
Electronic Thesis and Dissertation Repository

9-8-2015 12:00 AM

Secondary Electrohydrodynamic Flow Generated by Corona and Dielectric Barrier Discharges

Mohammadreza Ghazanchaei, *The University of Western Ontario*

Supervisor: Dr. Kazimierz Adamiak, *The University of Western Ontario*

A thesis submitted in partial fulfillment of the requirements for the Doctor of Philosophy degree in Electrical and Computer Engineering

© Mohammadreza Ghazanchaei 2015

Follow this and additional works at: <https://ir.lib.uwo.ca/etd>



Part of the [Electrical and Electronics Commons](#), [Engineering Physics Commons](#), [Fluid Dynamics Commons](#), [Numerical Analysis and Computation Commons](#), [Partial Differential Equations Commons](#), [Plasma and Beam Physics Commons](#), and the [Power and Energy Commons](#)

Recommended Citation

Ghazanchaei, Mohammadreza, "Secondary Electrohydrodynamic Flow Generated by Corona and Dielectric Barrier Discharges" (2015). *Electronic Thesis and Dissertation Repository*. 3295.
<https://ir.lib.uwo.ca/etd/3295>

This Dissertation/Thesis is brought to you for free and open access by Scholarship@Western. It has been accepted for inclusion in Electronic Thesis and Dissertation Repository by an authorized administrator of Scholarship@Western. For more information, please contact wlsadmin@uwo.ca.

SECONDARY ELECTROHYDRODYNAMIC FLOW GENERATED BY CORONA AND DIELECTRIC BARRIER DISCHARGES

(Thesis format: Integrated Articles)

By

Mohammadreza Ghazanchaei

Graduate Program in Engineering Science
Department of Electrical and Computer Engineering

A thesis submitted in partial fulfillment
of the requirements for the degree of
Doctor of Philosophy

The School of Graduate and Postdoctoral Studies
The University of Western Ontario
London, Ontario, Canada
September, 2015

© Mohammadreza Ghazanchaei 2015

Abstract

One of the main goals of applied electrostatics engineering is to discover new perspectives in a wide range of research areas. Controlling the fluid media through electrostatic forces has brought new important scientific and industrial applications. Electric field induced flows, or electrohydrodynamics (EHD), have shown promise in the field of fluid dynamics. Although numerous EHD applications have been explored and extensively studied so far, most of the works are either experimental studies, which are not capable to explain the in depth physics of the phenomena, or detailed analytical studies, which are not time effective. The focus of this study is to provide the model that in a reasonable computational time is able to give us accurate results in different electric-fluid interactions. So, the main goals of this study is to provide a model to simulate all essential physical phenomena, applicable in different EHD systems.

So, in this thesis, first, a two-dimensional numerical solver is presented for the dynamic simulation of the Dielectric Barrier Discharge (DBD) and the Corona Discharge (CD) in point to plane configuration. The simulations start with the single-species model and the different steps of the numerical technique are tested for this simplified model. The ability of the technique to model the expected physical behavior of ions and electric field is investigated. The studied physics were implemented in different geometry configurations such as wire to plane, wire to wire, and plane to plane geometries. The electrostatic field and ionic space charge density due to corona discharge were computed by numerically solving Poisson and current continuity equations, using a Finite Element method (FEM). The detailed numerical approach and simulation procedure is discussed and applied throughout the thesis. Then, the technique is applied to a more complicated model in order to address several existing EHD applications. The complicated mutual interaction between the three coexisting phenomena of electrostatic field, the charge transport, and fluid dynamics, which affect the EHD process, were taken into account in all the simulations. Calculations of the gas flow were carried out by solving the Reynolds-averaged Navier-Stokes (RANS) equations using FEM. The turbulence effect was included by using the $k-\varepsilon$ model included in commercial COMSOL software. An additional source term was added to the gas flow equation to include the effect of the electrostatic body force. In all the simulations, the effects of different parameters on the

overall performance of the system and its characteristics are investigated. In some cases, the simulation results were compared with the existing experimental data published in literature.

Keywords

Corona discharge, Dielectric barrier discharge, electrohydrodynamics, numerical simulation, transient simulation, finite element method, electric field intensity, discharge current, charge transport, surface charge accumulation, electrostatic body force, EHD pump, active airflow control, boundary layer, velocity profile, drag force.

Co-Authorship Statement

This thesis has been written by Mohammadreza Ghazanchaei under supervision of Dr. Kazimierz Adamiak and Dr. G.S. Peter Castle. Parts of the material presented in this thesis have been published in several peer-reviewed journals and refereed conference proceedings as listed below. The research in each publication has been conducted by the principal author and guided/supported by or in collaboration with the underlined authors, who are the research supervisors or members of the advisory committee.

Chapter 3 presents a numerical investigation of the quasi stationary modeling of Dielectric Barrier Discharge (DBD) under AC sinusoidal voltage. Finite element method is used in this chapter in order to include the effect of space charge density on electric field distribution in point to plane geometry. Behaviour of corona current and space charge density under different voltage/ frequency combinations is investigated. The investigation and numerical analysis were conducted by the principal author. The co-authors help to improve the understanding of the physics related to DBD and constructing a numerical model. Some recommendations and revisions were made by the co-authors as well. The material in Chapter 3 has been published in:

Mohammadreza Ghazanchaei, Kazimierz Adamiak, G.S. Peter Castle, "Quasi-stationary numerical model of the dielectric barrier discharge," J. Electrostat., Vol.72:4, pp. 261-269, Aug.2014(Also Presented at Electrostatics Society of America (ESA), Cocoa Beach, USA, June 2013)

In Chapter 4 the 2D numerical model is presented for non-parallel electrohydrodynamic pumps with DC positive applied voltage. The main contribution of the work is to present an analogy between ideal power source and EHD pump. The concept of the short circuit, and open circuit was interpreted in the form of velocity and pressure. The pressure vs. velocity graphs were extracted for different applied voltage and angle of orientation, for control purposes. Effect of the ion mobility on the electromechanical energy conversion is studied. The mathematical analysis, numerical simulation, and justification of the related experiments with the studied model were performed by the principal author. Co-authors helped to understand the model observations and proposed several

recommendations to justify the simulation results with experiments. Some recommendations and revisions were made by the co-authors as well. The material in Chapter 4 has been published in:

Mohammadreza Ghazanchaei, Kazimierz Adamiak, G.S. Peter Castle, "Predicted flow characteristics of a wire-nonparallel plate type electrohydrodynamic gas pump using the Finite Element Method," J. Electrostat., Vol. 73, pp. 103-111, Feb. 2015 (also presented at Electrostatics Society of America, Notre Dame, USA, June 2014)

In Chapter 5 the 2D model is developed in order to include all essential physics related to DC plasma formation on a flat plate. The contribution in this work is that this model is fully coupled and capable of solving all the phenomena in one solver using the Finite Element Method. Effects of different parameters of the model on plasma actuator characteristics are studied. The flow separation control was studied and the effectiveness of the proposed model to delay that separation for different angle of attack was investigated. The principal author performed the mathematical modeling and simulation analysis. The co-authors helped to understand the concept of the boundary layer control using corona discharge. Some recommendations and revisions were made by the co-authors as well. The material in Chapter 5 is being under-review in:

Mohammadreza Ghazanchaei, Kazimierz Adamiak, G.S. Peter Castle, "Numerical study on the DC corona discharge for the active airflow control along the flat plate," Ins. Phys., IOP: Electrostatics, Vol.1, pp.85, Southampton, UK, April, 2015

and reviewed in:

Mohammadreza Ghazanchaei, Kazimierz Adamiak, G.S. Peter Castle, "Numerical Modeling of EHD Interaction in the Boundary Layer of Air Flows," under review: Int. J. Flow Control, Feb. 2015

In Chapter 6 a 2D numerical analysis is developed in order to control the air flow over the flat plate using DBD. The main contribution in this work are: Modified approach for the calculation of space charge density for electrostatic body force calculation, observation of the quasi stationary fluctuation of the velocity in an actuator, capability of the proposed numerical algorithm to compute electrostatic, charge transport and fluid

flow model with the same solver, and capability of the system to evaluate the total force on the moving air. Besides, the parametric study has been done to investigate the effect of physical and geometrical characteristics of the model, on the system performance. The mathematical analysis and numerical investigations were performed by the principal author. The co-authors helped in the further understanding of the plasma formation mechanism involving DBD. The co-authors clarified several difficulties in explaining the observations. Meantime, some recommendations and revisions were made by the co-authors. The material in Chapter 6 has been published in:

Mohammadreza Ghazanchaei, Kazimierz Adamiak, G.S. Peter Castle, "Modeling of dielectric barrier discharge actuator for airflow control," CANCAM 2015, London, Canada, June 2015

Mohammadreza Ghazanchaei, Kazimierz Adamiak, G.S. Peter Castle, "Investigation on dielectric barrier discharge actuator to control airflow boundary layer," Electrostatic Society of America (ESA) Annual Meeting on Electrostatics, Pomona, USA, June 2015

and is currently under review in:

M.R. Ghazanchaei, K. Adamiak, G.S.P. Castle, "Modeling of dielectric barrier discharge actuator for airflow control," under review: J. Phys. D: Appl. Phys., Mar. 2015

Acknowledgments

First of all, I give my best regards and gratefulness to Prof. K. Adamiak, and Prof. G.S.P Castle. During the past four years, they were the most influential persons to me. Their great insight and profound knowledge was of great help for me. I would like to thank them for their consistent help, support, and guidance, and invaluable comments during the course of this project. I could not have asked for more from them, and will always be grateful for their encouragement and guidance.

I wish to thank my other thesis committee members: Dr. Anestis Dounavis, Dr. Rajiv Varma, Dr. Cedric Briens and Dr. Nicolas Benard.

I also like to acknowledge the helpful discussions and advises of all professors and colleagues who helped me with their valuable hints and comments on my works. I had a great opportunity to discuss and get feedback from many professors through annual reviews, local and international conferences.

I am grateful to NSERC of Canada and UWO for their financial support, and CMC Microsystems for the providing an access to COMSOL commercial software. I also acknowledge and admire my colleagues for their assistance and friendship, helping me during the course of this project.

Last but not least, I take this opportunity to thank my family: my dear mother Leila, my dear father Soleiman, and my beautiful sisters, Afsaneh, Fatemeh, Ghazal, and Zohreh for their unconditional love and support they gave me during these years. I would like to dedicate this work to my parents and to my cool nephew, Borna, and my lovely niece Baran.

Table of Contents

Abstract	ii
Co-Authorship Statement.....	iiv
Acknowledgments.....	vii
Table of Contents	viiiviii
List of Tables	xiii
List of Figures	xiv
Nomenclature	xviii
Acronyms	xxii
Chapter 1	1
1 Introduction	1
1.1 Corona discharge and its applications.....	1
1.1.1 Features of Corona Discharge.....	3
1.1.2 Types of Corona Discharge	3
1.2 Dielectric-Barrier Discharges	5
1.2.1 The History of DBD.....	5
1.2.2 The Physics of Dielectric Barrier Discharge	6
1.3 Electrohydrodynamic pump.....	7
1.3.1 What is EHD?	8
1.3.2 EHD pump design and features	9
1.4 Airflow control by plasma actuators.....	10
1.4.1 Corona discharge actuator.....	11
1.4.2 Dielectric barrier discharge actuator.....	13
1.5 Objectives	16
1.6 Thesis Outline	18

References	19
Chapter 2.....	25
2 Mathematical Models and Numerical Algorithms in EHD.....	25
2.1 Mathematical Models and Numerical Algorithms in Electric Corona Simulation.....	25
2.2 Literature Review on Mathematical Models for the Dielectric Barrier discharge	29
2.3 Literature Review on the Numerical Techniques on EHD Simulation.....	31
2.4 Mathematical Model and Governing Equations	34
2.4.1 Electrostatic Field and Charge Transport	34
2.4.2 Fluid Flow	35
2.5 Boundary Conditions	40
2.5.1 Complementary equations for modeling dielectric barrier discharge.....	41
2.6 Finite Element implementation in COMSOL.....	42
2.6.1 Current	44
2.6.2 Electrokinetic conversion.....	46
2.7 Conclusions.....	47
References:.....	48
Chapter 3.....	56
3 Quasi-stationary numerical model of the dielectric barrier discharge	56
3.1 Introduction.....	56
3.2 Mathematical model.....	58
3.2.1 Governing equation.....	58
3.2.2 Complementary equations for modeling dielectric barrier discharge.....	60
3.2.3 Boundary conditions	61
3.3 Numerical algorithm	62
3.3.1 Electric current.....	63
3.4 Simulation results.....	64

3.5 Conclusion	71
References	72
Chapter 4	74
4 Predicted flow characteristics of a wire-nonparallel plate type electrohydrodynamic gas pump using the Finite Element Method	74
4.1 Introduction.....	74
4.2 Model description	77
4.2.1 Geometry.....	77
4.2.2 Electrical model	78
4.2.3 Airflow model.....	79
4.2.4 Boundary conditions	80
4.3 Numerical Algorithm	81
4.4 Simulation results and discussion	82
4.4.1 Electric current.....	82
4.4.2 Flow pattern	83
4.4.3 Pressure vs. velocity characteristics.....	84
4.4.4 Efficiency	88
4.4.5 Wall angle effect.....	89
4.4.6 Conclusions.....	91
Acknowledgments.....	92
References.....	92
Chapter 5	95
5 Numerical Modeling of Electrohydrodynamic Interactions in the Boundary Layer of Air Flows.....	95
5.1 Introduction.....	95
5.2 Model description	98
5.2.1 Geometry.....	98

5.2.2	Boundary layer	98
5.2.3	Fluid flow model	99
5.2.4	Electrical model	1000
5.3	Numerical method	1022
5.4	Results and discussion	1033
5.4.1	Current	1033
5.4.2	Velocity profile	1055
5.4.3	Effect of the Voltage Level	1077
5.4.4	Total force	109
5.4.5	Efficiency	1111
5.4.6	Angle of attack	1122
5.5	Summary	1144
	References	1144
Chapter 6	1188
6	Modeling of dielectric barrier discharge actuator for airflow control.....	1188
6.1	Introduction.....	1188
6.2	Model description	1211
6.2.1	Fluid flow model.....	1222
6.2.2	Electrical model	1233
6.3	Numerical algorithm	1255
6.4	Results and discussion	1266
6.4.1	Electric field intensity	1266
6.4.2	Electric current.....	1277
6.4.3	Flow velocity	1288
6.4.4	Force calculation.....	1311
6.4.5	Parametric study.....	1322

6.5 Conclusions.....	138
Acknowledgments.....	13939
References	13939
Chapter 7.....	1422
7 Conclusions and Future Study	1422
7.1 Conclusions.....	1422
7.1.1 Single-Species Model of Dielectric Barrier Discharge.....	1422
7.1.2 Wire-nonparallel plate electrohydrodynamic gas pump.....	1444
7.1.3 Electrohydrodynamic Interactions in the Boundary Layer of Air Flows	145
7.1.4 DBD plasma actuator for airflow control	146
7.2 Recommendations for Future Study	1477
7.2.1 Modeling.....	147
7.2.2 Experimental studies.....	147
7.2.3 EHD pump design for cooling an electronic circuit	148
7.2.4 Sliding Discharge.....	148
7.2.5 Different applications of Plasma actuators	149
Curriculum Vitae	150

List of Tables

Table 4.1: Boundary conditions for the EHD pump model	81
Table 4.2: Average outlet velocity for the same pressure difference for the basic configuration	84
Table 4.3: Total energy conversion and efficiency of the pump	88
Table 4.4: Wall angle effect on velocity, pressure and air flow rate	91

List of Figures

Figure 1.1: Model of the positive corona discharge	4
Figure 1.2: Basic dielectric-barrier discharge configurations	6
Figure 1.3: Ion transport and choking effect on DBD	7
Figure 1.4: Various geometries for the corona discharge plasma actuator	12
Figure 1.5: Configuration of the Dielectric Barrier Discharge plasma actuator	13
Figure 2.1: Schematic geometry of the electrodes	45
Figure 3.1: Typical configuration for DBD investigated in this study	58
Figure 3.2: Electric field intensity on the needle’s tip with (Poissonian Model) and without (Laplacian Model) the effect of the accumulated charge	64
Figure 3.3: Waveform of the discharge current	65
Figure 3.4: Distribution of space charge in the air gap	65
Figure 3.5: Accumulated surface charge on dielectric layer	66
Figure 3.6: Distribution of space charge along the axis of symmetry as a function of a period	67
Figure 3.7: Waveform of discharge current just above the onset voltage at 5 kHz	67
Figure 3.8: Total space charge in domain for the voltage just above onset level (V=3.2 kV) at 5 kHz	68
Figure 3.9: Waveform of the discharge current for the voltage just above onset level (V=3.2kV) at 50 Hz	68
Figure 3.10: Total space charge for the voltage just above onset level at 50 Hz	69

Figure 3.11: Maximum current and maximum space charge in domain at different voltages and at 5 kHz	70
Figure 3.12: Maximum current (left hand side) and maximum space charge (right hand side) in domain at different frequencies and at 7.5 kV	71
Figure 4.1: EHD pump configuration for wire to non-parallel plate system (not to scale)	78
Figure 4.2: Discharge current per unit length of corona wire for EHD gas pump as a function of applied voltage	82
Figure 4.3: Flow patterns under different applied voltage for the same level of pressure difference ($\Delta P = 0.02$ Pa, wall angle = 3°)	83
Figure 4.4: Short circuit and blocked mode of the EHD pump (wall angle = 3°)	85
Figure 4.5: Flow patterns of the pump by changing the reverse pressure from zero up to maximum pressure for the same level of wire voltage (wall angle = 3°)	86
Figure 4.6: Predicted pressure vs. velocity characteristics for different levels of the applied voltage	87
Figure 4.7: Flow streamlines for different wall angles at $V=8$ kV and $\Delta P = 0$	90
Figure 5.1: Configuration for the corona wire and grounded wire	98
Figure 5.2: Flow over a flat plate	99
Figure 5.3: Corona discharge current versus voltage	104
Figure 5.4: Velocity profile for the system with/without corona at $x=1$ cm ahead of corona wire for $U_\infty=2$ m/s.	105
Figure 5.5: Velocity profiles without discharge (\square) and with corona discharge (\blacksquare) at $x=1$ cm for $U_\infty=2, 5, 10$ and 12 m/s.	106
Figure 5.6: Velocity profiles induced by corona discharge for the input voltage 38kV for different x values.....	107

Figure 5.7: Velocity profiles for $U_\infty \approx 0$ and different applied voltages (a) 26kV, (b) 30kV, (c) 34 kV, (d) 38kV	108
Figure 5.8: Velocity profiles induced by the ionic wind along a line normal to the wall for different applied voltages at $x=1\text{cm}$ ahead of the corona wire	109
Figure 5.9: Boundary layer formation around the flat plate	109
Figure 5.10: Total force calculation at $x=1\text{ cm}$ ahead of corona wire versus airflow velocity U_∞ in absence and in presence of the corona discharge	111
Figure 5.11: Efficiency versus applied voltage for $U_\infty=5\text{ m/s}$	112
Figure 5.12: Velocity distribution with (left) and without (right) the corona effect for input velocity $U_\infty=0.5\text{ m/s}$ and a flat plate at (a) 0° , (b) 10° , (c) 20°	113
Figure 6.1: Idea of DBD actuator (not to scale).....	121
Figure 6.2: Electric field intensity on the tip of exposed electrode with (Poissonian Model) and without (Laplacian Model) the effect of the charge accumulated in air and dielectric surface	127
Figure 6.3: Voltage (kV) and current (mA/m) waveforms in DBD	128
Figure 6.4: Velocity profile along a direction normal to the surface at $x=10\text{mm}$ ahead of the exposed electrode.....	129
Figure 6.5: Velocity distribution around the object without (left) and with EHD flow (right)	129
Figure 6.6: Velocity profiles above the DBD actuator for different distances from the discharge electrode	130
Figure 6.7: Time evolution of the x velocity component.....	130
Figure 6.8: Total force calculation at $x=5\text{ mm}$ ahead of exposed electrode versus free airflow velocity U_∞ in absence and in presence of the DBD	131

Figure 6.9: Evolution of the maximum induced air velocity with voltage magnitude and frequency.....	132
Figure 6.10: Maximum current for different voltage magnitudes and frequencies	133
Figure 6.11: Space charge density distribution (plasma extension) for different applied voltages	134
Figure 6.12: Velocity evolution at the same point for two different frequencies of the applied voltage.....	135
Figure 6.13: Normalized fluctuation level for different frequency levels	135
Figure 6.14: Plasma extension (space charge density) for two different radii of the exposed electrode (left) 0.04mm, (right) 0.08mm.	136
Figure 6.15: Velocity evolution at the same point for two different radii of the exposed electrode.....	136
Figure 6.16: The effect of DBD on boundary layer for 15mm (left), and 10mm (right) electrode width	137
Figure 6.17: Maximum velocity for different widths of the ground electrode	138

Nomenclature

\vec{D}	<i>Electrostatic displacement vector ($C \cdot m^{-2}$)</i>
\vec{E}	<i>Electric field intensity ($V \cdot m^{-1}$)</i>
V, V_{ap}, V_{max}	<i>Electric potential, applied voltage, maximum voltage (V)</i>
ρ_c	<i>Ionic charge density ($C \cdot m^{-3}$)</i>
\vec{j}	<i>Current density vector ($A \cdot m^{-2}$)</i>
$\epsilon, \epsilon_0, \epsilon_r$	<i>Permittivity, permittivity of Air, Relative Permittivity ($F \cdot m^{-1}$)</i>
$\mu_e, \mu_{p,e}, \mu_{n,e}$	<i>Mobility of ions, positive ions, and Negative Ions ($m^2 \cdot V^{-1} \cdot s^{-1}$)</i>
\vec{u}, V_G	<i>Vector and magnitude of gas velocity ($m \cdot s^{-1}$)</i>
D	<i>Diffusion coefficient ($m^2 \cdot s^{-1}$)</i>
k_B	<i>Boltzmann constant ($m^2 \cdot kg \cdot s^{-2} \cdot K^{-1}$)</i>
e_0	<i>Electron charge (C)</i>
T, T_0	<i>Actual temperature, Standard temperature (K)</i>
ρ	<i>Gas density ($Kg \cdot m^{-3}$)</i>
μ, μ_t	<i>Airflow viscosity, eddy viscosity ($kg \cdot m^{-1} \cdot s^{-1}$)</i>
\vec{F}	<i>External body force</i>
S_x, S_y	<i>Source terms of the x and y momentum</i>
Re	<i>Reynolds number</i>
L	<i>Length scale of the flow (m)</i>
U_b, u'_i	<i>Mean and fluctuating velocity components ($m \cdot s^{-1}$)</i>
ϕ	<i>Scalar quantities such as pressure, or energy</i>
k	<i>Turbulence kinetic energy</i>
ϵ	<i>Turbulence dissipation rate</i>
ρ_s	<i>Surface charge density</i>
T_I	<i>Turbulence intensity</i>
R	<i>Electrode radius (m)</i>
β	<i>Experimentally found constant for charge injection ($C \cdot m \cdot V^{-1}$)</i>
E_0	<i>Onset value of electric field ($V \cdot m^{-1}$)</i>
f	<i>Frequency (Hz)</i>
A_G	<i>Discharge cross section (m^2)</i>
S_G	<i>Averaged gas flow rate ($L \cdot min^{-1}$)</i>

v_i *Drift velocity of ions ($m.s^{-1}$)*
 I *Corona current (A)*

Acronyms

CD	<i>Corona Discharge</i>
DBD	<i>Dielectric Discharge Barrier</i>
AC	<i>Alternating Current</i>
DC	<i>Direct Current</i>
FEM	<i>Finite Element Method</i>
BEM	<i>Boundary Element Method</i>
FDM	<i>Finite Difference Method</i>
FVM	<i>Finite Volume Method</i>
MoC	<i>Method of Characteristics</i>
FCT	<i>Flux Corrected Transport</i>
PDE	<i>Partial Differential Equations</i>
RANS	<i>Reynolds-averaged Navier-Stokes</i>
EHD	<i>Electrohydrodynamics</i>
ESP	<i>Electrostatic precipitator</i>
PIV	<i>Particle Image Velocimetry</i>
1D, 2D, 3D	<i>One, two, three dimensional</i>

Chapter 1

1 Introduction

Diverse applications of EHD have been proposed in different fields of physics and engineering. From the electrical engineering point of view, the mechanisms related to the corona discharge and dielectric barrier discharge as the driving force of the electric-fluid interaction seems to be the main subject of the EHD studies. Thus, in this chapter, the corona discharge, the dielectric barrier discharge and a summary of the research on their physics and applications are briefly reviewed first. Then, the general concept of the EHD phenomenon is described in detail. As a particular application, air pumping through EHD effects is reviewed and the models related to EHD pumps are explained. Finally, a review of the research regarding the EHD effects associated with boundary layer control is presented and the new trend of research in controlling the airflow through electrostatic forces is highlighted. Finally, the objectives of the research and the outline of this thesis are described.

1.1 Corona discharge and its applications

Corona discharge is a high voltage physical phenomenon involving the partial electrical breakdown of the gaseous medium between at least two electrodes with significantly different radii of curvatures. A so-called corona electrode is a sharp electrode with very small radius of curvature, usually supplied with a high electric potential and the other electrode is blunt with much larger radius of curvature and is usually grounded [1]. The partial electrical discharge, or electric corona discharge, occurs when the strength of the electric field near the corona electrode exceeds a certain critical value, but still not enough for a complete breakdown or arc. In studying the mechanism of the corona systems it is been found that the electric field near the sharp corona electrode is much larger than its value at points far from this electrode. Therefore, compared to a spark discharge, only a very small part of the gap between the two electrodes becomes ionized and conductive during the discharge; this is why corona is called a partial discharge phenomenon.

Corona discharges have been a field of study since the early 20th century as a detrimental mode of breakdown in high voltage engineering. The physical laws that govern the discharges were studied extensively by Townsend [2], Loeb [3], and Peek [4], both theoretically and experimentally. Townsend [2] derived an approximate relationship for the voltage-current characteristic of a steady state corona discharge. Peek [4] conducted experiments that were mainly concerned with establishing empirical laws to determine the corona losses from high voltage conductors. Using electric field distributions in simple conductor geometries, he derived the minimum gap distance required to initiate a steady state corona and also defined an empirical relationship to obtain the potential required to onset the corona in dry air for highly symmetric configurations.

These simple configurations form an approximation for more practical configurations used in experiments. The semi-empirical Peek's law defines the minimum electric field on the wire surface necessary to initiate the discharge. In 1947, Kaptzov [5] proposed that the electric field at the wire surface remains at the value specified by Peek's onset criterion irrespectively of the potential applied on the wire. Kaptzov's hypothesis is often used in simulations of corona discharge [1], [6] since it provides a methodology to avoid the reaction chemistry in the ionization zone.

Sigmond [7, 8] provided a comprehensive review on the physics of electrical coronas and their interaction with surfaces, with some emphasis on phenomena which seem of importance for high voltage insulation. Despite the fact that coronas may have unwanted effects, especially in electric power transmission by causing power loss, audible noise, electromagnetic interference, and ozone generation, they have been used for many years in different industrial applications. The main application of corona discharge in engineering devices and processes involves the transport of the very small charged particles and ions along the trajectories which follow the electric field lines. Examples of areas of engineering using this phenomenon are numerous: from cooling of microscale electronic circuits [9], to medium range industrial processes of chemical materials [10- 12], to macroscale efficient flow control for inner and outer of space aerodynamic applications [13, 14]. Different configurations for corona discharge have been investigated by many researchers. Corona electrodes typically consist of needles, wires or blades connected to a high voltage

power supply. Some examples of different configurations used for generating corona discharge are point-to-plane, multipoint-to-plane, wire-to-plane, wire-to-cylinder, wire between two planes, and multiwire-to-plane [15 -16]. It has been proved that the electrode configuration has a major role in different applications of corona discharge.

1.1.1 Features of Corona Discharge

As the electric field near the corona electrode increases, the free electrons existing in gas in this area are accelerated due to electric forces. When the accelerated electrons gain enough energy, they create an electron-positive ion pair upon their collision with neutral gas molecules. The newly generated electrons are accelerated and create more electron-ion pairs. Therefore, the number of electrons in the air gap increases exponentially. This process is known as the electron avalanche. As the applied voltage increases closer to the value of the breakdown voltage of the gas, the ionization process penetrates deeper into the air gap and arcing occurs. This is what happens during a lightning strike.

The value of the electric potential at which the corona starts is called the corona onset voltage. At voltages close to this value, corona current increases proportionally with voltage. Above this, the corona current increases more rapidly, approximately as a square function of the applied voltage.

1.1.2 Types of Corona Discharge

Corona discharge phenomena can be categorized into different types based on the applied voltage, electrode configuration, or the polarity of the electric potential supplied to a sharp electrode. A corona discharge can be operated in direct current (DC) mode, alternating current (AC) mode or in pulsed mode. DC corona discharges can be generated for both positive and negative polarity, depending on whether the positive or negative voltage source is applied to the corona electrode. The present research is conducted only for positive DC corona discharges and hence this thesis focuses primarily on positive coronas.

Generally, if a positive voltage is applied to the corona electrode, positive ions move towards the ground plane and electrons and negative ions move towards corona electrode. In negative corona on the other hand, the applied voltage and the direction of ions

movement is opposite to that of the positive corona case. The physics related to the positive and negative corona discharges are somewhat different. The negative coronas mostly consist of short pulses of very fast duration, called Trichel pulses, while positive coronas are more stable.

The processes in a DC positive corona are well understood [17, 18] and illustrated in Figure 1.1. In the general electrode configuration this type of corona starts with burst pulse corona. This regime consists of random and non-regular current pulses. As voltage increases this develops into glow corona, streamer corona and finally spark discharge.[11].

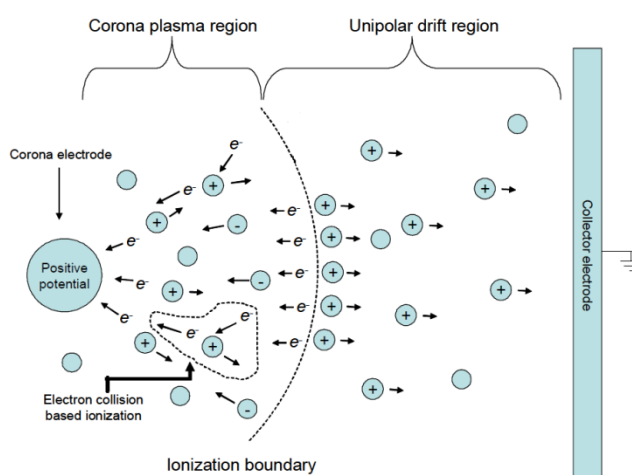


Figure1.1: Model of the positive corona discharge [17]

The glow discharge regime has a stable current at a fixed voltage, quiet operation and almost no sparking. The streamer regime is unstable, and emits audio and radio noise. It creates many thin and short duration current streamers originating from the area near the needle. The streamer regime of corona can be described as an incomplete breakdown and it is followed by a spark as voltage is further increased [11].

In this section the fundamental theory of corona discharges relevant to this research was reviewed. The more comprehensive study on the numerical simulation and mathematical models of corona discharges is discussed in next chapter.

1.2 Dielectric-Barrier Discharges

Dielectric Barrier Discharge (DBD) is used on a large industrial scale. A prominent feature is the simple scalability from small laboratory reactors to large industrial installations with megawatt input powers [19]. Industrial applications include ozone generation, pollution control, airflow control and surface treatment. Background of the research and the discharge physics of dielectric barrier discharges are discussed in this section.

1.2.1 The History of DBD

Dielectric-barrier discharges, or simply barrier discharges, have been known for more than a century. First experimental investigations were reported by Siemens [20] in the late 19th century and were related to the application of DBD to the ozone generation. Siemens proposed the name of silent discharge for this phenomenon, which still is frequently used in scientific literatures. Ozone formation in DBDs became an important research issue for many decades [21].

Later, Warburg conducted a series of investigations on the nature of the silent discharge. Most of the researches at the beginning of the 20th century were working on the design of industrial ozone generators utilizing DBDs. A significant contribution to characterizing the discharge was made by Buss, who found out that breakdown of atmospheric-pressure air between planar parallel electrodes covered by dielectrics always occurs in a form of large number of tiny short-lived current filaments. More information about the nature of the discharge, including the images of these filaments and oscilloscope recordings of current and voltage, were collected by a few researchers [22, 23]. Manley [24] proposed a method for determining the consumed power in DBDs by using voltage/charge figures and derived an equation for dissipated power. Extensive research activities employing modern diagnostic and modeling tools started around 1970. Originally aimed at a better understanding of the plasma physical processes in industrial ozone generation, these research efforts resulted not only in improved ozone generators, but also in a number of additional applications of DBD, such as surface modification, pollution control and, most recently, in manipulation of the airflow in aerodynamic applications.

1.2.2 The Physics of Dielectric Barrier Discharge

In many cases the term corona discharge is used in connection with DBD, although most authors prefer to use this term only for discharges between bare metal electrodes without dielectric. However, both discharges have some common features, for example strong local field distortions caused by space charge accumulation.

Typical planar DBD configurations are sketched in Figure 1.2. As a consequence of the presence of at least one dielectric barrier, these discharges require alternating voltage for their operation. The dielectric, being an insulator, cannot pass a DC current. Its dielectric constant and thickness, in combination with the time derivative of the applied voltage, determine the amount of displacement current that can be passed through the dielectric [19]. To generate ionic current in the discharge gap the electric field has to be high enough to cause breakdown in the gas. In most applications the dielectric limits the average current density in the gas space.

Preferred materials for the dielectric barrier are glass or silica glass, in special cases also ceramic materials and thin enamel or polymer layers. At very high frequencies the current limitation by the dielectric becomes less critical. For this reason DBDs are normally operated between line and a few kHz frequencies.

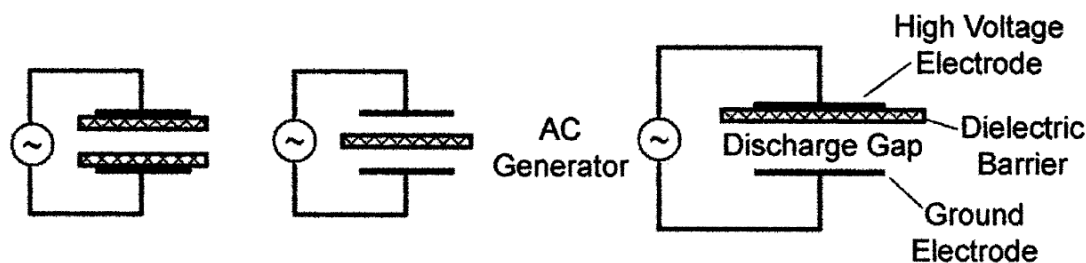


Figure 1.2: Basic dielectric-barrier discharge configurations [19]

Figure 3 illustrates the processes that occur in DBD during one cycle of AC voltage. By applying an electric field larger than the breakdown field local ionization in the gap occurs. By applying a negative voltage (left hand side on Figure 1.3), negative ions accumulate on the lower dielectric surface and positive ions accumulate on top one. So, the total electric field intensity is a combination of the electric field produced by the voltage source and the

field produced by the space charge collected on the dielectric surfaces. As the discharge progresses, electric field is reduced until ionization stops and the ionic current in the gas falls to zero.

When the sign of voltage reverses, the source field reinforces the field of accumulated charges. This enhanced field at the beginning of the new half cycle initiates gas ionization and a new ionic current, which transfers charge across the cell until the opposing space-charge field once again, extinguishes gas ionization in the gap [25].

The described choking effect due to the local field reduction depends on the lateral extension of the surface discharge, the properties of the dielectric barrier and, of course, on the gas properties.

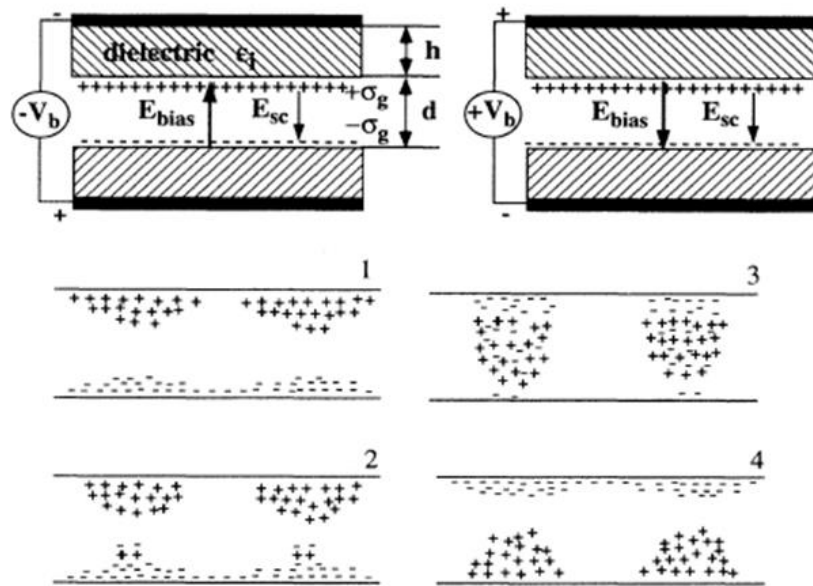


Figure 1.3: Ion transport and choking effect on DBD [28]

In next Chapter the detailed mathematical model of the DBD, as well as a comprehensive literature review on the numerical modeling is discussed.

1.3 Electrohydrodynamic pump

Phenomena that involve the direct conversion of electrical energy into kinetic energy of moving fluid are known as electrohydrodynamics (EHD) and have a variety of possible applications today. This section contains a literature review of the EHD effects associated

with high voltage discharges, from the first observation of the phenomenon to the most recent advancements on its mathematical modeling, as well as the proposed new applications, such as air pumping and boundary layer control.

1.3.1 What is EHD?

The first experiments on the electrohydrodynamic effects were performed long time ago by observing a weak wind blowing when holding a charged tube close to a human body [26]. Newton was the one who explored this phenomenon thoroughly, and named it as electric wind. This terminology was used for centuries; however, nowadays, the term ionic wind, or secondary electrohydrodynamic flow, are more common. Later, researchers could find some practical application for electric wind [19]. The first qualitative description of the phenomenon was proposed by Cavallo [27], who accurately described the physical mechanism of electric wind. Significant progress was made several decades later by Faraday [28], when he described the electric wind as a process of momentum transfer, caused by friction or collision between charged and uncharged gas particles, properly identifying the reason behind the movement of the air. However, even though the EHD effects had been observed, the scientists simply lacked the knowledge and experimental apparatus to fully explain it at that time.

Maxwell [29] performed the first qualitative analysis of the electric wind mechanism. The first quantitative analysis of the ionic wind was performed by Chattock [30]. He derived an experimentally verifiable relationship between pressure and electric current for a parallel plane electrode configuration. Later on, Peek [4] published his work focusing on dielectric phenomena and provided vast information on corona-related effects and mechanisms, which had critical importance to future researchers. Townsend noticed that the net mechanical force is generated when the asymmetrical electrodes were connected to a high-voltage power source. He published an article predicting that the ionized particles (ions) are created by the high-voltage electrode.

Interest in EHD phenomena increased during the past decades due to the very promising applications in various fields of engineering and science. Two major categories of the research in this area are the air pumping and the boundary layer control.

1.3.2 EHD pump design and features

Robinson [31] was the first who proposed the feasibility of designing a functional electrostatic blower or EHD pump. By experimentally testing a needle-to-ring electrode geometry, he evaluated the conversion efficiency from electrical to mechanical energy via corona discharges. Advantages of EHD pumps over mechanical pumps, such as no moving parts with a very simple construction and no noise or vibrations during the system operation, were clearly highlighted in his work.

However, the results of his experiments showed that the efficiency of an electrokinetic energy conversion was less than 1%. The low electrokinetic energy conversion efficiency beside the ozone generation and electrode corrosion are the main problems of EHD pumps. There have been a few experimental studies focused on improving the efficiency of EHD pumps. Important work toward this goal was reported in [32], which focused on improving the electrical to mechanical energy conversion efficiency of the needle to ring and needle to mesh electrode configurations.

Later, the research was extended to the cascading designs, consisting of a few consecutive stages [33]. Through a parametric study, the authors of this paper found that the wind speed is a linear function of the voltage applied to the corona electrode, as well as a square root function of the current, multiplied with an empirical constant. As the efficiency of EHD pumps is proportional to the velocity of the flow [34], it was also shown that cascading EHD pumps increase not only the exit wind velocity of the EHD pump, but the overall efficiency of the device as well. Moon *et al.* [35] later presented a more complex needle-to-mesh EHD pump, with the corona electrode surrounded by a ring at the same voltage potential. With this design, the research team claimed to have improved the efficiency of EHD pump by 2.5 times compared with the simple needle-to-mesh electrode design.

Furthermore, the researchers tested both positive and negative corona discharges and their effect on flow velocity. Study of different configuration for the EHD pump was other interesting research area. In [36], the performance of multiple EHD pump geometries were experimentally tested using needles as the corona electrodes and several different grounded

electrodes. The study gave very useful conclusions regarding the dependence between air pressure and the applied voltage. It has been revealed that the radius of the needle is a vital factor for the overall performance of the EHD pump.

A later study, assessing the effect of the voltage on the wind velocity using a needle-to-ring electrode configuration, discovered that the EHD pump operated properly with a positive voltage applied to the emitter, can reach exit air velocities in excess of 2 m/s [37]. Future research by the same author concentrated on further optimization of the design, which enhanced the performance of the EHD pump by implanting the collector electrode to the tube walls and also explored the performance of a cascading design consisting up to seven stages [38].

Despite the fact that the needle-to-mesh electrode configuration remained by far the most popular for years, during the past decade researchers also began exploring EHD pumps based on different electrode configurations. Tsubone et al. performed series of experimental investigation over wire-plate type EHD gas pump. In [39] they study the effect of grounded electrode location and polarity for a wire-non-parallel plate type EHD gas pump. The experiments were conducted for the negative and positive applied voltages. This configuration for the EHD gas pump was used to fully explain the mechanism of unidirectional EHD generation.

However, although the study included very detailed results on the experimental investigations, the experimental prototypes doesn't appear to be optimized and no recommendations were discussed how to optimize the electrode configuration.

1.4 Airflow control by plasma actuators

The active flow control is of huge importance in the aerodynamic community. Efficient flow control systems are capable of manipulating the flow to achieve desired effects, such as drag reduction, and mitigating noise and vibration. These applications typically involve techniques, such as separation control and laminar to turbulent transition suppression. Recently, the introduction of plasma actuators in this field has demonstrated much promise.

Plasma based devices exploit the momentum coupling between the surrounding gas and plasma to manipulate the flow.

Unlike mechanical flow control techniques, plasma actuators require low power consumption [40], involve no moving mechanical parts and have a very short response time. For these reasons, the plasma actuator has become a very attractive device in numerous potential applications.

Plasma actuators can be sub-categorized into two major families: the corona discharge and the dielectric barrier discharge. The major difference between the DBD and the corona discharge actuators is the presence of a dielectric barrier separating the corona and grounded electrode in the former configuration. The dielectric barrier introduces a region of large electric field, allowing for the application of larger potential differences and thus larger electric field intensities in the plasma region. In addition, the presence of the dielectric barrier increases the stability of the plasma, preventing a glow to spark transition at typical potentials for which this would occur on the surface corona discharge.

1.4.1 Corona discharge actuator

Actuation due to corona discharge is typically implemented due to the ignition of the plasma through the partial ionization of the surrounding air. This actuator involves the placement of two electrodes, both exposed to the air, on the surface of a dielectric separated by some distance. Typical corona discharge plasma actuator geometries can be seen in Figure 1.4. Applying DC high voltage across the electrodes ignites weakly ionized plasma that is capable of inducing flows up to few meters per second [41].

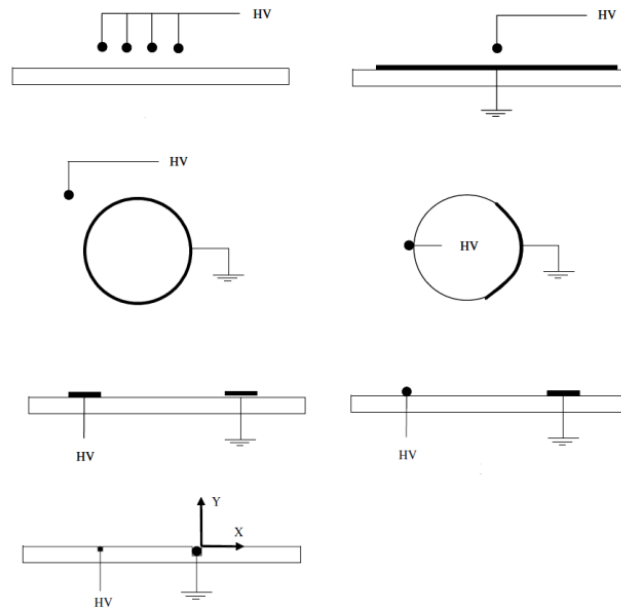


Figure 1.4: Various geometries for the corona discharge plasma actuator [41]

Preliminary research in this field has started in the 1950s. However, the first scientific paper was published by Velkoff [42] in 1968. From then up to late 90s, several research groups worked on airflow control by DC surface corona discharges, both experimentally [43] and theoretically [44]. It could be said that using plasma actuator has considerably influenced research on airflow control since few years ago and this subject has been growing considerably.

Velkoff et al. [42] used a plasma actuator consisting of four HV wire electrodes placed above the surface of a flat plate. They demonstrated that the velocity profile on the plate could be affected by the application of an electric field. For the same configuration, Malik et al. [45] reported an electric wind of several m/s contributing to drag reduction. In 1992, Soetomo [46] experimentally observed a drag reduction effect induced by AC and DC corona discharges along a flat plate. In this case, the corona discharge was established between two razor blades flush-mounted on the wall of a glass flat plate. Noger et al [47] used a point to plane configuration in order to manipulate airflow around a cylinder. Continuous works have been done on the surface corona based actuator and characterizing its electrical and mechanical properties by a group of researchers in France and Argentina [48-59]. Their studies focused on using two wire electrodes placed inside a groove at the wall surface. The corona electrode diameter was much smaller compared to that of the

grounded electrode in order to induce a stronger electric field. The electrical properties of this surface discharge as a function of different geometric parameters have been studied. The authors demonstrated that the surface discharge is very sensitive to these parameters. They found that the major disadvantage of the corona discharge actuators is the glow to arc transition that occur at large potential differences. This transition introduces a large surge of current towards the anode, effectively creating a short circuit. This problem could be solved by DBD plasma actuators.

1.4.2 Dielectric barrier discharge actuator

Recently, the most commonly used plasma actuators have been based on the dielectric barrier discharge (DBD). A typical configuration of the DBD is shown in Figure 1.5. Many parametric studies have been dedicated to investigating the properties of the plasma actuator's geometrical parameters. Two electrodes are typically separated by a dielectric barrier, usually glass, Kapton or Teflon.

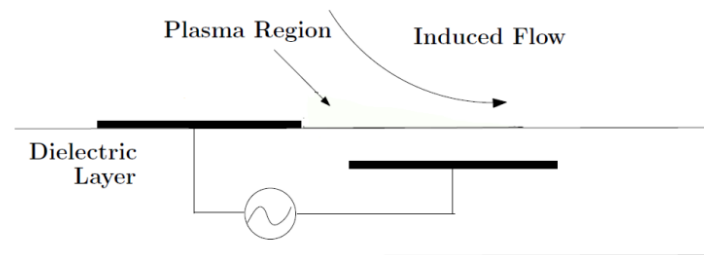


Figure 1.5: Configuration of the Dielectric Barrier Discharge plasma actuator

When a high voltage AC signal of sufficient amplitude and frequency is applied between the electrodes, the intense electric field partially ionizes the surrounding air producing the plasma sheet on the dielectric surface. The collisions between the neutral particles and accelerated ions generate a net body force on the surrounding fluid leading to the formation of ionic wind. The body force can be used to impart the desired flow control. The momentum coupling of the plasma and fluid induces an initial vortex that propagates downstream. This can be observed through the PIV measurements reported by Post et al. [60]. This result confirms that the plasma actuator eventually evolves into a wall-jet directed in the downstream direction.

Currently, the design of plasma actuators has primarily been focused towards the optimization of the momentum-air coupling for maximizing the induced flow. This has been accomplished through a variety of techniques from geometrical modifications to waveform optimization, incorporating a large set of variables that contribute to the performance of the plasma actuator. These variables are primarily divided into two categories: the geometrical parameters and the electrical operating conditions.

The geometrical parameters define the placement of the electrodes around the dielectric barrier. These include the electrode gap, electrode thickness, electrode width and span length, as well as the dielectric thickness. In a typical application, these parameters are fixed and are not typically controlled in real-time. One of the key parameters that has a significant influence on the induced flow is the thickness of the exposed electrode. Enloe et al. [61] were the first to investigate the effect of this parameter. They used two sets of actuators that differ in exposed electrode shape. They found that despite the fact that the two exposed electrode were different, the structure of the plasma remained unchanged in all cases. However, they further observed that the efficiency of the plasma actuator is strongly dependent on the thickness and diameter of the exposed electrode.

Hoskinson et al. [62] investigated the effect of the electrode thickness of the plasma actuator using a stagnation probe. In addition to this, three different materials were investigated for the exposed electrode. The results presented in this paper have suggested that changing the dielectric material has little effect on the induced force for the exposed electrode.

Another important geometrical parameter of the plasma actuator is the width of the encapsulated electrode. As observed by Enloe et al. [61], and Orlov et al. [63], the extent of the plasma was limited by the width of the encapsulated electrode and it would not be generated more than a few millimetres past the trailing edge. Similar results were also observed by Forte et al. [64] in a different plasma actuator configuration.

Finally, the electrode separation gap also plays a significant role in the optimization of the plasma actuator. This parameter governs the chord distance between the trailing edge of the exposed electrode and leading edge of the encapsulated electrode. Forte *et al.* [64]

studied the effects of this parameter on the maximum induced velocity. These results indicated that there is a fine balance between maximizing the electric field intensity with a small gap width and creating tangentially oriented force vectors with a larger gap width. However, there is no reason to believe that this result is universal to all actuator geometries and operating conditions. Thus, more studies must be performed on the effects of actuator gap on the performance of the actuator in different configurations.

The electrical parameters of the plasma actuators are the most important for the boundary layer control. These parameters include the applied voltage and frequency. The applied voltage is directly responsible for the strength of the electric field and, thus, the magnitude of the induced flow. Since the charges are constantly rearranged to cancel out the external electric field, a varying voltage is required to maintain plasma ignition. Finally, the driving frequency controls the number of times the plasma is ignited within a specific time period. Investigations into the effect of the applied voltage have been performed by various studies including Enloe et al. [61], Forte et al. [64] and Thomas et al. [65].

Plasma actuator models can be generally classified to belong to one of two families, defined by the method in which the charge density is calculated. The first consists of chemistry based models that attempt to spatially resolve the plasma phenomena directly, and the second are algebraic models that are based on the solution of Poisson's equation. The significant difference between the two is that the latter generally require assumptions on the behaviour of either the charge density or electric field intensity produced by the actuator. The chemistry based method typically consists of drift-diffusion type models [66]. These models track the chemical species present in the plasma, such as electrons and ions, using a set of transport equations. Using empirically found relationships, essential features such as ionization and recombination are modeled. Generally speaking, these models are capable of accurately resolving and predicting the plasma phenomena that occur with plasma actuator operation. The most sophisticated chemistry model that applies to the plasma actuator is the model proposed by Likhanskii et al. [66]. In this model, three chemical species are modeled: electrons, positive ions, and negative ions. Although the chemistry model proposed by him has the potential to resolve the plasma phenomena directly, the computational cost presents a significant limitation in its implementation.

Additionally, no investigation has been performed into the solution of this model over commonly used kHz frequencies, which would require an extremely large number of iterations to complete at the nanosecond time steps were required for numerical stability. Because of this, the chemistry based methods are not typically feasible for the design and optimization of plasma actuators and thus not particularly useful for simulations of flow control. For the above-mentioned reasons, the focus of the present study is on algebraic models [67- 69].

Based on above introduction the main objectives of this research and the outline of this work in order to achieve those goals are as below.

1.5 Objectives

The main objectives of this thesis are as follows:

- 1) To present a feasible mathematical model for simulating the AC dielectric barrier discharge in point-to-plane configuration and a numerical technique for solving the model.**

Many researchers have investigated the dielectric barrier discharge experimentally. However, because of its very complicated physics very few investigations have been devoted to its numerical modeling. The DBD is a very complicated phenomenon for which an analytic solution is not available. Also, the governing equations for modelling the behaviour of charge carriers are not easily solvable. Therefore, presenting a technique which can deal with the nonlinear hyperbolic equations required for modelling this problem is very desirable. Meanwhile, most of the presented models use non effective numerical algorithm for the highly non uniform phenomenon or dielectric barrier discharge phenomenon is approximated by a static or one-dimensional (1D) models. Therefore, presenting a model which can accurately predict the physical behaviour of the dielectric barrier discharge has still been missing. A single-species model used in this study can be useful for some engineering applications, where a simplified model suffices. In this thesis, a dynamic, single species, 2D model for predicting the characteristics of the DBD is presented.

2) To investigate the effect of different parameters of the model on characteristics of the dielectric barrier discharge.

Some of the parameters used in modelling DBD differ widely in the literature and various values are used in different papers. Since knowing the effect of these parameters on the discharge characteristics is important, the effect of parameters such as voltage level, frequency, mobility, and dielectric constant are investigated in this thesis and the observations are reported.

3) To investigate the fundamental characteristics of a non-parallel plate EHD pump, using a coupled-physics EHD numerical model taking into account charge generation, charge transport, electric field and fluid dynamics.

Although the basic principles of EHD pump operation have been long understood, there are relatively few examples of successful designs of practical devices. The works up to now have been based either on the experimental investigations of the prototypes or simplified numerical techniques. However, several problems, such as the prediction of the velocity vs. pressure characteristics have not been investigated. The major goal explored in this thesis is the optimization of electrostatic air pumps.

4) To identify a model for the corona discharge plasma actuator that is capable of predicting an accurate flow response for given a set of the actuator parameters and operating conditions.

Due to the large number of variables involved in the design of the plasma actuator (electrode width, applied voltage, driving frequency, etc), there is a considerable level of complexity that is involved. An accurate model that is capable of predicting the output of the actuator under variations in geometry, voltage and frequency can alleviate the current trial-and-error design approach that is typically implemented. Furthermore, optimizing the performance of the plasma actuator is most easily achieved when the underlying physics is understood through an accurate model. The work presented in this study provides a systematic study of a plasma actuator. Consequently, variations of voltage and specific geometrical parameters are investigated in terms of their effect on the maximum velocity output by the plasma actuator.

5) To propose a numerical model for the dielectric barrier discharge plasma actuator that is capable to actively control the air flow boundary layer.

Dielectric barrier discharge actuators have shown much promise for active flow control. Proper design and optimization of plasma actuators require a model capable of accurately predicting the induced flow for a range of geometrical and excitation parameters. A number of models have been proposed in the literature, but have primarily been developed on geometric and physical characteristics, dependent to specific application or experimental results. As one of the main goals of this thesis, the quasi-stationary velocity fluctuation is modeled and the solution to minimize this fluctuation was studied.

1.6 Thesis Outline

This thesis is divided into seven chapters. A summary of each chapter is as follows.

Chapter 1: This chapter focuses on explaining the mechanism of corona discharge and dielectric barrier discharge in producing the secondary electrohydrodynamic flow. It also reviews the history of the corona discharge and dielectric barrier discharge, as well as the literature on the electrostatic air movers and plasma actuators, describes the objectives of the thesis and outlines the chapters.

Chapter 2: This chapter's focus is on the numerical techniques proposed for modelling corona discharge and dielectric barrier discharge. First, a comprehensive review on the numerical techniques used for solving different equations governing corona and DBD is presented. Secondly, the numerical techniques selected in this thesis are explained in detail. FEM is used for the electric field, charge transport, and fluid flow computations. In this chapter, the complete set of equations for modelling the DBD is presented and the solution methodology is explained. Moreover, some basic physical characteristics of the discharge such as the displacement current and efficiency of the electrokinetic energy conversion have been formulated.

Chapter 3: In this chapter, a numerical algorithm for the dynamic simulation of DBD in air, assuming single species charge carriers is proposed. The simulation results show the

behaviour of corona current and space charge density under different voltage/ frequency combinations.

Chapter 4: In this chapter, an EHD pump is numerically simulated. The mechanism of its operation is explained in detail. Optimized geometry is advised by assuming the maximum flow rate as an objective function. The general voltage vs. pressure characteristics of a pump was presented.

Chapter 5: In this chapter, DC corona plasma actuator over a flat plate is numerically modeled. This model is fully coupled and capable of solving all the phenomena in one solver using the Finite Element Method. Effects of different parameters of the model on plasma actuator characteristics are studied. The parameters of interest are: voltage magnitude, angle of attack and free stream velocity level. A general formula for calculating the total force acting on the air is presented.

Chapter 6: In this chapter, the numerical results for the DBD plasma actuator are presented. Velocity fluctuation is numerically captured as one of the main features of the velocity profile. Effect of different parameters such, as corona wire thickness, grounded electrode width, voltage and frequency on system performance has been discussed.

Chapter 7: This chapter summarizes the results presented in the thesis. Some suggestions for future studies on this subject are also proposed.

References

- [1] K. Adamiak, P. Atten, "Simulation of corona discharge in point-plane configuration", J. Electrost., Vol. 61:2, pp.85-98, 2004
- [2] J. Townsend, "Electricity in gases", Oxford University Press, 1915
- [3] L. Loeb, "Electrical coronas, their basic physical mechanisms", University of California Press, 1965
- [4] F. W. Peek, "Dielectric phenomena in high voltage engineering", New York: McGraw Hill, 2006.
- [5] N. Kaptzov, "Elektricheskiye yavleniya v gazakh i vacuume", OGIZ, Moscow, 1947
R. S. Sigmund, "Electrical breakdown of gases", New York: Wiley, 1978

- [6] M. Goldman, R. S. Sigmond, "Corona and insulation", IEEE Trans. Elect. Ins., Vol. 17:2, pp.90-105, 1982
- [7] N.E. Jewell-Larsen, P.Q. Zhang, C.P. Hsu, I.A. Krichtafovitch, A.V. Mamishev, "Coupled-physics modeling of electrostatic fluid accelerators for forced convection cooling", 9th AIAA/ASME Therm. Phys. Heat Trans. Conf., San Francisco, USA, 2006
- [8] A.E. Bergles, "Heat transfer in electronic and microelectronic equipment", Troy, New York, Hemisphere Publishing Corporation, 1990
- [9] G. C. Noll, "Ozone production by corona discharges", J. Inst. Environ. Sci. Tech. Vol. 45:1, pp.98-106, 2002
- [10] J.S. Chang, P.A. Lawless, O. Yamamoto, "Corona discharge process", IEEE Trans. Plasma Sci., Vol. 19:6, pp.1152-66, 1991
- [11] C. Junhong, J.H. Davidson, "Model of the negative DC corona plasma: comparison to the positive DC corona plasma", Plasma Chem. Plasma Proc., Vol. 23:1, pp.83-102, 2003
- [12] A. Soldati, S. Banerjee, "Turbulence modification by large-scale organized electrohydrodynamic flows", Phys. Fluids, Vol. 10:7, pp.1742- 56, 1998.
- [13] S. El-Khabiry, G. Colver, "Drag reduction by DC corona discharge along an electrically conductive flat plate for small Reynolds number flows", Phys. Fluids, Vol. 9:3, pp.587-99, 1997.
- [14] B. Khaddour, P. Atten, J.L. Coulomb, "Numerical solution and experimental test for corona discharge between blade and plate", IEEE Trans. Mag., Vol. 43:4, pp.1193-6, 2007
- [15] L.M. Dumitran, L. Dascalescu, P.V. Notingher, P. Atten, "Modeling of corona discharge in cylinder-wire-plate electrode configuration", J. Electrostat., Vol. 65:12, pp.758-63, 2007
- [16] R. Morrow, "Theory of positive corona in SF₆ due to a voltage impulse", IEEE Trans. Plasma Sci., Vol. 19:2, pp.86-94, 1991
- [17] R. Morrow, "The theory of positive glow corona", J. Phys. D: Appl. Phys., Vol. 30:22, pp.3099-114, 1997.

- [18] U. Kogelschatz, "Dielectric-barrier discharges: Their history, discharge physics, and industrial applications", *Plasma Chem. Plasma Proc.*, Vol. 23:1, pp.1-46, 2003
- [19] W. Siemens, "Ueber die elektrostatische Induction und die Verzögerung des Stroms in Flaschendräten", *Ann. Phys. Chem.*, Vol.102, pp.66–120 1857
- [20] P. Hautefeuille, J. Chappuis, "Recherches sur l'ozone", *Compt. Rend. Acad. Sci.* 1881.
- [21] M. Suzuki, "On the nature of chemical reaction in silent discharge", *Proc. Japan Acad.*, Vol.26:9, pp.20-4, 1950
- [22] M. Suzuki, Y. Naito, "On the nature of chemical reaction in silent discharge II", *Proc. Japan Acad.*, Vol. 26:9, pp.469-76, 1952
- [23] T. C. Manley, "The electric characteristics of the ozonator discharge", *J. Elec. chem. Soc.*, Vol.84:1, pp.83-96, 1943
- [24] W. Breazeal, K. M. Flynn, E. G. Gwinn, "Static and dynamic two-dimensional patterns in self-extinguishing discharge avalanches", *Phys. Rev.*, Vol. 52:2, pp.1503-15, 1995
- [25] N. Cabeo, "Philosophia Magnetica", Cologne, Germany: Ferrara, 1629
- [26] T. Cavallo, "A complete treatise of electricity", London, U.K.: Edward, 1777
- [27] M. Faraday, "Experimental researches in electricity", Carlsbad, USA: Faraday, 1834
- [28] J. C. Maxwell, "Treatise in electricity and magnetism", Oxford, U.K.: Oxford Univ. Press, 1873
- [29] A. P. Chattock, "On the velocity and mass of the ions in the electric wind in air", *Phil. Mag.*, Vol.48:294, pp.401-20, 1899
- [30] M. Robinson, "Movement of air in the electric wind of the corona discharges", *AIEE Trans.*, pp.143-50, 1961
- [31] O. M. Stuetzer, "Ion drag pumps", *J. Appl. Phys.*, Vol. 31:1, pp.136–46, 1960
- [32] C. Kim, D. Park, K. C. Noh, J. Hwang, "Velocity and energy conversion efficiency characteristics of ionic wind generator in a multistage configuration", *J. Electrostat.*, Vol. 68:1, pp.36–41, 2010
- [33] H. Bondar, F. Bastien, "Effect of neutral fluid velocity on direct conversion from electrical to fluid kinetic energy in an electro-fluid dynamics (EFD) device," *J. Phys. D: Appl. Phys.*, Vol. 19:9, pp.1657–63, 1986
- [34] J.D. Moon, D.H. Hwang, S.T. Geum, "An EHD gas pump utilizing a ring/needle electrode", *IEEE Trans. Dielectr. Elec. Ins.*, Vol. 16:2, pp.352–58, 2009

- [35] K. Asano, K. Yatsuzuka, "Fundamental study of EHD pump with needle-cylinder electrodes", Conf. Elect. Ins. Dielectr. Phenomena, Vol.2, pp.785-88, Austin, USA, 1999
- [36] M. Rickard, D. Dunn-Rankin, F. Weinberg, F. Carleton, "Characterization of ionic wind velocity," J. Electrostat., Vol. 63:6, pp.711–16, 2005
- [37] M. Rickard, D. Dunn-Rankin, F. Weinberg, F. Carleton, "Maximizing ion-driven gas flows", J. Electrostat., Vol. 64:6, pp.368–76, 2006
- [38] H. Tsubone, J. Ueno, B. Komeili, S. Minami, G.D. Harvel, K. Urashima, C.Y. Ching, J.S. Chang, "Flow characteristics of DC wire-non-parallel plate electrohydrodynamic gas pumps", J. Electrostat., Vol. 66:1, pp.115–21, 2008
- [39] E. Moreau, "Airflow control by non-thermal plasma actuators", J. Phys. D: Appl. Phys., Vol.40, pp.605–36, 2007
- [40] J. D'Adamo, G. Artana, E. Moreau, G. Touchard, "Control of the airflow close to a flat plate with electrohydrodynamic actuators", Proc. ASME U.S.-Euro. Fluids Eng. Div. Conf., Vol.1, pp. 1339-44, Montreal, Canada, 2002
- [41] H. Velkoff, J. Ketchman, "Effect of an electrostatic field on boundary layer transition", J. AIAA, Vol.16, pp.1381–3, 1968
- [42] A. Soldati, S. Banerjee, "Turbulence modification by large scale organized electrohydrodynamic flows", Phys. Fluids, Vol.10, pp.1742–56, 1998
- [43] S. El-Khabiry, G.M. Colver, "Drag reduction by a DC corona discharge along an electrically conductive flat plate for small Reynolds number flow", Phys. Fluids, Vol.9, pp.587–99, 1997
- [44] M.R. Malik, L. Weinstein, M. Hussaini, "Ion wind drag reduction", 21st AIAA Conf. Aero. Sci. Meeting, Pap. No. 83-0231, Reno, USA, 1983
- [45] F. Soetomo, "The influence of high voltage discharge on flat plate drag at low Reynolds number air flow", MS Thesis Iowa State University, 1992.
- [46] C. Noger, G. Touchard, J.S. Chang, "Active controls of electrohydrodynamically induced secondary flow in corona discharge reactor", Proc. 2nd Int. Sym. Plasma Tech. Pollution Control, pp. 136-141, Bahia, Brazil, 1997

- [47] L. Leger, E. Moreau, G. Artana, G. Touchard, "Modification de l'écoulement d'air autour d'une plaque plane par une décharge couronne", Proc. Colloque de la Société Française d'Electrostatique, France, 2000
- [48] G. Artana, J. D'Adamo, G. Desimone, G. Diprimio, "Air flow control with electrohydrodynamic actuators", 2nd Int. Workshop on Conduction Convection and Breakdown in Fluid, pp.190-3, Grenoble, France, 2000
- [49] G. Artana, G. Desimone, G. Touchard, "Study of the changes in the flow around a cylinder caused by electroconvection", Proc. IOP Conf. Electrostat., pp. 147-51, Cambridge, UK, 1999
- [50] L. Leger, E. Moreau, G. Artana, G. Touchard, "Influence of a DC corona discharge on the airflow along an inclined flat plate", J. Electrostat. Vol. 50-51, pp.300-6, 2001
- [51] L. Leger, E. Moreau, G. Touchard, "Control of low velocity airflow along a flat plate with a DC electrical discharge", 36th IEEE Ind. App. Conf., Vol.3, pp.1536-43, Chicago, USA, 2001.
- [52] G. Artana, G. DiPrimio, G. Desimone, E. Moreau, G. Touchard, "Electrohydrodynamic actuators on a subsonic airflow around a circular cylinder", 32nd AIAA Conf. Plas. Dynamics & Lasers, Pap. No. 2001-3056, Anaheim, USA, 2001
- [53] G. Artana, J. D'Adamo, L. Leger, E. Moreau, G. Touchard, "Flow control with electrohydrodynamic actuators", 39th AIAA Conf. Aero. Sci. & Exhibit, Pap. No. 2001-0351, Reno, USA, 2001
- [54] L. Leger, E. Moreau and G. Touchard, "Electrohydrodynamic airflow control along a flat plate by a DC surface corona discharge - velocity profile and wall pressure measurements", 1st AIAA Flow Control Conf., Pap. No. 2002-2833, , St. Louis, USA, 2002
- [55] E. Moreau, L. Leger, G. Touchard, "Three-phase traveling wave surface discharge along an insulating flat plate in air: application to electrohydrodynamically airflow control", IEEE Conf. Elec. Ins. & Dielectr. Phenom., pp.272-8, Mexico, 2002
- [56] C. Louste, E. Moreau, G. Touchard, "DC corona surface discharge along an insulating flat plate in air: experimental results", IEEE Conf. Elec. Ins. & Dielectr. Phenom., pp.822-6, Mexico, 2002

- [57] L. Leger, E. Moreau, G. Touchard, "Effect of a DC corona electrical discharge on the airflow along a flat plate", *IEEE Trans. Ind. App.*, Vol.38:6, pp.1478–85 2002
- [58] G. Artana, J. D'Adamo, L. Leger, E. Moreau, G. Touchard, "Flow control with electrohydrodynamic actuators", *J. AIAA*, Vol. 40:9, pp.1773–9, 2002
- [59] M.L. Post, "Plasma actuators for separation control on stationary and unstationary airfoils", PhD thesis, Univ. of Notre Dame, 2004
- [60] C.L. Enloe, T.E. McLaughlin, R.D. VanDyken, K.D. Kachner, E.J. Jumper, T. Corke, M. Post, O. Haddad, "Mechanisms and responses of a single dielectric barrier plasma actuator: Geometric effects", *J. AIAA*, Vol. 42:3, pp.595-604, 2004
- [61] A.R. Hoskinson, N. Hershkowitz, D.E. Ashpis, "Force measurements of single and double barrier DBD plasma actuators in quiescent air", *J. Appl. Phys.*, Vol.41, pp.1-9, 2008
- [62] D.M. Orlov, "Modeling and simulation of single dielectric barrier discharge plasma actuators", PhD thesis, Univ. of Notre Dame, October 2006
- [63] M. Forte, J. Jolibois, J. Pons, E. Moreau, G. Touchard, M. Cazalens, "Optimization of a dielectric barrier discharge actuator by stationary and non-stationary measurements of the induced flow velocity: application to airflow control", *Exp. Fluids*, Vol. 43:6, pp.917–28, 2007
- [64] F. Thomas, T. Corke, M. Iqbal, A. Kozlov, D. Schatzman, "Optimization of dielectric barrier discharge plasma actuators for active aerodynamic flow control", *J. AIAA*, Vol.47:9, pp.2169-78, 2009.
- [65] A. Likhanskii, M. Shneider, S. Macheret, R. Miles, "Modeling of dielectric barrier discharge plasma actuators driven by repetitive nanosecond pulses", *Phys. Plas.*, Vol.14, pp.073501, 2007
- [66] W. Shyy, B. Jayaraman, A. Andersson, "Modeling of glow discharge-induced fluid dynamics", *J. Appl. Phys.*, Vol.92:11, pp.6434- 43, 2002
- [67] K. Singh, S. Ro, "Modeling plasma actuators with air chemistry for effective flow control", *J. Appl. Phys.*, Vol.101, pp.123308, 2007
- [68] Y.B. Suzen, P.G. Huang, J.D. Jacob, "Numerical simulations of plasma based flow control applications", 35th AIAA Fluid Dynamics Conf. & Exhibit, Pap. No. 2005-4633, Toronto Canada, 2005

Chapter 2

2 Mathematical Models and Numerical Algorithms in EHD

Despite the widespread applications of Corona Discharge (CD) and Dielectric Barrier Discharge (DBD), many published works just reported the experimental data and there is still a huge challenge for a reliable and accurate model, which can be used in the computer simulation of these phenomena. Different types of numerical techniques have been used by different researchers who have attempted to model CD and DBD. Those numerical techniques vary with respect to their applications, the memory requirements, computation speed and accuracy. However, there is still no generally stable algorithm regardless of the configuration or application for modeling of corona discharge. In this chapter, based on the fundamental physics described already, different theoretical and numerical techniques are reviewed for modeling CD and DBD problems. Then, a detailed numerical approach and simulation procedure, including all the essential physics and valid for arbitrary geometry, are presented to predict the characteristics of discharges.

2.1 Mathematical Models and Numerical Algorithms in Electric Corona Simulation

During the last several decades, many efforts have been made to have a better understanding of the electric corona discharge and many theoretical, experimental and numerical results have been published. Due to the complexity of the equations governing corona discharge, finding analytical solutions for these equations is not possible unless some major simplifications are made or the problem geometry is highly symmetric. Therefore, numerical simulation is principally the only feasible approach for the corona discharge modeling. The use of numerical tools for studying this phenomenon has recently reached an advanced degree of development.

Studies on numerical modeling of corona discharges are generally divided into two main categories, those that simulate the whole process including the ionization zone and those that simulate just the drift region. All essential processes, such as ionization, attachment and recombination, occur in the ionization zone, a thin layer close to the corona electrode, where many different ionic species are generated. Therefore, by studying the reaction

chemistry within the ionization zone, predicting the concentrations of various ionic species is possible. A full numerical model of the corona discharge in the time domain, including all processes in the ionization layer, has been attempted by few authors [1, 2]. A few other studies have concentrated on the reaction chemistry within the ionization zone [3, 4]. Morrow [5] has solved the continuity equations for electrons, negative ions, positive ions coupled with Poisson's equation in a spherically symmetrical coordinate system for concentric-sphere electrodes. Chen and Davidson [6-8] have conducted a series of simulations modeling the ionization zone. Their studies comprised of two elements. The governing equations were the drift equations for the ions and the drift-diffusion equation for the electrons. Diffusion was found to be insignificant in the case of ions and neglected. This model was one dimensional in a cylindrical geometry and hence all concentrations varied only in the radial direction. Yanallah et al. [9, 10] also conducted simulations of the ionization zone using a similar procedure.

Although such works can be interesting for detailed study of physical processes, in the practical applications they are not useful. Due to its complexity, such an algorithm generally leads to very time consuming computations caused by a very fine spatial discretization, very irregular dynamics and rapid time variation of some parameters. While the whole process is rather complicated, the net effect is that ions, of the same polarity as that of the corona electrode, are drifting to the other electrode [11]. Almost all the authors interested in engineering applications of the corona discharge completely ignore the processes in the ionization layer, which is justified by its small thickness, generally in the same order of magnitude as the radius of curvature of corona electrode [12].

Many versions of the basic mono-polar corona model exist and they use various numerical techniques [13-15]. The fundamental procedure for simulation of a corona discharge is similar in all of these studies. The only difference is in the numerical techniques used to solve the equations. Most often the numerical algorithm is based on back-and-forth iterations for solving electric field and space charge density until convergence is reached.

In the early stage of corona research the electric potential was calculated from the Finite Difference (FDM) approximation [16]. In this technique, the derivatives in the partial differential equations are replaced with finite differences. The whole region is discretized and a mesh is formed. The finite difference approximation is then applied to every node of a mesh. As a result, the differential equations are transformed to linear algebraic equations. The simplicity of this technique is one of the advantages of FDM. However, since this technique needs a rectangular mesh, it is difficult to apply FDM to problems with irregular computational domains. For problems with complicated geometry, FDM must use a large mesh which leads to time consuming calculations. Another disadvantage of this technique is that it cannot handle the sharp geometry of the discharge electrode very well [17, 18], therefore, using this technique for modeling corona discharge is not recommended.

FEM was the next proposed technique, and it eventually became a dominant one, for solving Laplace and Poisson equations [19-23]. FEM is based on minimizing the energy of the system instead of direct solution of the equations. Therefore, it can determine the energy related parameters with a much better accuracy. In order to use FEM, the whole domain should be discretized into a set of triangular, quadrilateral or other type of elements depending on the problem configuration. A simple matrix equation for each element is then obtained, and by assembling these matrix equations, a global set of algebraic equations can be formulated. After introducing the boundary conditions, this global set of equations is solved to obtain the values of the unknown functions at each node. The advantage of FEM over FDM is its ability in solving problems with complicated geometries. It can use unstructured grids, which is much more flexible than a structured grids required for FDM, as it results in a smaller mesh and makes the calculations less time consuming. By increasing the number of elements, or the order of interpolating polynomials in each element, accuracy of the technique can be easily improved.

Some other authors proposed the Boundary Element Method (BEM) [24] to obtain the Laplacian components of electric field intensity. In BEM only the boundaries need to be discretized with boundary conditions at infinity naturally satisfied, which reduces the number of nodes and, consequently, the size of the algebraic system to be solved. The boundary techniques are better suited to strong field gradients, but the main disadvantage

of BEM is that it is time consuming for problems with space charge and it is impossible to use it for non-linear problems.

Finite Volume Method (FVM) is another technique proposed for corona discharge problems. This technique also converts partial differential equations into algebraic equations. Similarly to the FDM, values of unknown solution are calculated at discrete nodes of a mesh. In the FVM, the volume integrals in a partial differential equation containing divergence terms are converted to surface integrals using the divergence theorem. These terms are then evaluated as fluxes at the surfaces of each finite volume. Because the flux entering a given volume is identical to that leaving the adjacent volume, these methods are conservative. Another advantage of the FVM is that it can be easily formulated for both structured and unstructured meshes. This method is used in many computational fluid dynamics packages.

Each of these techniques has its own advantages and disadvantages and in few cases authors have combined different methods in one algorithm. As an example, a combination of BEM-FEM was used by Adamiak and Atten [11].

The space charge density distribution in corona discharge can be determined from the charge continuity equation. The space charge density also depends on the electric field and the electric field depends on the space charge. In order to obtain the Poissonian component of the electric field with considering charge transport different approaches were presented by many researchers. All of the numerical algorithms that have been proposed for the simulation of corona discharge can be classified into two groups: simple or hybrid ones. In simple algorithms, the same technique is used for the calculation of electric field and space charge density while the hybrid techniques use simultaneously two or more numerical methods.

Adamiak [24] used a combined algorithm using BEM for obtaining the electric potential and Method of Characteristics (MoC) technique to determine the charge density distribution in the wire-duct configuration. The proposed technique was reliable but time consuming. Later, Zhao and Adamiak [25] presented a hybrid technique based on the FEM and MoC for the simulation of electric corona discharge. Although this approach proved

to have considerable efficiency and speed, interfacing both numerical techniques was rather difficult. Davidson et al. [26] used the same hybrid numerical model to predict electric field and space charge density in 3D point-to-plane and barbed plate-to-plane configurations. Although their results had a good accuracy, the model was very complicated. Adamiak and Atten [11] simulated the electrical conditions in point-to-plane configuration using a combined BEM-FEM-MoC algorithm, which produced a much smoother distribution of the electric field. This technique was based on BEM and FEM techniques for obtaining the harmonic and space charge components of the electric field, respectively, and on MoC to determine the charge density distribution. Atten *et al.* [27] combined FEM, FVM and MoC for the simulation of electric corona discharge. They used FEM for the electric field calculation and the combination of FVM and MoC for the space charge density calculations.

The above techniques were applied for modeling a steady-state single-species corona discharge. Few attempts have been made for modeling transient corona discharge. Zhang and Adamiak [28] proposed a dynamic model for the negative corona discharge in the point-plane geometry. They used a hybrid BEM-FEM technique to calculate the electric field parameters and MoC for the charge-transport prediction. This model was valid for single-species discharge only but successfully simulated the full current waveform under different waveforms of the applied voltage: step, square and pulse. Combination of FEM with Flux Corrected Transport (FCT) technique is another useful technique for solving charge continuity equations. This technique has been proposed by Morrow [29], who successfully applied it to solve the charge continuity equation. Sattari et al. [30] applied FEM to calculate electric field distribution and the hybrid FEM-FCT technique for the space charge density calculations.

2.2 Literature Review on Mathematical Models for the Dielectric Barrier discharge

In order to have a better insight into DBD phenomena, a study of the different models of DBD systems and their basic characteristics is necessary. Barrier discharges can be operated in various modes such as diffuse, patterned, and filamentary. Also under certain circumstances apparently homogeneous diffuse discharges [31], and regularly spaced glow

discharge patterns [32-34] can be observed. A good review of the various modes and terms has been presented by Kogelschatz [35]. There have been numerous models developed for DBDs in air that include complicated chemistry. These models usually include 20–30 reaction equations, each with different reaction times and energy outputs. These equations account for electron, ion-neutral and neutral-neutral reactions in different gases that are present in the air [36, 37]. Font [38] considered the plasma discharge in a 2D asymmetric plasma actuator that included only nitrogen and oxygen reactions. With this model, they were able to simulate the propagation of a single streamer from the bare electrode to the dielectric surface and back. Likhanskii et al. [39] modeled the weakly ionized-air plasma as a four-component mixture of neutral molecules, electrons, and positive and negative ions that included ionization and recombination processes. Massines et al. [40] developed a 1D model for the DBD dynamics based on the numerical solution of the electron and ion continuity, and momentum transfer equations coupled to Poisson's equation. Their model predicted the space and time variations in the electric field, and the electron and ion densities. The authors accounted for the charge accumulation on the dielectric as the discharge develops and derived the voltage boundary conditions for dielectrics by considering an equivalent circuit of the gas gap in series with the equivalent capacitor of the dielectric. Later, Massines et al. [41] presented a two dimensional analysis for a parallel electrode configuration. This study provided a helpful insight for understanding the DBD behavior. Paulus et al. [42] developed a 2D model to study the time-dependent evolution of the potential and the electric field surrounding dielectric materials by applying a pulse voltage. The simulation showed that the charged particles move toward the regions of high electric potential, creating high electric field strength near the electrode's edges. One of the latest investigations on modeling of DBD was performed by Shang et al. [43, 44], which was based on FDM. The DBD was studied by drift diffusion plasma model including Poisson equation. The simulation replicates the self-limiting feature of the DBD for preventing transition of the corona to spark and the numerical results somehow match with experimental data.

Generally speaking, such detailed models can precisely describe all different processes involved in DBD. However, they are computationally time-consuming and require significant computer resources. Such simulations are not suitable to be a part of a design

tool that would be used in the iterative optimization. Although quite a few articles have been published on using DBD in numerous industrial applications [45- 48], but so far no reliable and accurate model has been presented in order to interpret the physics of this phenomenon in these different applications. Moreover, in many cases optimization techniques are required in order to achieve a better system performance.

2.3 Literature Review on the Numerical Techniques on EHD Simulation

Although utilizing the FEM to model electrostatic problems dates back to 1960s, the modeling of high voltage discharges and EHD flows has witness an explosive growth since 2007, due to advances in computing equipment. Modern computers have reach required capabilities and are able to handle very fine spatial discretization, especially when electrodes with curvatures of very small radii are involved.

The fluid motion generated by corona discharge has been employed by many investigators in chemical processing and thermal management of electronic equipment and circuitry [49- 51]. Few authors focused their studies on the theoretical and numerical investigation of the EHD flows. Examples of numerical models for EHD based system are found in the literature with majority of them appearing in the last several years [52-56].

Studies of basic geometries, such as wire-to-wire [51], cylinder-to-wire-to-plane [52], wire-to-cylinder [53] and needle-to-plane [54], were published during the past few decades. One of the first models was developed by Mathew et al. [57] for a two-wire-to-duct electrode arrangement. The study investigated the airflow enhancement in a duct due to EHD generated flows. More recent work has also been focused on EHD flows in channels [58-60]. A mathematical model for the needle-to-plate EHD air pump has been developed, verified by a parallel experimental study using a needle-to-mesh EHD air pump [61]. Yabe et al. [62] investigated the EHD flow produced by the corona discharge in a 2D electrode arrangement of a wire-plate system. The results of numerical simulations of the Navier–Stokes equations were presented. However, a more detailed analysis of the EHD flow was presented by Yamamoto and Velkoff [52]. Their simulation results revealed the interaction between EHD flow and main flow. Later, Zhao and Adamiak [25] carried out a

fundamental study of the EHD flow in the point-plane geometry, focusing on a more rigorous model of the corona discharge. A hybrid algorithm was proposed, which included the 2D Finite Element Method (FEM) for the electric potential distribution and the Method of Characteristics (MoC) for the charge transport, assuming a single species discharge model and laminar flow. A similar approach was used to simulate the air flow pattern in the wire-plate electrostatic precipitator, without [63] and with the effect [64] of the particle charge. A 2D model has been presented by Feng [65], who investigated the EHD flow associated with corona discharge in a rectangular shield. It was shown that the magnitude of the flow increases with the size of the collecting electrodes. Chang et al. [66] have investigated the mechanism of EHD gas pump in a wire non-parallel plate electrode. A 1D model was presented and compared with the experiments for different location of corona wire and for both positive and negative applied voltage at atmospheric pressure and room temperature, where air was used as the working fluid. The results show that the net flow in such configuration significantly depends on the location of the corona wire, relative to the grounded electrode. Based on this model, a few experiments were carried out in order to visualize the flow patterns, as well as to measure the velocities of the EHD flows using PIV technique [67, 68].

In the past decade there has been increasing interest in application of DBD for flow control. This seems to be the result of the special characteristics of this technique, such as no moving parts with fully electronic control, a fast time response for unsteady applications, a very low mass, the efficient conversion of the input power without parasitic losses, and the ability to be mounted on a surface without the addition of cavities and holes [69]. A model for the body force produced by the plasma on the neutral air was presented by Roth et al. [70]. This model was based on a derivation of the forces in gaseous dielectrics. It was found that the body force is proportional to the gradient of the squared electric field.

One of the first suggested models of plasma actuators proposed by Shyy et al. [71], where the maximum generated electric field was assumed to be equivalent to that in a parallel plate capacitor with an equivalent potential difference across the exposed and encapsulated electrodes. A further assumption was imposed suggesting that the electric

field decays linearly in the horizontal and vertical directions from its prescribed maximum value located at the trailing edge of the exposed electrode. The electric field intensity diminished at the trailing edge of the encapsulated electrode and at a prescribed plasma height creating a triangular region of plasma generation. There are several disadvantages of this model that restrict its generality for all actuator geometries. First, there is no accurate solution for the spatial charge density and it was assumed at a constant value. The space charge density is an important factor, which affects the volume force intensity and is highly dependent on the applied electric field. Therefore, neglecting its spatial variance can have a dramatic effect on the overall force distribution and accuracy of the model. The inclusion of this parameter is critical since it plays a significant role in the performance of plasma actuators as it governs the electric field strength, thereby affecting the ignition of the plasma. Despite these shortcomings, the model provides an attractive method for calculating the Lorentz force at very small computational cost. Singh [72] used the results of the body forces obtained from a first-principle simulation along with empirical observations of actuator behavior to develop an approximation for the 2D body-force components. This approach makes the calculation of the body force a curve-fitting problem that is only valid for a single-actuator configuration. Similar to Shyy et al.'s model, it does not include temporal characteristics of the body force and the net body force does not scale properly with voltage. A more complicated model was proposed by Suzen et al. [73], which involved fewer parameters while at the same time capturing more features of the plasma physics. The model is focused on applying Gauss's law and solving the electric potential from Laplace's equation. These authors assumed that the charge density on the dielectric surface follows a half-Gaussian distribution with the maximum value matched from the experiment. Since this value was defined for the specific actuator geometry and is thus constant, the parameter is not able to account for geometrical changes or voltage and frequency variation.

As can be seen, finding an exact solution for the electrostatic fluid interaction regardless of the application, geometry and applied voltage (AC or DC), is challenging. The aim of this study is to develop a theoretical, mathematical and numerical model to include all those effects.

2.4 Mathematical Model and Governing Equations

2.4.1 Electrostatic Field and Charge Transport

This study is based on solving the space charge transport by neglecting the ionization layer and considering unipolar ions in the domain drifting toward ground plate with constant mobility (μ_e). In the absence of magnetic fields, the equations defining the electric field are [30]:

$$\nabla \cdot \vec{D} = \rho_c \quad (2-1)$$

$$\nabla \cdot \vec{J} = -\frac{\partial \rho_c}{\partial t} \quad (2-2)$$

$$\vec{D} = \varepsilon \vec{E} \quad (2-3)$$

$$\vec{E} = -\nabla V \quad (2-4)$$

where \vec{D} is the electrostatic displacement vector, ρ_c is the space charge density, \vec{J} is the electric current density, ε is the gas permittivity, \vec{E} is the electric field and V is the electric potential.

The electric potential is thus governed by Poisson's equation:

$$\nabla^2 V = -\frac{\rho_c}{\varepsilon} \quad (2-5)$$

The ionic charges are accelerated by the Coulomb force and move towards the ground electrode. The charge drift creates an electric current with a density defined as:

$$\vec{J} = \rho_c(\mu_e \vec{E} + \vec{u}) - D \nabla \rho_c \quad (2-6)$$

where \vec{J} is the current density, μ_e the mobility of ions, D the ions diffusion coefficient and \vec{u} the gas velocity, which may include both the EHD flow and the externally produced airflow. The three terms on the right hand side of Eq. (2-6) are drift, convection and diffusion currents, respectively. D is the diffusion coefficient and is equal to [30]:

$$D = \frac{k_B T \cdot \mu_e}{e_0} \quad (2-7)$$

where k_B is the Boltzmann constant, which is equal to $1.38065 \times 10^{-23} (\text{m}^2 \text{k}_g / \text{s}^2 \text{K})$, T is the absolute temperature, e_0 is the electron charge, equal to $1.602 \times 10^{-19} (\text{C})$.

Generally, since the drift velocity of ions in Eq. (2- 6) is usually about two orders of magnitude larger than the typical velocity of the gas flow [74], the convective component in the ionic current density can be neglected. As a result the electric field and space charge density will be independent of the fluid motion. However, in this study in some applications we are interested to see the effect of the flow velocity rate on the current level. Therefore, a fully coupled model has been implemented. Eq. (2-6) can be substituted into Eq. (2-2) to derive the continuity equation,

$$\frac{\partial \rho_c}{\partial t} + \nabla \cdot (\rho_c (\mu_e \vec{E} + \vec{u})) - D \nabla^2 \rho_c = 0 \quad (2-8)$$

This is the most generic form of the continuity equation. Obviously, when we are not interested in gas velocity, the convective part would be eliminated, and when we are studying the steady state condition the derivative of the charge density over time could be eliminated.

The simulation of the corona discharge phenomenon requires the simultaneous solution of Poisson's equation to account for the field modification due to space charge and the continuity equations to account for the migration of the space charge. Therefore, the corona discharge is governed by a set of two partial differential equations with two unknown distributions: Eq. (2-5) with the unknown potential V and Eq. (2-8) with the unknown space charge density ρ .

2.4.2 Fluid Flow

Under the assumption that the ambient air is incompressible Newtonian fluid, which is valid for the small pressure drop in the system, it has constant density and viscosity and the flow is steady and turbulent, the airflow has to satisfy the continuity and the Navier–Stokes equation. The Navier–Stokes equations result from the Newton's second law of motion (momentum equation), which states that the rate of change of momentum equals the sum of forces on the fluid particle [75].

$$\frac{\partial(\rho \vec{u})}{\partial t} + \nabla \cdot (\rho u \vec{u}) = -\frac{\partial P}{\partial x} + \nabla \cdot (\mu \nabla \vec{u}) + S_x \quad (2-9)$$

$$\frac{\partial(\rho \vec{u})}{\partial t} + \nabla \cdot (\rho u \vec{u}) = -\frac{\partial P}{\partial y} + \nabla \cdot (\mu \nabla \vec{u}) + S_y \quad (2-10)$$

Taking into account the assumption of an incompressible flow of a Newtonian fluid with constant density and viscosity, the Navier–Stokes equations can be simplified to a form:

$$\rho \left(\frac{\partial \vec{u}}{\partial t} + \vec{u} \cdot \nabla \vec{u} \right) = -\nabla P + \mu \nabla^2 \vec{u} + \vec{F} \quad (2-11)$$

where S_x , S_y are the source terms of the x-momentum, and y- momentum equations respectively, ρ is the gas density, P the static pressure, μ is the fluid viscosity and \vec{F} the external body force, in this case equal to the Coulomb force, which is responsible for the corona generated EHD flow.

If temperature effects are neglected, the only other equation (apart from initial boundary conditions) needed is the mass conservation or continuity equation, given in its most general form as:

$$\frac{\partial \rho}{\partial t} + \nabla \cdot (\rho \vec{u}) = 0 \quad (2-12)$$

Under the incompressible flow assumption, density is constant and the equation will simplify to:

$$\nabla \cdot \vec{u} = 0 \quad (2-13)$$

2.4.2.1 Turbulent model

Turbulence is a property of the flow field and it is mainly characterized by a wide range of flow scales which depend on the geometry: from the largest, to the smallest quickly fluctuating scales, and all the scales in between. The tendency for an isothermal flow to become turbulent is measured by the Reynolds number [76]:

$$R_e = \frac{\rho \vec{u} L}{\mu} \quad (2-14)$$

where L is length scale of the flow.

Flows with high Reynolds numbers tend to become turbulent and this is the case for most engineering applications. The modeling procedure involves computing the flow Reynolds number (R_e) to determine if turbulence modeling is necessary. If the Reynolds

number based on the characteristic length of the channel and the existing external gas flow is above a critical value then the fluid flow is considered as turbulent. The Navier-Stokes equations can be used for turbulent flow simulations, although this would require a large number of elements to capture the wide range of scales in the flow. So, the exact time dependent solutions of the Navier-Stokes equations in complex geometries for turbulent flows, which can represent the smallest scales of the motions, are unlikely to be achievable in the near future [77]. An alternative approach is to divide the flow into large resolved scales and small unresolved scales. The small scales are then modeled using a turbulence model with the goal that the model is numerically less expensive than resolving all present scales. This averaged representation often provides sufficient information about the flow.

In Reynolds averaging, the solution variables in the instantaneous Navier- Stokes equations are decomposed into the mean and fluctuating components. For the velocity components:

$$u_i = U_i + u'_i \quad (2-15)$$

where U_i and u'_i are the mean and fluctuating velocity components, respectively. The subscript “i” represents each dimensional component of the velocity, for example, it indicates X, Y for 2D Cartesian system. Likewise for other scalar quantities:

$$\phi = \bar{\phi} + \phi' \quad (2-16)$$

where ϕ denotes a scalar, such as pressure, or energy.

Decomposition of flow fields into an averaged part and a fluctuating part is followed by insertion into the Navier-Stokes equation. Then averaging gives the Reynolds-averaged Navier-Stokes (RANS) equations:

$$\begin{aligned} \frac{\partial U_i}{\partial x_i} &= 0 \\ \frac{\partial}{\partial t}(\rho U_i) + \frac{\partial}{\partial x_i}(\rho U_i U_j) &= -\frac{\partial P}{\partial x_i} + \frac{\partial}{\partial x_j} \left[\mu \left(\frac{\partial U_i}{\partial x_j} + \frac{\partial u_j}{\partial x_i} - \frac{2}{3} \delta_{ij} \frac{\partial U_i}{\partial x_j} \right) \right] \\ &+ \frac{\partial}{\partial x_j} (-\rho \overline{u'_i u'_j}) + f_i \end{aligned} \quad (2-17)$$

A comparison with Eq. (2-11) indicates that the only difference is the appearance of a term on the left-hand side of Eq. (2-17). This term represents interaction between the fluctuating velocities and is called the Reynolds stress tensor. This means that in order to obtain the mean flow characteristics, information about the small-scale structure of the flow is needed. In this case, that information is the correlation between fluctuations in different directions.

A common method employs the Boussinesq hypothesis [77] to relate the Reynolds stresses to the mean velocity gradients:

$$-\rho \overline{u'_i u'_j} = \mu_t \left(\frac{\partial U_i}{\partial x_j} + \frac{\partial U_j}{\partial x_i} \right) - \frac{2}{3} \left(\rho k + \mu_t \frac{\partial U_i}{\partial x_i} \right) \delta_{ij} \quad (2-18)$$

2.4.2.2 Standard $k - \varepsilon$ turbulent model

In this model, two additional transport equations (for the turbulence kinetic energy, k , and turbulence dissipation rate, ε)

$$\frac{\partial}{\partial t} (\rho k) + \frac{\partial}{\partial x_i} (\rho k U_i) = \frac{\partial}{\partial x_j} \left[\left(\mu + \frac{\mu_t}{\sigma_k} \right) \frac{\partial k}{\partial x_j} \right] - \rho \overline{u'_i u'_j} \frac{\partial U_j}{\partial x_i} - \rho \varepsilon \quad (2-19)$$

$$\frac{\partial}{\partial t} (\rho \varepsilon) + \frac{\partial}{\partial x_i} (\rho \varepsilon U_i) = \frac{\partial}{\partial x_j} \left[\left(\mu + \frac{\mu_t}{\sigma_\varepsilon} \right) \frac{\partial \varepsilon}{\partial x_j} \right] - C_\varepsilon \left(\overline{u'_i u'_j} \frac{\partial U_j}{\partial x_i} \right) \quad (2-20)$$

are solved, and the eddy viscosity μ_t is computed as a function of k and ε using the following expression:

$$\mu_t = \rho C_\mu \frac{k^2}{\varepsilon} \quad (2-21)$$

In these equations $C_\varepsilon, C_\mu, \sigma_\varepsilon, \sigma_k$ are constant coefficients.

2.4.2.3 Turbulence intensity

The turbulence intensity, T_I , often referred to as turbulence level, is defined as the ratio of the root mean square of the turbulence velocity fluctuations, u' , to the mean flow velocity, U , as:

$$T_l = \frac{u'}{U} = \sqrt{\frac{2k}{3}} / U, \quad U = \sqrt{U_x^2 + U_y^2} \quad (2-22)$$

Two thirds the turbulence kinetic energy assumes isotropic turbulence and corresponds to averaging the fluctuating components $\left(u' = \sqrt{\frac{1}{3}(u_x'^2 + u_y'^2)} = \sqrt{\frac{2}{3}k}\right)$. The conservation equations and assumption presented in this section can be found in standard gas dynamics, compressible fluid flow textbooks [78].

2.4.2.4 Body force effect

The force acting on the neutral gas is due to electron-molecule and ion-molecule collisions, and this force per unit volume is equal to the momentum transferred per unit volume and per unit time from charged particles to neutral molecules. If we neglect the mean velocity of the neutral molecules with respect to the charged particles drift velocity, and by using the definition of charged particle mobility, the total force acting per unit volume f_i and f_e due to ions and electrons on the neutral molecules can be written as a function of charged particle current densities and mobilities [79]:

$$f = f_i - f_j = \frac{J_i}{\mu_{e,i}} - \frac{J_e}{\mu_{e,e}} \quad (2-23)$$

The current densities in the collisional plasma are well described by the drift-diffusion equations:

$$J_i = \rho_{c,i} \mu_{e,i} \vec{E} - D_i \nabla \rho_{c,i} \quad (2-24)$$

$$J_e = \rho_{c,e} \mu_{e,e} \vec{E} - D_e \nabla \rho_{c,e} \quad (2-25)$$

In the ionization region the force on molecules due to electrons is almost negligible, since the electron mobility is much larger than the ion mobility.

In a non-neutral region, the charged particle density gradients can be neglected with respect to the electric field terms. So, the electric force acting on the charged particles is entirely transmitted to the neutral molecules through collisions and we have

$$f \approx (\rho_{c,i} - \rho_{c,e}) \vec{E} \quad (2-26)$$

Generally the ion number density in non-neutral regions is much higher than the electron number density. This is, for example, the case in a glow discharge, in the drift region. In this case the force per unit volume acting on the gas molecules simplifies to:

$$f \approx \rho_{c,i} \vec{E} \quad (2-27)$$

The simple argument above and the numerical results show that the force exerted by the charged particles on the neutral gas in the conditions studied here are significant only in the drift region of the discharge where the ion current density is large.

2.5 Boundary Conditions

The boundary conditions for the potential are very straightforward: a given electric potential (V_{ap}) at the corona electrode and zero at the ground planes. The value of space charge density at different points of the corona electrode is the required boundary condition for space charge density. However, specifying this value is not so easy. One possible approach is to use a hypothesis first suggested by Kaptzov [80]. This hypothesis suggests that if the corona discharge occurs at some point of the electrode and charge is injected, the electric field at this point remains at the value equal to that at the corona onset. The potential of the electrode at the point from which the very first time charge is injected to the domain defines the corona onset level, and the corresponding value of the electric field will be the critical electric field, which remains nearly constant during the discharge. In highly symmetrical arrangements of electrodes, for example cylindrical or hemispherical ones, there exists an analytical solution for the onset electric field. The result is known as Peek's equation and in air it has the following forms [81]:

- cylindrical geometry:

$$E_0 = 3.1 \times 10^6 \delta \left(1 + \frac{0.308}{\sqrt{\delta R}} \right) \left[\frac{V}{m} \right], \quad (2-28)$$

- spherical geometry:

$$E_0 = 3.1 \times 10^6 \delta \left(1 + \frac{0.308}{\sqrt{0.5 \delta R}} \right) \left[\frac{V}{m} \right] \quad (2-29)$$

where $\delta = T_0 P / T P_0$, T_0 the standard temperature, T the actual temperature, P_0 the standard pressure, P the actual pressure of gas, and R is the electrode radius in cm. It must be

emphasized that these Peek's equations can be used only, if the electric field is the same at all points of the discharge electrodes.

The values of the charge density should be selected in order to satisfy the Kaptzov condition. The electrode tip has a spherical shape, but the electric field is not constant and slightly varies from one point of the surface to another. Formally speaking, the corona onset voltage and critical electric field would have to be different at different points. However, for the simplification of the algorithm, a constant critical electric field has been assumed as calculated from Peek's formula for the spherical electrode. The initial density of the space charge has to be guessed, or taken from a previous solution at similar conditions. After the problem is solved the electric field on the electrode surface is compared with Peek's value and the electric charge updated. Beside some well-founded techniques, the following simple formula proved to be very effective [11]:

$$\rho_{new} = \rho_{old} + \beta(E - E_0) \quad (2-30)$$

where β is an experimentally found constant.

This approach provides an indirect boundary condition for space charge density. Its distribution on the corona electrode surface is iterated until the corona electrode electric field is sufficiently close to Peek's value.

The boundary conditions for the airflow are straightforward: the collecting plate and corona electrode surface act as stationary walls, where all components of the velocity vector are zero. The outside boundary of the domain is defined as velocity inlet and outflow. Since the computational domain is open in this area, the air is free to flow in both directions.

2.5.1 Complementary equations for modeling dielectric barrier discharge

The main point in simulating DBD is to include surface charge accumulation on the dielectric surface. This surface charge plays a controlling role in the self-limiting feature of DBD for transition from discharge to spark. To include the quenching action of the dielectric barrier, the introduction of an additional boundary condition is required, which

can handle charge accumulation at the dielectric surface and the resulting local reduction of the electric field in the discharge gap. According to the Maxwell equation, the tangential and normal components of the electrical intensity and electrical displacement at the interface of plasma and dielectrics must satisfy the following continuity conditions:

$$\vec{n} \times (E_d - E_a) = 0, \quad (2-31)$$

$$\vec{n} \cdot (D_d - D_a) = \rho_s \quad (2-32)$$

In the above equations, the subscripts d and a designate the variables either residing in the dielectric or air. The local derivative of surface charge density is defined as:

$$\frac{\partial \rho_s}{\partial t} = \vec{n} \cdot \vec{J} \quad (2-33)$$

The current density \vec{J} is defined in Eq. (2- 6), so, the surface charge accumulation is calculated by:

$$\rho_s = \int J_n dt + C_0 \quad (2-34)$$

2.6 Finite Element implementation in COMSOL

FEM is versatile and powerful for handling problems with complex geometries and in non-homogeneous media. Another advantage of this technique is in programming flexibility and elegance.

Six steps are involved in this method [82]:

- Discretization of the solution region into elements: these elements can be 1D, 2D or 3D depending on the configuration of the problem.
- Interpolation of the solution: in this step, the unknown variable inside the element is interpolated based on the nodal values.
- Deriving governing equations for each element.
- Assembling matrix equations for all elements in the solution region to form a global set of equations.
- Introducing the boundary conditions.

- Solving the resulting system of equations using matrix inversion or iterative techniques.

The aim of this section is to give an introductory overview of FEM as it is implemented in COMSOL commercial software. Because of the generality of this technique, a general purpose computer program can be developed and can be used for a wide range of problems.

The first step in using COMSOL is to create the solid geometry of the system under investigation and to generate the mesh for the computational domain. The setup of regions, boundary conditions and equations is followed by the solution of a set of partial differential equations (PDEs). Those PDEs could be as the form of classical PDE, such as the Poisson and charge transport equations, or momentum and continuity equations.

The Poisson and current continuity equations, Eq. (2-5) and Eq. (2-8), with two unknown distributions: potential and space charge density (ρ_c), are the two governing equations describing the corona discharge model. These equations are solved using the proposed 2D FEM numerical technique. The entire algorithm to obtain the electrical characteristics consists of two iterative loops, the inner loop for calculating the electric field and the space charge density in the domain, and the outer loop for calculating the charge density on the corona electrode surface. In summary, the iterative procedure includes the following steps:

1. Make an initial guess for the space charge density on the corona wire surface
2. Solve Eq. (2-5) for finding the potential and field intensity distributions
3. Solve the current conservation equation, for the space charge density using FEM
4. Update the charge density on the surface of the wire by comparing the actual electric field intensity with Peek's value
5. Rescale the space charge density within the domain considering the new charge density on the corona wire surface
6. Return to step 2 and repeat the procedures until the electric field magnitude on the wire surface is sufficiently close to Peek's value.

The next step is solving the airflow governed by time-averaged Navier- Stokes equation. In the whole thesis, the airflow is assumed to be incompressible, and the momentum and mass conservation equations, Eq. (2-11) and Eq. (2-13), are solved using FEM method. The k- ϵ turbulent model with turbulence intensity between 5-10% is usually assumed. The obtained electric field and space charge density distributions are used for calculating the electric body force, in Eq. (2-11), responsible for generating secondary EHD flow, are entered into every single cell of the discretized COMSOL model.

Therefore, a two-way coupling between airflow phases should be considered. The procedure for analysis of the whole process can be summarized as follows:

1. Evaluate the electric potential and ionic space charge distribution in the whole channel by solving the Poisson and current continuity equations using the FEM technique,
2. Solve the fluid flow with the effect of electrostatic body forces,
3. Return to Step 1, adding the charged ions velocity to current continuity equations to calculate the new ionic charge density and electric potential distributions in the channel, to calculate new electrostatic body force,
4. Stop the iterations when the average electric field magnitude on the wire surface is sufficiently close to Peek's value or the calculated corona discharge current agrees with the experimental measurements.

Finally, all local parameters of the corona actuator, including the space charge density, the electric field and the potential for every point in the simulation domain can be obtained.

2.6.1 Current

Fig.2.1 shows schematically the geometry of the electrodes, the direction of the electric fields and the drift velocities. In this study, a formula for the discharge current is derived for general electrode geometry from the energy balance equation in which the displacement current is explicitly taken into account [83].

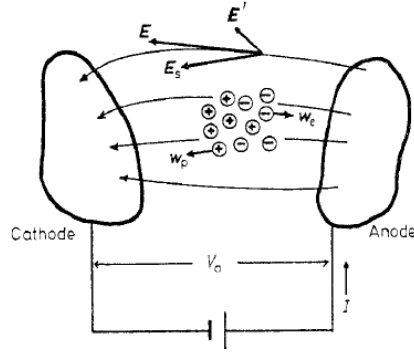


Figure 2.1: Schematic geometry of the electrodes [84]

The equation for the net charge density without including the diffusion and convection and for the general case with positive and negative ions having different mobilities is as follows

$$\frac{\partial \rho_c}{\partial t} = -\nabla \cdot [(\mu_{c,p}\rho_{c,p} - \mu_{c,n}\rho_{c,n})\vec{E}] = -\nabla \cdot \vec{\Gamma} \quad (2-35)$$

\vec{E} is electric field modified by the space charge:

$$\vec{E} = \vec{E}_s + \vec{E}' \quad (2-36)$$

where \vec{E}_s is the static applied field without effect of space charge and \vec{E}' is the field produced by the space charge. The general relations between the charge density and the electric field intensity such as $\nabla \cdot \vec{E}_s = 0$, $\nabla \cdot \vec{E}' = \rho_c/\epsilon$ and $-\vec{E}' = \nabla V'$ are valid, where V' is the potential of the field caused by the space charge.

For this case, the energy balance equation including the displacement current is

$$V_{ap}I = \iiint \vec{j} \cdot \vec{E} dv = \iiint \vec{\Gamma} \cdot \vec{E} dv + \epsilon \iiint (\partial \vec{E}/\partial t) \cdot \vec{E} dv \quad (2-37)$$

where I is the total corona current.

The first term of Eq. (2-37) can be divided into two terms

$$\iiint \vec{\Gamma} \cdot \vec{E}_s dv + \iiint \vec{\Gamma} \cdot \vec{E}' dv \quad (2-38)$$

By using the divergence theorem and the Green's first identity, the second term in Eq. (2-38) can be integrated by parts to yield

$$- \oint V' \vec{\Gamma} \cdot d\mathbf{S} + \iiint V' \nabla \cdot \vec{\Gamma} dv \quad (2-39)$$

The final form of the energy balance equation becomes [84]

$$V_{ap} I = \iiint \vec{\Gamma} \cdot \vec{E}_s dv + \varepsilon \iiint (\partial \vec{E}_s / \partial t) \cdot \vec{E}_s dv \quad (2-40)$$

The final form of current equation for time-dependent electric fields, including positive and negative ions with different mobility is

$$I = \frac{1}{V_{ap}} \iiint (\mu_{e,p} \rho_{c,p} - \mu_{e,n} \rho_{c,n}) \vec{E} \cdot \vec{E}_s dv + \frac{\varepsilon}{V_{ap}} \iiint \frac{\partial \vec{E}_s}{\partial t} \cdot \vec{E}_s dv \quad (2-41)$$

Throughout this study different forms of this current equation have been used in order to evaluate the discharge current depending upon the conditions assumed. If the DC voltage is applied to the system the variation of the electric field over time would be zero and the second term in Eq. (2-42) would be equal to zero. Consequently the current equation would be

$$I = \frac{1}{V_{ap}} \iiint (\mu_{e,p} \rho_{c,p} - \mu_{e,n} \rho_{c,n}) \vec{E} \cdot \vec{E}_s dv \quad (2-42)$$

Moreover, in a general case the mobility of positive and negative ions were assumed to be the same. By doing more simplifications, the current equation could be calculated as follows

$$I = \frac{1}{V_{ap}} \iiint \rho_c \mu_e \vec{E} \cdot \vec{E}_s dv \quad (2-43)$$

2.6.2 Electrokinetic conversion

From the velocity profiles, the induced kinetic power and then electro-mechanical efficiency of the EHD actuators could be computed. For corona-induced kinetic power, Robinson [74] assumed that the kinetic power corresponds to the energy derivative and showed

$$P_{mech} = \frac{1}{2} \rho A_G V_G^3 \quad (2-44)$$

Sigmond and Lagstad [75] established a theoretical model where they considered that

$$P_{mech} = \frac{1}{2} \rho S_G V_G^2 \quad (2-45)$$

They demonstrated that the electro-mechanical efficiency of the corona discharge is given by

$$\eta = \frac{P_{mech}}{P_{elec}} = V_G / 2v_i \ll 1 \quad (2-46)$$

where A_G is the discharge cross section, V_G the gas velocity, S_G the averaged gas flow rate through the discharge cross section and v_i the drift velocity of ions.

In the previous models the velocity variations along the y axis is not taken into consideration. The more complete model was developed by Moreau [69] based on the energy conservation equation. In this model velocity profile is taken into account and the mechanical power corresponding to the kinetic energy density is expressed as

$$P_{mech} = \frac{1}{2} \rho L_s \int V_G^3 dy \quad (2-47)$$

with L_s the span wise electrode length. To determine the mechanical power of a surface discharge per unit of electrode length, the value is divided by L_s . Therefore, the electrical power per unit length, and then the electro-mechanical efficiency of the plasma actuator, could be derived.

2.7 Conclusions

In this Chapter, a comprehensive review on different proposed techniques for simultaneously solving the Poisson equation, charge continuity equation and fluid flow equations were explained. Among these techniques, the FEM seems to be best suited for simulating discharge cases investigated in this thesis. The full mathematical algorithm to calculate the electrical characteristics such as electrical current and power consumption are described in detail. Other important characteristic of the corona actuator is the active force on the air above the actuator. The complete formulation for calculating the acting force on the airflow moving over a flat plate is described in detail in Chapter 5.

References:

- [1] G.E. Georghiou, R. Marrow, A.C. Metaxas, "A two-dimensional, finite element, flux corrected transport algorithm for the solution of gas discharge problems", *J. Phys. D: Appl. Phys.*, Vol. 33, pp.2453-66, 2000
- [2] A.P. Napartovich, Y.S. Akishev, A.A. Deryugin, I.V. Kochetov, M.V. Pankin, N.I. Trushkin, "Numerical Simulation of Trichel-pulse Formation in a Negative Corona", *J. Phys. D: Appl. Phys.*, pp.2726-36, Vol. 30, 1997
- [3] E. Landers, "Distribution of electrons and ions in a corona discharge", *Proc. IEE*, Vol. 125: 9, pp. 1069-73, 1978
- [4] Y. Takahashi, M. Yoshida, Y. Anma, S. Kobayashi, M. Endo, "Thickness and luminosity distribution of positive corona sheath in air", *J. Phys. D: Appl. Phys.*, Vol.15, pp. 639-53, 1982
- [5] R. Morrow, "The theory of positive glow corona", *J. Phys. D: Appl. Phys.*, Vol. 30: 22, pp. 3099, 1997
- [6] J. Chen, J.H. Davidson, "Electron density and energy distributions in the positive DC corona: Interpretation for corona-enhanced chemical reactions", *Plas. Chem. Plas. Proc.*, Vol.22, pp.199-224, 2002
- [7] J. Chen, J.H. Davidson, "Ozone production in the positive DC corona discharge: Model and comparison to experiments," *Plas. Chem. Plas. Proc.*, Vol.22, pp. 495-522, 2002
- [8] J. Chen, J.H. Davidson, "Ozone production in the negative DC corona: dependence of discharge polarity," *Plas. Chem. Plas. Proc.*, Vol.23, pp. 501-18, 2003
- [9] K. Yanallah, S. Hadj Ziane, A. Belasri, Y. Meslem, "Numerical modeling of ozone production in direct current corona discharge", *J. Molec. Struc.*, Vol.777, pp.125-9, 2006
- [10] K. Yanallah, F. Pontiga, A. Fernandez-Rueda, A. Castellanos, "Experimental investigation and numerical modelling of positive corona discharge: ozone generation", *J. Phys. D: Appl. Phys.*, Vol. 42, p. 065202, 2009
- [11] K. Adamiak, P. Atten, "Simulation of corona discharge in point-plane configuration", *J. Electrostat.*, Vol.61, pp. 85-98, 2004

- [12] K. Adamiak, V. Atrazhev, P. Atten, "Corona discharge in the hyperbolic point-plane configuration: direct ionization criterion versus approximate formulations", IEEE Trans. Dielectr. Elec. Insul., Vol.12: 5, pp. 1025-34, 2005
- [13] K. Adamiak, X. Deng, "The electric corona discharge in a triode system", IEEE Trans. Ind. Appl., Vol.35, pp. 767-73, 1999
- [14] R. Lakeh, M. Molki, "Patterns of airflow in circular tubes caused by a corona jet with concentric and eccentric wire electrodes", J. Fluids Eng., Vol. 132: 1, pp. 081201, 2010
- [15] D.B. Go, S.V. Garimella, T.S. Fisher, R.K. Mongia, "Ionic winds for locally enhanced cooling," J. Appl. Phys., Vol.102, pp. 053302, 2007
- [16] J.R. McDonald, W.B. Smith, H.W. Spencer, L.E. Sparks, "A mathematical model for calculating electrical conditions in wire duct electrostatic precipitation devices," J. Appl. Phys., Vol.48, pp.2231, 1977
- [17] P. Atten, K. Adamiak, B. Khaddour, J.L. Coulomb, "Simulation of corona discharge in configurations with a sharp electrode", J. Optoelec. Adv. Mat., Vol.6: 3, pp.1023-8, 2004
- [18] J.R. McDonald, W.B. Smith, H.W. Spencer, L.E. Sparks, "A mathematical model for calculating electrical conditions in wire-duct electrostatic precipitation devices", J. Appl. Phys., Vol. 48, pp.2231-43, 1977
- [19] J.L. Davis, J.F. Hoburg, "Wire-duct precipitator field and charge computation using finite element and characteristics method", J. Electrostat., Vol.14, pp.187-99, 1983
- [20] A.J. Butler, Z.J. Cendes, J.F. Hoburg, "Interfacing the finite element method with the method of characteristics in self-consistent electrostatic field models", IEEE Trans. Ind. Appl., Vol.25, pp.533-8, 1989
- [21] G.Ghione, R.D. Graglia, "Two-dimensional finite-boxes analysis of monopolar corona fields including ion diffusion", IEEE Trans. Magnet., Vol.26, pp.567- 70, 1990
- [22] P.L. Levin, J.F. Hoburg, "Donor cell-finite element descriptions of wire duct precipitator fields, charges, and efficiencies", IEEE Trans. Ind. Appl., Vol. 26: 4, pp. 662-70, 1990
- [23] M. N.O. Sadiku, "Numerical techniques in electromagnetics", Boca Raton: CRC Press, 1992

- [24] K. Adamiak, "Simulation of corona in wire-duct electrostatic precipitator by means of the boundary element method", *IEEE Trans. Ind. Appl.*, Vol.30:2, pp.381-6, 1994
- [25] L. Zhao, K. Adamiak, "Numerical simulation of the electrohydrodynamic flow in a single wire-plate electrostatic precipitator", *IEEE Trans. Ind. Appl.*, Vol.44: 3, pp.683-91, 2008
- [26] J. H. Davidson, P. J. McKinney, P. Linnebur, "Three-dimensional (3D) model of electric field and space charge in the barbed plate-to-plate precipitator", *IEEE Trans. Ind. Appl.*, Vol. 32: 4, pp. 858-66, 1996
- [27] P. Atten, L. J. Coulomb, B. Khaddour, "Modelling of electrical field modified by injected space charge", *IEEE Trans. Magnet.*, Vol.41:5, pp.1436-9, 2005
- [28] J. Zhang, K. Adamiak, "A dynamic model for negative corona discharge in point-plane configuration", *Proc. of ESA/IEJ/IEEE-IAS/SFE Joint Conference on Electrostatics*, Vol.2, pp.588-97, Berkeley, USA, 2006
- [29] R. Morrow, "Theory of negative corona in oxygen", *Phys. Rev. A*, Vol. 32, pp.1799-809, 1985
- [30] P. Sattari, G.S.P. Castle, K. Adamiak, "FEM-FCT-Based Dynamic Simulation of Corona Discharge in Point-Plane Configuration", *IEEE Trans. Ind. Appl.*, Vol.46: 5, pp.1699-706, 2010
- [31] K.G. Donohoe, T. Wydeven, "Plasma polymerization of ethylene in an atmospheric pressure pulse-discharge", *J. Appl. Poly. Sci.*, Vol.23:9, pp.2591-601, 1979
- [32] D.G. Boyers, W.A. Tiller, "Plasma bubble domains: A magnetic bubble analog", *Appl. Phys. Lett.*, Vol.41, pp.28, 1982
- [33] E. Ammelt, D. Schweng, H.G. Purwins, "Stripe Turing structures in a two-dimensional gas discharge system", *J. Phys. Rev. E*, Vol.55: 6, pp.6731-40, 1993
- [34] W. Breazeal, K. M. Flynn, E. G. Gwinn, "Static and dynamic two-dimensional patterns in self-extinguishing discharge avalanches", *J. Phys. Rev. E*, Vol.52, pp.1503, 1995
- [35] U. Kogelschatz, "Filamentary, patterned and diffuse barrier discharges", *IEEE Trans. Plasma Sci.*, Vol.30:4, pp.1400-08, 2002
- [36] S.T. Pai, X.M. Guo, T.D. Zhou, "Closed form analytic solution describing glow discharge plasma", *Phys. Plasmas*, Vol.3, pp.3842-52, 1996

- [37] V. Gibalov, G. Pietsch, “The development of dielectric barrier discharges in gas gaps and surfaces”, *J. Phys. D: Appl. Phys.*, Vol.33, pp.2618–36, 2000
- [38] G.I. Font, “Boundary layer control with atmospheric plasma discharges”, *AIAA/ASME/SAE/ASEE Joint Conf. Exhibit*, Pap. No. 2004-3574, Fort Lauderdale, USA, 2004
- [39] A.V. Likhanskii, M.N. Shneider, S.O. Macheret, R.B. Miles, “Modeling of interaction between weakly ionized near-surface plasmas and gas flow”, *44th AIAA Conf. Aero. Sci. Meet. Exhibit*, Pap. No. 2006-1204, Reno, USA, 2006
- [40] F. Massines, R.B. Gadri, P. Decomps, A. Rabehi, P. Segur, C. Mayoux, “Atmospheric pressure dielectric controlled glow discharges: diagnostics and modeling”, *AIP Conf. Proc.*, Vol.363, pp. 306, New jersey, USA, 1996
- [41] F. Massines, A. Rabehi, P. Decomps, R.B. Gadri, P. Segur, C. Mayoux, “Experimental and theoretical study of a glow discharge at atmospheric pressure controlled by dielectric barrier”, *J. Appl. Phys.*, Vol.83, pp.2950, 1998
- [42] M. Paulus, L. Stals, U. Rude, B. Rauschenbach, “Two-dimensional simulation of plasma-based ion implantation”, *J. Appl. Phys.*, Vol. 85, pp.761–6, 1999
- [43] J.S. Shang, P.G. Huang, “Modeling of ac dielectric barrier discharge”, *J. Appl. Phys.*, Vol.107, pp. 113302, 2010
- [44] J.S. Shang, P.G. Huang, “Electrodynamics force of dielectric barrier discharge”, *J. Appl. Phys.*, Vol. 109, pp.113301, 2011
- [45] N. Zouzou, B. Dramane, E. Moreau, G. Touchard, “EHD flow and collection efficiency of a DBD ESP in wire- to- plane and plane- to- plane configurations”, *IEEE Trans. Ind. Appl.*, Vol. 47, pp.336-43, 2011
- [46] R. Gouri, N. Zouzou, A. Tilmatine, L. Dascalescu, “Enhancement of submicron particle electrostatic precipitation using dielectric barrier discharge in wire to square tube configuration”, *J. Electrostat.*, Vol.71, pp.240-5, 2012
- [47] F. Thomas, T. Corke, M. Iqbal, A. Kozlov, D. Shatzman, “Optimization of SDBD plasma actuators for active aerodynamic flow control”, *J. AIAA*, Vol.47, pp.2169, 2009
- [48] M. Forte, J. Jolibois, F. Moreau, G. Touchard, M. Cazalens, “Optimization of a dielectric barrier discharge actuator by stationary and non-stationary measurements of

- the induced flow velocity: application to flow control”, *Exp. Fluids*, Vol.43: 6, pp.917-28, 2007
- [49] L. Zhao, K. Adamiak, “EHD flow in air produced by electric corona discharge in pin-plate configuration”, *J. Electrostat.*, Vol.63, pp.337-50, 2005
- [50] E. Moreau, C. Louste, G. Touchard, “Electric wind induced by sliding discharge in air at atmospheric pressure”, *J. Electrostat.*, Vol.66, pp.107-14, 2008
- [51] B. Komeili, J.S. Chang, G.D. Harvel, C.Y. Ching, D. Borocilo, “Flow characteristics of wire-rod type electrohydrodynamic gas pump under negative corona operations”, *J. Electrostat.*, Vol.66, pp.342-53, 2008
- [52] T. Yamamoto and H. R. Velkoff, “Electrohydrodynamics in an electrostatic precipitator”, *J. Fluid Mech.*, Vol.108, pp.1-18, 1981
- [53] D. Blanchard, L. M. Dumitran, P. Atten, “Effect of electro-aero-dynamically induced secondary flow on transport of particles in an electrostatic precipitator”, *J. Electrostat.*, Vol.51, pp.212-7, 2001
- [54] T. Yamamoto, M. Okuda, “Three-dimensional ionic wind and electrohydrodynamics of tuft/point corona electrostatic precipitator”, *IEEE Trans. Ind. Appl.*, Vol. 39, pp.1602-7, 2003
- [55] H.J. Schmid, S. Stolz, H. Buggisch, “On the modeling of the electro-hydrodynamic flow field in electrostatic precipitators”, *J. Flow Turb. Comb.*, Vol.68, pp.63-89, 2002
- [56] A. Soldati, S. Banerjee, “Turbulence modification by large-scale organized electrohydrodynamic flows”, *Phys. Fluids*, Vol.10, pp.1742, 1998
- [57] J. Mathew, F.C. Lai, “Enhanced heat transfer in a horizontal channel with double electrodes”, *Proc. of IEEE Ind. Appl. Annual Meeting*, Vol.2, pp.1472-9, Orlando, USA, 1995
- [58] M. Molki, K.L. Bhamidipati, “Enhancement of convective heat transfer in the developing region of circular tubes using corona wind”, *Int. J. Heat and Mass Transfer*, Vol. 47: 19, pp.4301-14, 2004
- [59] N. Kasayapanand, “Numerical study of electrode bank enhanced heat transfer,” *Appl. Thermal Eng.*, Vol.26: 14, pp. 1471-80, 2006
- [60] N. Kasayapanand, J. Tiansuwan, W. Asvapoositkul, N. Vorayos, T. Kiatsiriroat, “Effect of the electrode arrangements in a tube bank on the characteristic of

- electrohydrodynamic heat transfer enhancement: low Reynolds number”, *J. Enh. Heat Trans.*, Vol.9: 5, pp.229- 42, 2002
- [61] Y. Hanein, C. G. J. Schabmueller, G. Holman, P. Lucke, D. D. Denton, K. F. Bohringer, “High-aspect ratio submicrometer needles for intracellular applications”, *J. Micromech. & Microeng.*, Vol.13: 4, pp. 91-5, 2003
- [62] A. Yabe, Y. Mori, K. Hijikata, “EHD study of the corona wind between wire and plate electrodes”, *J. AIAA*, Vol.16: 4, pp.340-5, 1978
- [63] L. Zhao, K. Adamiak, “Numerical simulation of the electrohydrodynamic flow in a single wire-plate electrostatic precipitator”, *IEEE Trans. Ind. App.*, Vol.44:3, pp.683-91, 2008
- [64] K. Adamiak, P. Atten, “Numerical simulation of the 2-D gas flow modified by the action of charged fine particles in a single-wire ESP”, *IEEE Trans. Dielectr. Elec. Ins.*, Vol.16:3, pp.608-14, 2009
- [65] J.O. Feng, “Application of Galerkin finite element method with Newton iterations in computing steady-state solutions of unipolar charge currents in corona devices”, *J. Comp. Phys.*, Vol.151, pp.969-89, 1999
- [66] J.S. Chang, H. Tsubone, Y.N. Chun, A.A. Berezin, K. Urashima, “Mechanism of electrohydrodynamically induced flow in a wire-non-parallel plate electrode type gas pump”, *J. Electrostat.*, Vol.67, pp.335-9, 2009
- [67] M. Kocik, J. Podliński, J. Mizeraczyk, J.S. Chang, “Particle image velocimetry measurements of wire nonparallel plates type electrohydrodynamic gas pump”, *IEEE Trans. Dielectr. Elec. Ins.*, Vol. 16: 2, pp. 312-9, 2009
- [68] M. Kocik, J. Podliński, J. Mizeraczyk, K. Urashima, J.S. Chang, “Flow distribution measurement in wire-nonparallel plate type electrohydrodynamic gas pump by a particle image velocimetry”, *IEEE Trans. Dielectr. Elec. Ins.*, Vol. 16: 3, pp. 601-7, 2009
- [69] E. Moreau, “Airflow control by non-thermal plasma actuators”, *J. Phys. D: Appl. Phys.*, Vol.40, pp. 605–36, 2007
- [70] J.R. Roth, D.M. Sherman, S.P. Wilkinson, “Electrohydrodynamic flow control with a glow discharge surface plasma, *J. AIAA*, Vol.38, pp.1166–72, 2000

- [71] W. Shyy, B. Jayaraman, and A. Andersson, "Modeling of glow discharge-induced fluid dynamics", *J. Appl. Phys.*, Vol.92: 11, pp. 6434-43, 2002
- [72] K. Singh, S. Roy, "Force approximation for a plasma actuator operating in atmospheric air", *J. App. Phys.* Vol.103, pp.013305:1-10, 2008
- [73] Y. Suzen, P. Huang, J. Jacob, "Numerical simulations of plasma based flow control applications", 35th AIAA Fluid Dynamic Conf. Exhibit, Pap. No. 2005-4633, Toronto, Canada, 2005
- [74] M. Robinson, "Movement of air in the electric wind of the corona discharge", *AIEE Trans.*, pp.143-50, 1961
- [75] D. Pnueli, C. Gutfinger, "Fluid Mechanics", Cambridge University press, 1992
- [76] H. H. Schlichting, "Boundary layer theory", New York: McGraw-Hill, 2000
- [77] N. Farnoosh, "Three dimensional modeling of electrostatic precipitator using hybrid finite element flux corrected transport technique", Ph.D. Thesis, University of Western Ontario, 2011
- [78] J. Hoffman, C. Johnson, "Turbulent incompressible flow, applied mathematics: body and soul", Vol. 4, New York: Springer, 2006
- [79] J. Boeuf, and L. Pitchford, "Electrohydrodynamic force and aerodynamic flow acceleration in surface dielectric barrier discharge", *J. Appl. Phys.*, Vol. 97, pp.103307, 2005
- [80] N.A. Kaptzov, "Elektricheskiye Yavleniya v Gazakh i Vakuume", OGIZ, Moscow, 1947
- [81] A.M. Meroth, T. Gerber, C.D. Munz, P.L. Levin, A.J. Schwab, "Numerical solution of non-stationary charge coupled problems", *J. Electrostat.*, Vol.45, pp.177-98, 1999
- [82] M. Sadiku, "Numerical techniques in electromagnetics with MATLAB", 3rd edition, Boca Raton: CRC Press, 2009
- [83] N. Sato, "Discharge current induced by the motion of charged particles", *J. Phys. D: Appl. Phys.*, Vol.13, pp. L3-6, 1980
- [84] R. Morrow, and N. Sato, "The discharge current induced by the motion of charged particles in time-dependent electric fields; Sato's equation extended", *J. Phys. D: Appl. Phys.*, Vol.32, pp.L20-2, 1999

- [85] R.S. Sigmond and I.H. Lagstadt, "Mass and species transport in corona discharges",
High Temp. Chem. Proc., Vol.2, pp.221-9, 1993

Chapter 3

3 Quasi-stationary numerical model of the dielectric barrier discharge

The aim of this study is to present a numerical algorithm for investigating the dynamic characteristics of a simple model of the dielectric barrier discharge in air. The proposed algorithm is based on the finite element method and is capable of determining the distribution of electric field intensity and space charge density in the point-plane geometry, when the plane is covered with a thin dielectric layer and the needle is energized with a sinusoidal voltage. The simulation results show the behavior of corona current and space charge density for a few values of the input voltage and frequency. The aim of this parametric study is to investigate the effect of voltage, and frequency on the time variation of the discharge.

3.1 Introduction

The dielectric barrier discharge (DBD) is used in various important applications, such as ozone generation, pollution control, electrostatic precipitation, fluid flow control and many other industrial processes. This discharge is closely related to corona discharge (CD) since both discharges have common features, such as the strong distortion of the local field caused by space charge distribution [1]. Although, the electric field, established by the electrodes, in corona discharge can be produced by dc voltage, ac voltage or pulse voltage, a dielectric barrier discharge requires alternating voltages for its operation [2]. The dielectric layer deposited on one or both electrodes cannot pass a dc current, but the electric current can exist and it is induced by drifting ions. Barrier discharges can be operated in various modes. At atmospheric pressure, the local electrical breakdown in a form of large number of micro discharges is the normal situation for most gases [3]. Under certain circumstances it is possible to obtain apparently homogeneous, diffuse discharges [4] or regularly spaced glow discharge patterns [5]. At lower pressures, diffuse glow discharges can always be obtained [3]. Due to these numerous regimes of operation, during the last several decades, many efforts have been made to have a better understanding of the dielectric barrier discharge and many theoretical, experimental and numerical results have

been published. Massines et al. [6] developed a 1D model for the DBD dynamics based on the numerical solution of the electron and ion continuity, and momentum transfer equations coupled to Poisson's equation. The authors accounted for the charge accumulation on the dielectric surface, as the discharge develops, and derived the voltage boundary conditions for dielectrics by considering an equivalent circuit of the gas gap in series with the equivalent capacitor of the dielectric. Later Massines et al. [7] presented a two-dimensional analysis for a parallel electrode configuration. This study provided a helpful insight for understanding the DBD behavior. One of the recent investigations on modeling of DBD, based on the Finite Difference Method (FDM) was performed by Shang et al. [8], [9]. The qualitative electro-dynamics of the DBD in air was studied using three components in a drift diffusion plasma model including Poisson's equation. The computational simulation confirms the self-limiting feature of the DBD, preventing the corona to spark transition, and the numerical results agree to some extent with the experimental data. However, since the authors used FDM there is still a problem with spatial discretization of complicated geometries. Gouri et al. [10] investigated one of the most common applications of DBD in the electrostatic precipitator (ESP). The electrical characteristics of the precipitator, such as the current waveform, have been analyzed. Sensitivity analysis has shown that the particle collection efficiency of the ESP increases with the applied voltage. However, this depends on the frequency range and both at low or very high frequencies the efficiency can be poor. Dramane et al. [11] varied the system geometry in order to investigate the effect of channel geometry on the system operation. This included the thickness, length and number of tubes.

Although quite a few articles using DBD in numerous industrial applications have been published, still no reliable and accurate model has been presented in order to interpret the physics of this phenomenon and most of the works are based on the experimental setups. Complications in modeling the dielectric barrier discharge are generally related to the complexity of reactions in the ionization layer and randomness of the discharge regime in some configurations. In order to overcome these problems, a single species DBD model for a point to plane configuration is presented in this paper. The Finite Element Method (FEM) was used to solve the governing equations for both the electric field and distribution of unipolar space charge using the COMSOL multi-physics commercial software. The

basic characteristics of the discharge, including the total current, electric field distribution, surface charge accumulation and space charge density distributions are reported. In addition, in order to investigate the effect of frequency and amplitude of voltage on the discharge characteristics the simulation has been done for different levels of these parameters.

3.2 Mathematical model

3.2.1 Governing equation

Figure 3.1 shows a typical configuration for dielectric barrier discharge in the point-plane geometry.

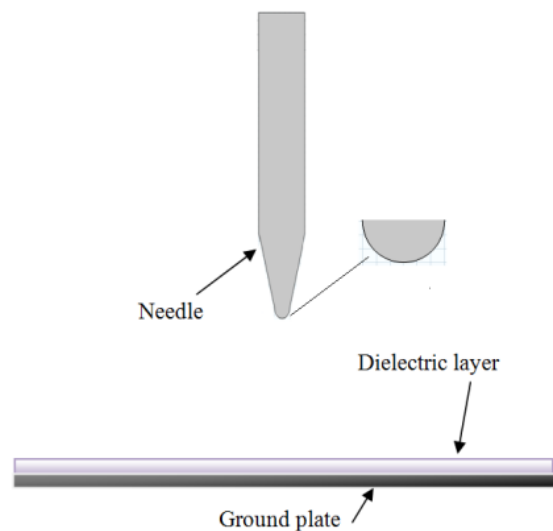


Figure 3.1: Typical configuration for DBD investigated in this study

A hemispherical needle with a tip radius curvature R and length L is perpendicular to an infinitely large plate at a distance D . A sinusoidal electric potential with the maximum value of V_{\max} is applied to the needle. The ambient gas is air at room temperature and atmospheric pressure. As this is a single species model, it is assumed that the ionization layer is neglected and positive or negative ions with constant mobility are assumed to be injected from the corona electrode. In the absence of magnetic field, the equations governing the electric field are [12]:

$$\nabla \cdot \vec{D} = \rho_c \quad (3-1)$$

$$\nabla \cdot \vec{J} = -\frac{\partial \rho_c}{\partial t} \quad (3-2)$$

$$\vec{D} = \epsilon_0 \vec{E} \quad (3-3)$$

$$\vec{E} = -\nabla V \quad (3-4)$$

where \vec{D} is the electrostatic displacement, ρ_c is the space charge density, \vec{J} is the electric current density, ϵ_0 is the gas permittivity, \vec{E} is the electric field and V is the electric potential. The electric field is thus governed by Poisson's equation:

$$\nabla^2 V = -\frac{\rho_c}{\epsilon_0} \quad (3-5)$$

The ionic charges are accelerated by the Coulomb force and move towards the ground plates. The charge drift creates an electric current with a density defined as:

$$\vec{J} = \rho \left(\mu_e \vec{E} + \vec{u} \right) - D \nabla \rho_c \quad (3-6)$$

where μ_e is the mobility of ions, D is the ions diffusion coefficient and \vec{u} is the gas velocity. Three terms on the right hand side of Equation (3.6) are drift, convection and diffusion currents, respectively. Diffusion coefficient and is equal to:

$$D = \frac{k_B T \mu_e}{e_0} \quad (3-7)$$

where k_B is the Boltzmann constant equal to $1.38065 \times 10^{-23} (m^2 \cdot kg/s^2 \cdot K)$, T is the absolute temperature, e_0 is the electron charge, equal to $1.602 \times 10^{-19} (C)$.

Since the drift velocity of ions is usually about two orders of magnitude larger than the typical velocity of the gas flow, the convective component in the ionic current density can be neglected, so:

$$\vec{J} = \rho \mu_e \vec{E} - D \nabla \rho_c \quad (3-8)$$

Eq. (3.8) can be substituted into (3.2) to derive the continuity equation,

$$\frac{\partial \rho_c}{\partial t} + \nabla \cdot \left(\rho \mu_e \vec{E} - D \nabla \rho_c \right) = 0 \quad (3-9)$$

Therefore, the electric problem of the corona discharge is governed by a set of two partial differential equations with two unknown distributions: Eq. (3.5) with the unknown potential and Eq. (3.9) with the unknown space charge density.

3.2.2 Complementary equations for modeling dielectric barrier discharge

The main point in simulating DBD is to include surface charge accumulation on the dielectric surface. This surface charge produces a field directed against the electric field produced by the voltage source to an extent that the ionization eventually stops. Actually, the surface charge accumulation plays a controlling role for the self-limiting feature of DBD preventing transition from a corona to a spark discharge. To include this phenomenon it is necessary to introduce an additional boundary condition, which can include the charge accumulation on the dielectric surface and the resulting reduction of the electric field in the discharge gap. According to Maxwell equations, the tangential and normal components of the electrical intensity and electrical displacement at the interface between air and dielectric material must satisfy the following conditions [8]:

$$\vec{n} \times (\vec{E}_d - \vec{E}_a) = 0 \quad (3-10)$$

$$\vec{n} \cdot (\vec{D}_d - \vec{D}_a) = \rho_s \quad (3-11)$$

In the above equations, the subscripts d and a, correspond to dielectric or air. The time derivative of surface charge density is related to the normal current density:

$$\frac{\partial \rho_s}{\partial t} = \vec{n} \cdot \vec{J} \quad (3-12)$$

The current density \vec{J} is defined in Eq. (3-8), so, the surface charge accumulation can be calculated as:

$$\rho_s = \int J_n dt + C_0 \quad (3-13)$$

Integral form of the surface charge density on the dielectric includes total charge at each time steps and C_0 which defines the total accumulated charge in previous time steps. Basically by C_0 , charge accumulation on the barrier surface would be controlled by same polarity charge and likewise; charge elimination on the barrier surface is controlled by opposite polarity charge.

3.2.3 Boundary conditions

The boundary conditions for the potential are straightforward: a given electric potential (V_{ap}) on the corona electrode and zero on the ground plane [13]. However, formulation of proper boundary conditions for the space charge density is not so easy because the ionization layer has been neglected. One possible approach is to use Kaptzov's hypothesis, which can be used to create a simple algorithm, which helps to establish the charge injection law. Kaptzov suggested that if the corona discharge occurs at some point on the electrode, the electric field at this point remains constant at the value it takes at the corona onset.

The potential of the electrode at the point where the charge is injected to the domain for the first time defines the corona onset level, and the corresponding value of the electric field will be the critical electric field, which remains nearly constant during the discharge. In this configuration we can apply Peek's equation which in air it has the following form:

$$E_0 = 3.1 \times 10^6 \delta \left(1 + \frac{0.308}{\sqrt{0.5\delta R}} \right) \quad (3-14)$$

where $\delta = T_0 P / TP_0$, R is the electrode radius in cm, T_0 the standard temperature, T the actual temperature, P_0 the standard pressure and P the actual pressure of gas. It must be emphasized that Peek's equation can be used only, if the electric field is the same at all points on the discharge electrode.

The values of the charge density should be selected in order to satisfy the Kaptzov condition. The electrode tip has a spherical shape, but the electric field is not constant and slightly varies from one point of the surface to another. Formally speaking, the corona onset

voltage and critical electric field would have to be different at all points. However, for the simplification of the algorithm, a constant critical electric field has been assumed. The initial density of the space charge has to be guessed, or taken from a previous solution at similar conditions. After the problem is solved the electric field on the electrode surface is compared with Peek's value and the electric charge updated. While some well-established techniques are often advised, here the following simple formula to update the space charge density on the surface of corona electrode proved to be very effective [13]:

$$(\rho_c)_{new} = (\rho_c)_{old} + \beta(E - E_0) \quad (3-15)$$

where β is an experimentally found constant. Practically, this approach provides an indirect boundary condition for space charge density. Its distribution on the corona electrode surface is iterated until the corona electrode electric field is sufficiently close to Peek's value.

3.3 Numerical algorithm

The processes occurring in the dielectric barrier discharge during a cycle of AC voltage are more complicated than that for a corona discharge. By applying an electric field larger than the breakdown field local ionization occurs, which initiates the electric current in the domain. During the positive half cycle the positive ions will accumulate on the dielectric surface. So, the total electric field intensity is a combination of the electric field produced by the voltage source and the field produced by the space charge collected on the dielectric surface. As the discharge progresses, the charge accumulated on the dielectric surface reduces the local electric field to such an extent that ionization stops and the current is quenched. When the sign of the applied voltage reverses, the electric field due to external voltage is reinforced due to the surface charge accumulation. This enhanced field at the beginning of the new half cycle initiates a current in the opposite direction, which transfers negative charge to the dielectric surface. The process continues until the opposing space-charge field once again extinguishes the ionic current across the gap [14].

Following this description, an iterative numerical algorithm for the dielectric barrier discharge simulation has been developed. The simulation starts from some initial guess of the space charge density and then the conventional FEM procedure is employed to obtain

the Poisson component of the electric potential from Eq. (3.5). After calculating V , the electric field is calculated by differentiating the potential distribution. Using the values of calculated electric field, the new charge density distribution is obtained by solving Eq. (3.15). This process continues and the iterative algorithm updates the injected charge density on the corona electrode surface until the electric field values are sufficiently close to Peek's value. Finally, all local parameters of the electric dielectric barrier discharge, including the space charge density, the current density, the electric field and the potential for every point in the simulation domain can be obtained. It should be noted that the electric field varies strongly in both space and time. Near the discharge electrode the electric field variation is particularly steep, which demands a very fine spatial mesh, while in the remaining region the electric field is more uniform. A non-uniform spatial mesh is therefore essential for an accurate numerical treatment. In addition, the numerical algorithm for determining space charge density should fulfill a few important requirements [12]. It should give positive, accurate results, free from nonphysical density fluctuation and numerical diffusion, should be computationally efficient, and should be easily adopted for any geometry.

3.3.1 Electric current

In this study, a formula for the discharge current is derived for general electrode geometry from the energy balance equation in which the displacement current is explicitly taken into account. \vec{E} is electric field modified by the space charge:

$$\vec{E} = \vec{E}_s + \vec{E}' \quad (3-16)$$

where \vec{E}_s is the static applied field without the effect of charge transport and \vec{E}' is the field produced by the space charge. It has been assumed that the computational model is based on a single species model without the effect of electrons. With a few simplifications the current equation can be calculated as follow [15]:

$$I = \frac{1}{V_{ap}} \iiint \rho_c \mu_e \vec{E}' \cdot \vec{E}_s dv \quad (3-17)$$

3.4 Simulation results

In this study, a cylindrical needle 1cm long is placed at the distance 3.1cm perpendicular to the circular aluminum plate, which has 25cm radius. The needle has a hemispherical tip with the radius of 95 μ m. A dielectric layer with thickness of 1mm is assumed to be placed on the ground plate, and the relative permittivity of this material is 6. At room temperature and atmospheric pressure the corona onset voltage for this configuration is evaluated to be 3.1kV. The voltage supplied to the needle varied between the corona onset level and 8kV.

The first simulation was done for a maximum sinusoidal input voltage of 7.5kV and a frequency of 5kHz. Total corona current between both electrodes and the distribution of the charge density on the ground plate were calculated. Figure 3.2 shows the distribution of the electric field intensity with and without the effect of accumulated charges in space and on the surface of the dielectric.

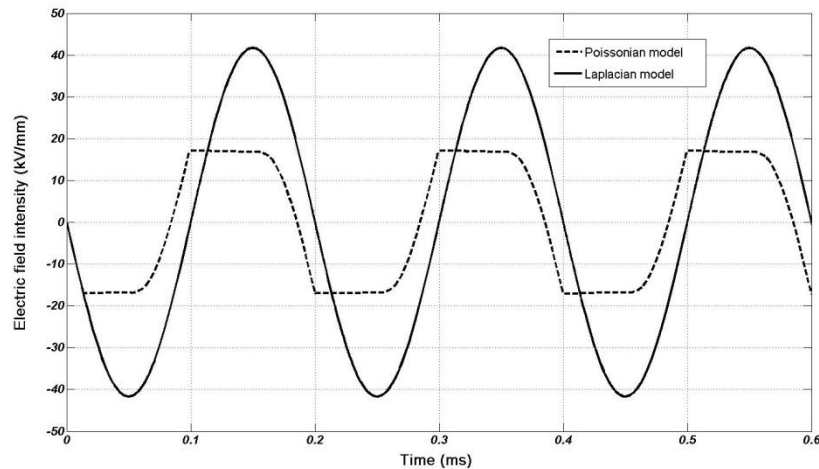


Figure 3.2: Electric field intensity on the needle's tip with (Poissonian Model) and without (Laplacian Model) the effect of the accumulated charge

Two observations are dominant in Figure 3.2. First, the electric field is distorted due to effect of injected space charge from the tip of the needle and the accumulated surface charge on the dielectric. The most important effect is that the electric field intensity reaches the value above Peek's value just before voltage zero crossing. So, it was observed that for this level of voltage and frequency the current is shifted with respect to the voltage as shown in Figure 3.3:

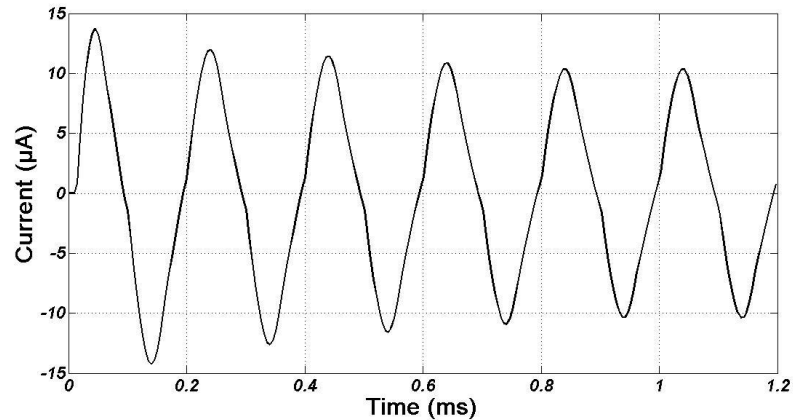


Figure 3.3: Waveform of the discharge current

The second observation is about the maximum electric field intensity on the needle's tip. The iterative algorithm is used to modify the injected charge and the iterations are terminated when the difference between both fields reaches an assumed value. So, the electric field magnitude is not exactly equal to Peek's value at all points on the needle's tip, and as a result there is some slight difference between the actual electric field and Peek's value.

In Figure 3.4 the total space charge in the air gap is shown as a function of time.

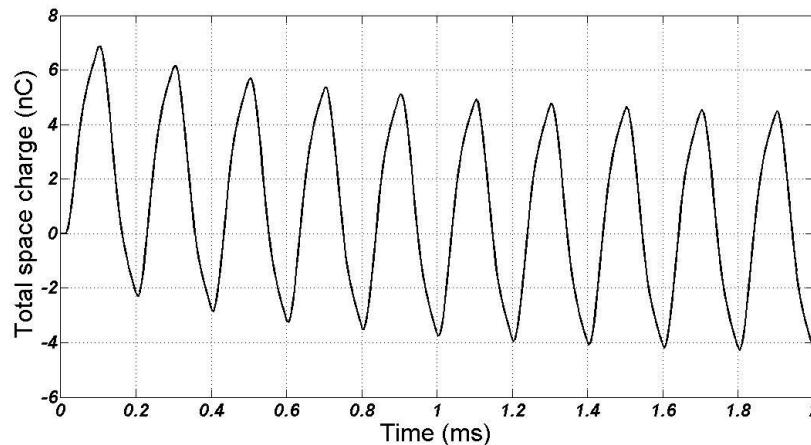


Figure 3.4: Distribution of space charge in the air gap

In the first positive half cycle, since there is no charge in the air gap, there is a short time delay before the charge injection occurs. This charge reaches its maximum level and after that the negative ions are injected in the negative half cycle. A zero crossing in this figure shows the time instant when the net amounts of negative and positive ions in the air

gap are equal. It is important to note that this point does not coincide with the zero crossing in the discharge current, because the sign of the current obeys the sign of the electric field intensity. It is obvious that after couple of periods the total space charge in the domain reaches the quasi-steady-state and the waveforms for both negative and positive cycles are identical.

The total surface charge on the dielectric at different instants of time is shown in Figure 3.5.

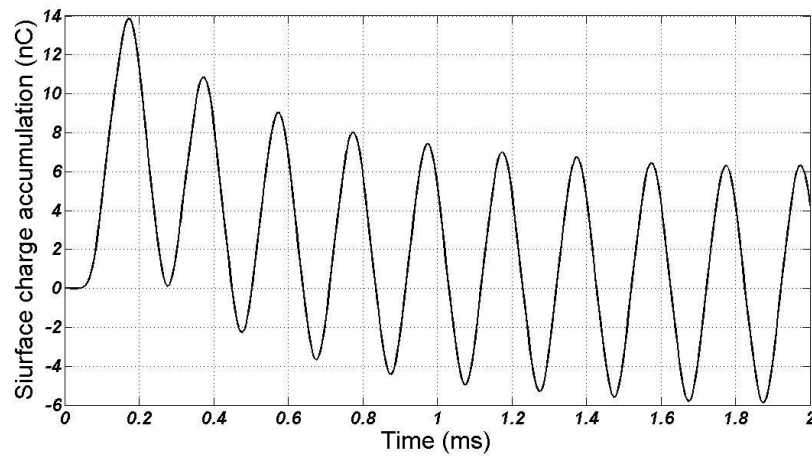


Figure 3.5: Accumulated surface charge on dielectric layer

Figure 3.6 shows the space charge density distribution in the air gap along the axis of symmetry. This depends on the voltage frequency. At higher frequencies, the ion transition time from the discharge electrode to the dielectric surface can be longer than the voltage period, therefore, at some points of the air gap there are still charges of one polarity, when the charges of opposite polarity start to be injected from the needle. At lower frequencies, like 50Hz, this may not happen, because ions have enough time to reach the collector before the needle starts to inject ions with opposite polarity. The period of one cycle at this frequency is 20ms.

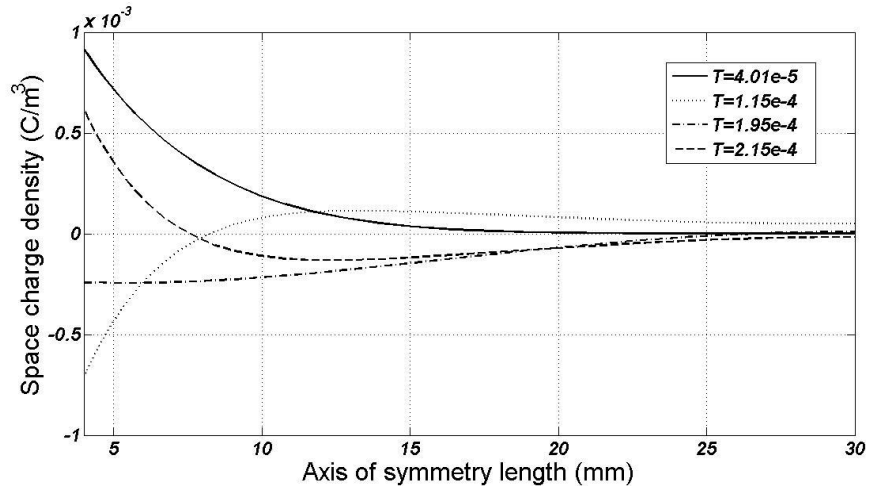


Figure 3.6: Distribution of space charge along the axis of symmetry as a function of a period

Note that at $t=4.01 \times 10^{-5}$ (s) (the positive half-cycle) just positive ions in the domain exist. For other values (for example $t=1.15 \times 10^{-4}$ (s), and $t=2.15 \times 10^{-4}$ (s)), both positive and negative are present. For $t=1.95 \times 10^{-4}$ (s) negative ions are dominant.

If all the parameters are kept the same as previous model, but the level of voltage is changed to $V_{\max}=3.2\text{kV}$, which is around the onset voltage, the waveform of the discharge current is shown in Figure 3.7.

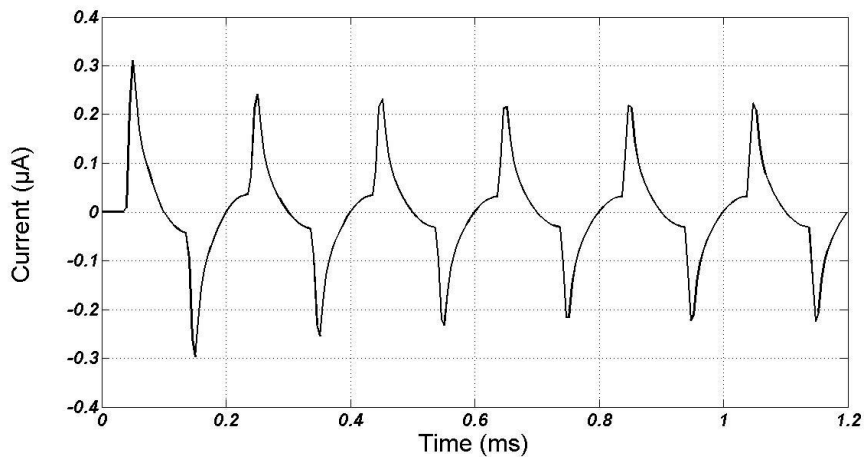


Figure 3.7: Waveform of discharge current just above the onset voltage at 5 kHz

When the maximum voltage is just above the onset level, the voltage rises above the onset for a short time and a small amount of charge is injected into the domain before injection stops. As a result, current starts to quickly decrease, but it still continues until the

next half cycle, when there is a charge injection in the opposite direction. Figure 3.8 shows the total space charge for the above case.

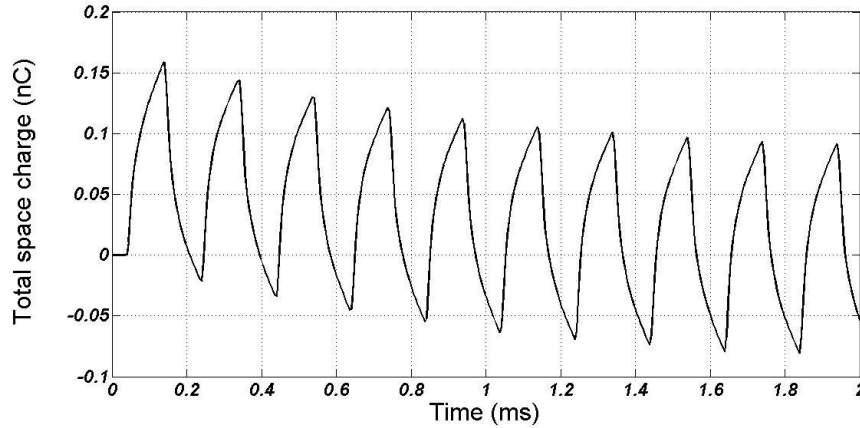


Figure 3.8: Total space charge in domain for the voltage just above onset level ($V=3.2$ kV) at 5 kHz

As shown, the waveform of the total charge in the domain is nearly the same as the basic model, but the maximum value for positive and negative ion density after a few cycles is much smaller than the previous case.

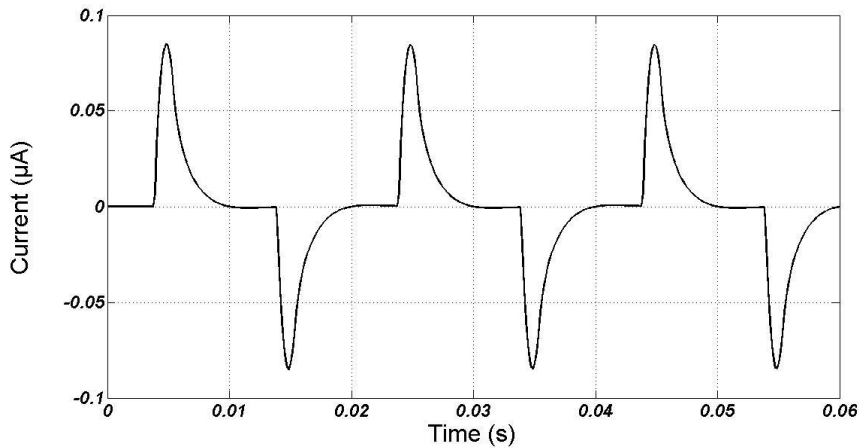


Figure 3.9: Waveform of the discharge current for the voltage just above onset level ($V=3.2$ kV) at 50 Hz

The waveform of discharge current is shown in Figure 3.9 for $V_{\max}=3.2$ kV, and frequency 50 Hz. When there is a charge injection, there is some discharge current in the domain. However, after the field at the tip falls below the onset value, the current in the domain quickly decreases. The charges have enough time to be deposited on the dielectric layer and at this moment the electric current drops to zero. Almost all the charges in the

domain are accumulated on the dielectric surface before the needle starts to inject charge in next voltage half-cycle. In Figure 3.10 the waveform of total charge in the domain is shown. Two differences can be observed as compared to the two previous cases at 5kHz. First of all, the steady-state in this case is reached after practically one cycle of the applied voltage. Secondly, in positive half cycle, positive ions are injected to the domain until the voltage drops below onset voltage. Between this point and the next half cycle, all charges in the domain have enough time to move to the dielectric layer and there are almost no charges with opposite sign in the domain at any instant of time. Because of this the current rises abruptly and then decays and at some points the current drops to zero, as there are no charges in the system to produce current.

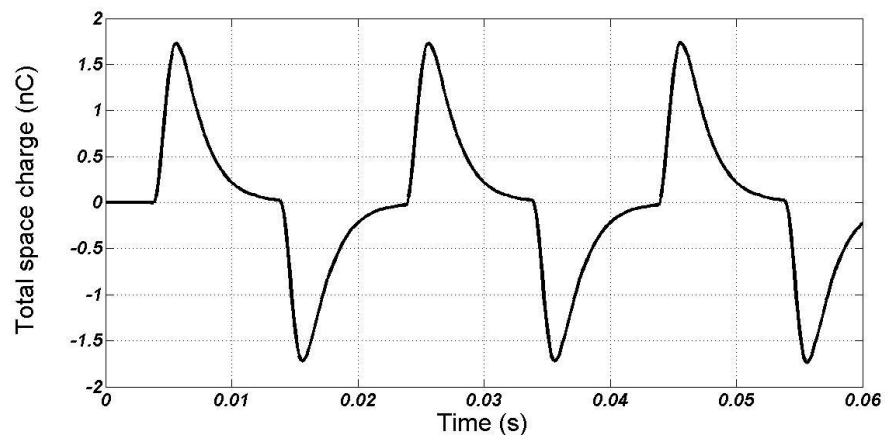


Figure 3.10: Total space charge for the voltage just above onset level at 50 Hz

Figure 3.11 shows the variation of the total space charge and the maximum current at 5kHz and for different voltage levels. As expected, at voltage levels below the onset voltage there is no charge injection and, as a result, there is no current in the domain. However, when the voltage is increased above the onset level the total corona current increases faster than linearly with the voltage. The total charge curve is almost linear.

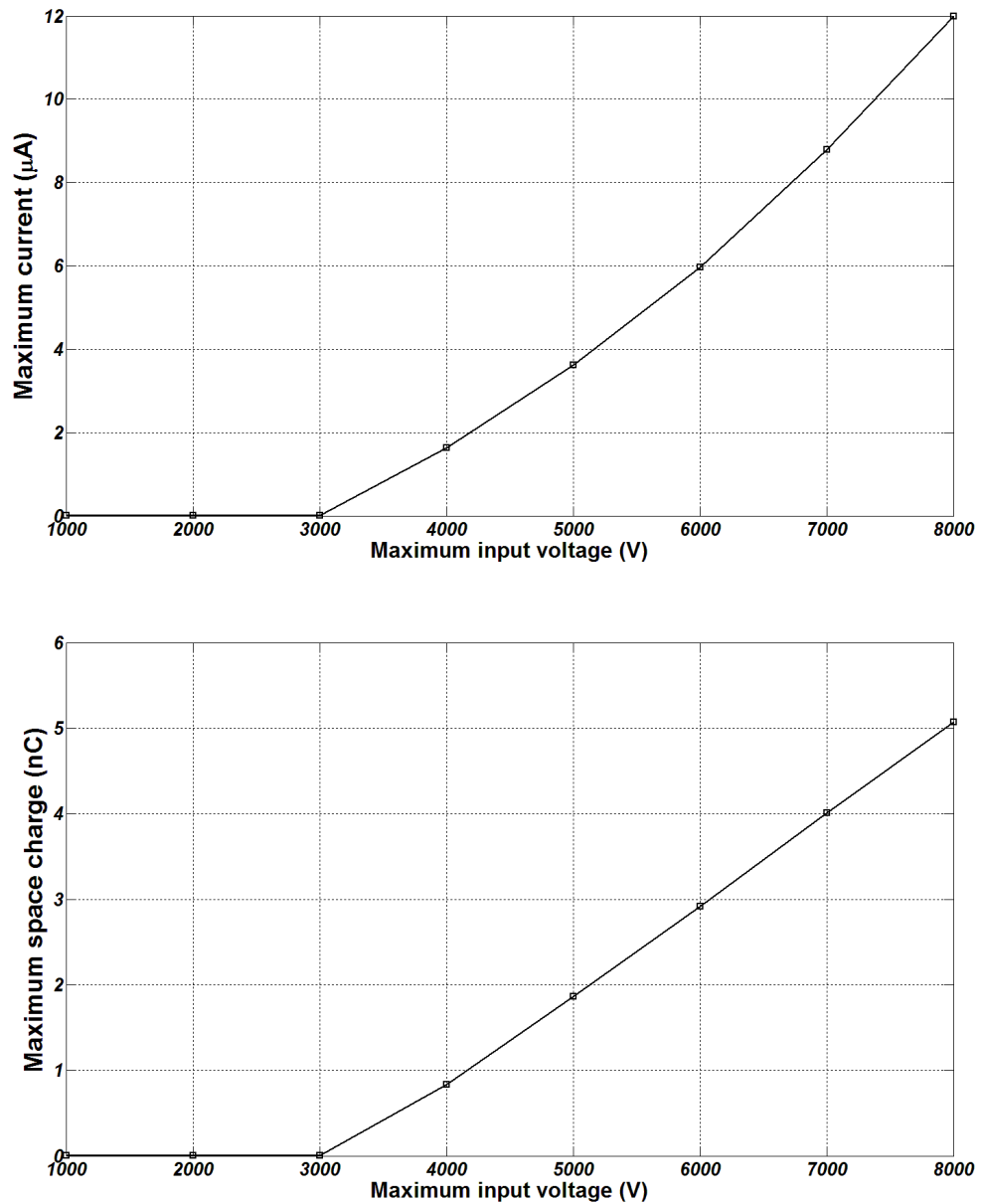


Figure 3.11: Maximum current and maximum space charge in domain at different voltages and at 5 kHz

Figure 3.12 shows the variation of the total space charge and maximum current at the fixed voltage and for different frequencies. As the frequency increases, the current level increases due to the fact that transition time from positive cycle to negative cycle gets smaller and clouds of both positive and negative ions are formed. However, the net charge in whole domain is smaller at higher frequencies, because at lower frequencies ions with

the same polarity are dominant in a half cycle, and starting from following cycle almost all the ions are settled on the dielectric layer.

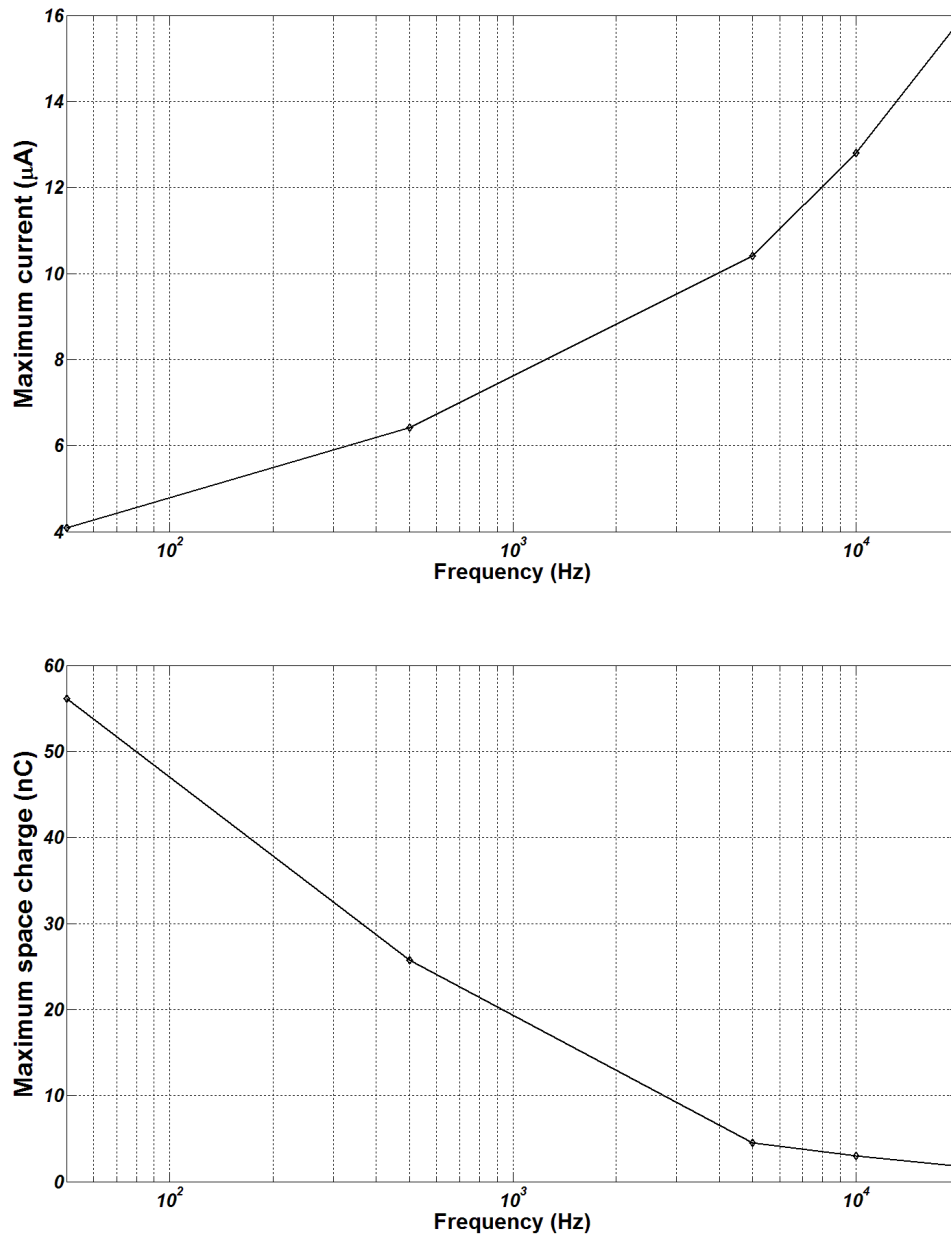


Figure 3.12: Maximum current (left hand side) and maximum space charge (right hand side) in domain at different frequencies and at 7.5 kV

3.5 Conclusion

In this chapter, a quasi-stationary single-species FEM model for simulating the dielectric barrier discharge has been proposed. The governing equations, which include the effect of

surface charge accumulation, have been derived. For the charge transport model a partial differential equation was employed and artificial diffusion has been added to obtain a stable algorithm. The main objectives of this study were to investigate the electrical behavior of the system, including electric field intensity, space charge density distribution, surface charge accumulation and total discharge current. Sensitivity analysis of voltage and frequency level has been carried out in order to investigate the time variation of the discharge. The results show the behavior of the corona current and space charge density for sinusoidal voltage at different frequencies and voltage levels. In the basic model, the current shifting was shown due to the effect of the reverse electric field produced by surface charge accumulation. Also, it was shown that for higher frequencies a combination of positive and negative ions contribute to the current generation. The shape of the current waveforms for positive and negative voltage half cycles is identical because the mobility of both species was equal. The ionization layer has been neglected and this is why the Trichel pulses in the negative half cycle were not observed. As expected, larger input voltage results in a larger current in the circuit. The average current depends on the frequency as well and increases as the frequency of input voltage increases.

References

- [1] U. Kogelschatz, "Dielectric-barrier discharges: Their history, discharge physics, and industrial applications", *Plasma Chem. Plasma Proc.*, Vol.23, pp.1-46, 2003
- [2] B. Eliasson, U. Kogelschatz, "Non-equilibrium volume plasma chemical processing", *IEEE Trans. Plasma Sci.*, Vol.19, pp.1063-77, 1991
- [3] U. Kogelschatz, "Filamentary, patterned, and diffuse barrier discharges", *IEEE Trans. Plasma Sci.*, Vol.30, pp.1400-8, 2002
- [4] S. Kanazawa, M. Kogoma, T. Moriwaki, S. Okazaki, "Stable glow plasma at atmospheric pressure", *J. Phys. D: Appl. Phys.*, Vol.21, pp.838-40, 1988
- [5] L. Yang, Y. Hao, E. Tu, X. Wang, J. Chen, "Mechanism and characteristic of dielectric barrier multi-pulse glow discharge in Helium at atmospheric pressure", *Proc. 9th Inter. Conf. Prop. Appl. Dielectr. Mat.*, pp.55-8, Harbin, China, 2009.

- [6] F. Massines, R.B. Gadri, P. Decomps, A. Rabehi, P. Segur, C. Mayoux, "Atmospheric pressure dielectric controlled glow discharges: diagnostics and modeling", Proc. Int. Conf. Phenom. Ionized Gases, ICPIG, pp.306-315 New Jersey, USA, 1996
- [7] F. Massines, A. Rabehi, P. Decomps, R. B. Gadri, P. Segur, C. Mayoux, "Experimental and theoretical study of a glow discharge at atmospheric pressure controlled by dielectric barrier", J. Appl. Phys., Vol.83, pp.2950-7, 1998
- [8] J. S. Shang, P. G. Huang, "Modeling of ac dielectric barrier discharge", J. Appl. Phys., Vol.107, pp.113302, 2010
- [9] J. S. Shanga, P. G. Huang, "Electrodynamic force of dielectric barrier discharge", J. App. Phys., Vol.109, pp.113301, 2011
- [10] R. Gouri, N. Zouzou, A. Tilmatine, L. Dascalescu, "Enhancement of submicron particle electrostatic precipitation using dielectric barrier discharge in wire to square tube configuration", J. Electrostat., Vol.71, pp.240-5, 2012
- [11] B. Dramane, N. Zouzou, E. Moreau, G. Touchard, "Electrostatic precipitation of submicron particles using a DBD in axisymmetric and planar configurations", IEEE Trans. Dielectr. Elec. Ins., Vol.6, pp.343-51, 2009
- [12] P. Sattari, G.S.P. Castle, K. Adamiak, "FEM FCT based dynamic simulation of corona discharge in point-plane configuration", IEEE Trans. Ind. App., Vol.46, pp. 1699-706, 2010
- [13] K. Adamiak, P. Atten, "Simulation of corona discharge in point-plane configuration", J. Electrostat., Vol.61, pp.85-98, 2004
- [14] W. Breazeal, K. M. Flynn, E. G. Gwinn, "Static and dynamic two-dimensional patterns in self-extinguishing discharge avalanches", Phys. Rev., Vol.52, pp.1503-15, 1995
- [15] N. Sato, "Discharge current induced by the motion of charged particles", J. Phys. D: Appl. Phys., Vol.13, pp.L3-6, 1980

Chapter 4

4 Predicted flow characteristics of a wire-nonparallel plate type electrohydrodynamic gas pump using the Finite Element Method

The aim of this study is to numerically investigate the interaction between the electrostatic field and the fluid flow in a wire-nonparallel plate configuration of electrodes. The governing equations: Poisson equation for electric field, continuity equation for charge transport and the momentum equation for gas flow were solved using the Finite Element Method assuming a highly non-uniform mesh distribution. The main outcome of this study is the determination of velocity versus pressure characteristics of the pump, which provides useful information for predicting the pump performance and for control purposes. In addition, the efficiency and optimum geometric configuration are evaluated using this model. The numerical results show that a higher voltage leads to larger velocity and higher pressure, where the gas velocity is a linear, but pressure is a non-linear function of the supplied voltage. It was also found that there is an optimum wall angle for which the air volumetric flow rate from the outlet of the pump reaches the maximum value.

4.1 Introduction

When a voltage above the corona onset level is applied between two electrodes, ions are created in the ionization layer and they drift from the high voltage electrode toward the grounded electrode(s) due to the Coulomb force. These ions collide with neutral gas molecules and exchange their momentum. The phenomenon of inducing the gas motion by corona discharge is known as the electric wind, corona wind or secondary electrohydrodynamic (EHD) flow. The whole process involves mutual interaction between the electric field, space charge density and gas flow. For the past several decades, a number of experimental and analytical investigations have been conducted to study the EHD phenomena.

Experimental investigations of velocity distributions in the EHD flow have been carried out using various techniques, such as particle-image velocimetry (PIV) [1], hot-wire anemometry [2] and laser Doppler anemometry [3]. These experimental observations have

proved the existence of the EHD flow and provided qualitative information about its characteristics.

One of the first numerical studies on the EHD flow produced by corona discharge in a 2D wire-plate electrode arrangement was presented by Yabe et al. [4], where the results of numerical simulations of the Navier–Stokes equations were presented. Later, Zhao and Adamiak [5] carried out a fundamental study of the EHD flow in the point-plane geometry, focusing on a more rigorous model of the corona discharge. A hybrid algorithm was proposed, which included the 2D Finite Element Method (FEM) for the electric potential distribution and the Method of Characteristics (MoC) for the charge transport, assuming a single species discharge model and laminar flow. A similar approach was used to simulate the air flow pattern in the wire-plate electrostatic precipitator, without [6] and with the effect [7] of the particle charge.

The above studies did not consider the effect of flow turbulence. For turbulent flow simulation, the direct Navier-Stokes approach can be used, although this would require a large number of elements to capture the wide range of local fluctuations in the flow. A number of studies were carried out for the EHD flow by solving the time-averaged Navier–Stokes equations with the $k - \varepsilon$ turbulence model [8]. Chun et al. [9] modeled the flow velocity field near the corona wire using the Finite Difference Method (FDM) and adopting the modified $k - \varepsilon$ turbulent model to include high and low Reynolds numbers. They have shown that the turbulence intensity is not just dependent on the flow Reynolds number; the EHD turbulence can be generated even for very small Reynolds numbers, if the EHD number is larger than the square of the critical Reynolds number. Although it has been mentioned that the equations were solved on a fine uniform rectilinear grid with a sufficient resolution to accurately model the system, since the configuration is highly non uniform, the FDM looks like an inadequate method to accurately model the whole phenomenon.

Other investigations on the EHD flow have been carried out in the wire-plate configuration [9, 10]. In this configuration, when a high voltage is applied to the corona wire without an external flow, the resulting EHD flow is symmetrical and no pumping effect is observed. However, it is possible to produce a net flow in one direction and obtain

a pumping effect by changing the orientation of the ground plates and forming a tilted electrode system. The basic concept of the pump is very attractive, as it directly converts the electric energy into the kinetic energy of the moving gas [11]. This type of pump may potentially have widespread applications in fluid transport, chemical transport and cooling of electronic circuits [12]. Compared to conventional gas pumps, the EHD pump offers some advantages, such as lack of moving components, simple construction, low noise operation, continuous control on the gas flow and the ability to reduce the pump size [13]. However, low efficiency of electrokinetic conversion and the generation of ozone are two major drawbacks of the EHD pumps [11].

Although the early reports on electrostatic pumps date back to the 18th century, one of the first attempts to comprehensively model this phenomenon was done much later by Robinson [11]. He derived a set of equations and carried out experiments on the needle-wire configuration. It has been proved experimentally that the level of current density produced by moving ions is almost negligible and could be ignored in the continuity equation. Other important ideas in this work were the concept of cascade pumps and calculation of the system efficiency. An approximate estimate of the pump efficiency, which was less than 1%, is probably correct, but the way the output power was calculated, based on a fixed velocity of air in the entire domain, and the relationship between the final efficiency and the device parameters, were questionable.

Recently, the wire to non-parallel plate pump has been investigated, both experimentally and numerically, by a few authors. Tsubone et al. [13] presented an experimental investigation of the effect of the location of the grounded electrode and the discharge polarity on the time averaged discharge current, velocity profile, volumetric flow rate and the pressure generation of the pump. The experimental results show that the volumetric flow rate, gas velocity and generated pressure increased for higher applied DC voltage, and that there is a non-linear relationship between the pressure and the gas velocity. Another series of experimental investigations on the effect of the polarity of the applied voltage and position of the grounded electrodes using PIV measurements have been carried out by Kocik et al. [14-15]. The results of these studies showed that the size of the vortices formed inside the EHD gas pump decrease with increased operating voltage.

One of the few numerical investigations has been done by Chang et al. [16]. The effect of corona wire position with respect to the edge of the ground electrodes and the angle of the flow channel electrodes were investigated. However, instead of using available numerical techniques to simulate the corona discharge, the authors assumed a 1D distribution of the electric field and the space charge density resulting from the analytical solution, even though their flow field was assumed to be 2D.

Until now, the published articles have been based either on the experimental investigations of the prototypes or simplified numerical techniques. However, several problems, such as the determination of the optimum wall angle for the maximum flow rate, prediction of the velocity vs. pressure characteristics, effect of the voltage level on the maximum capacity, and relation between the maximum velocity and pressure have not been investigated. The aim of this paper is to numerically investigate all these factors. The governing equations consisting of the Poisson equation for electric field, continuity equation for charge transport and the momentum equation for flow pattern using $k - \epsilon$ turbulent model were solved by using the Finite Element Method with a highly non-uniform mesh distribution.

4.2 Model description

4.2.1 Geometry

In the wire to parallel plate configuration without any external flow, applying the high voltage to the corona wire results in a symmetrical distribution of the electric field intensity and space charge density, which produces symmetric body force vectors on both sides of the corona wire. Hence, the observed EHD flow is symmetrical with four vortices and without any pumping effect. By changing the wall angle and making a tilted configuration with non-parallel plates, the electric field intensity upstream and downstream of the corona wire becomes asymmetric and unidirectional gas flow may be produced. The basic configuration for an EHD pump for 3° wall angle is shown in Figure 1 [17].

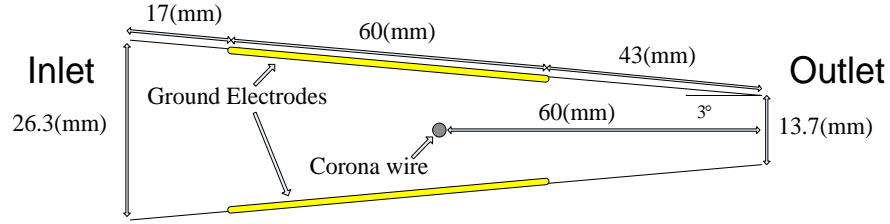


Figure 4.1: EHD pump configuration for wire to non-parallel plate system (not to scale)

The total length of the channel is 120 mm and the grounded electrode has dimensions of 60 mm \times 34 mm with 0.15 mm of thickness. The corona wire has a diameter of 0.23 mm and length of 34 mm. It is equidistant from both plates and always located 60 mm from the pump outlet. The vertical distance from grounded electrode to corona wire is 10 mm. When the plate angle changes, the distance between the corona wire and plates remains constant. This means that the inlet and outlet dimensions of the pump would be changed when the plate tilt angle varies.

4.2.2 Electrical model

The physics and governing equations for modeling a single species corona discharge are well established in numerous articles, for example in [18]. In the model used in this paper, the ionization layer around the corona wire has been neglected, and the ions, with the same polarity as the polarity of the wire voltage, are assumed to be injected from the corona electrode surface, accelerated by the Coulomb force and transported toward the ground electrode(s). This means that the electric field, space charge and gas flow are involved in the governing equations.

Poisson's equation governs the electric potential, and consequently the electric field intensity distribution for a given charge distribution [19]:

$$\nabla^2 V = -\frac{\rho_c}{\varepsilon} \quad (4.1)$$

The charge drift creates the electric current with a density defined as:

$$\vec{J} = \rho_c(\mu_e \vec{E} + \vec{u}) - D\nabla\rho \quad (4.2)$$

where \vec{J} is the electric current density, \vec{E} is the electric field intensity, \vec{u} is the gas velocity, ρ_c is the space charge density, ε is the gas permittivity, μ_e is the mobility of ions

and D is the ions diffusion coefficient. Three terms on the right hand side of Eq. (4.2) are drift, convection and diffusion currents, respectively. Under steady-state conditions, the current density must satisfy the charge conservation equation:

$$\nabla \cdot (\rho(\mu\vec{E} + \vec{u}) - D\nabla\rho) = 0 \quad (4-3)$$

Since the drift velocity of ions is usually about two orders of magnitude larger than the typical velocity of the gas flow [11], the convective component in the ionic current density can be neglected. Hence, the electric field and space charge density will be independent of the fluid motion.

4.2.3 Airflow model

In order to model the airflow, averaged distributions often provide sufficient information. The Reynolds-averaged representation of turbulent flow divides the flow velocity into an average component and a fluctuating component,

$$u_i = \bar{u}_i + u'_i$$

where u_i is the component of the velocity vector in the x_i direction and the mean velocity \bar{u}_i are determined by either time averaging or spatial averaging, depending on the flow under study. Moreover, u'_i denotes the turbulent part of the velocity. Decomposition of the flow fields into the averaged and the fluctuating component is followed by insertion into the Navier-Stokes equation. The Reynolds average Navier-Stokes (RANS) equation for an incompressible turbulent flow in the steady-state condition can be written as [19]:

$$\rho \frac{\partial}{\partial x_j} (\bar{u}_i \bar{u}_j) = \frac{\partial}{\partial x_j} \left\{ -\bar{p} \delta_{ij} + (\mu + \mu_T) \left(\frac{\partial \bar{u}_i}{\partial x_j} + \frac{\partial \bar{u}_j}{\partial x_i} \right) - \frac{2}{3} \rho k \delta_{ij} \right\} + F \quad (4-4)$$

where ρ is the gas density, p is the static pressure, δ_{ij} is the Kronecker delta, μ is the air viscosity, μ_T is the eddy-viscosity representing Reynolds stress tensor, and F is the external body force, in this case equal to the Coulomb force, $-\rho_{\text{ion}} \nabla V$. Different techniques can be used to capture the value for μ_T in the model. One of the most well known approaches and used in this study is the standard $k - \varepsilon$ model. In this version, the value of the eddy viscosity is derived using the turbulent kinetic energy (k), and the turbulent dissipation rate (ε). The detailed formulation to calculate the velocity has been provided in [20, 21].

4.2.4 Boundary conditions

The problem of the corona discharge is governed by two partial differential equations with unknown electric potential and space charge density. The boundary conditions for the potential are straightforward: a given DC electric potential (V_{ap}) on the corona electrode and zero potential on the grounded planes [16]. However, formulation of proper boundary conditions for the space charge density is not so easy because the ionization layer has been neglected. One possible approach is to use Kaptzov's hypothesis which assumes that when the corona discharge occurs at some point on the electrode, the electric field at this point remains at the corona onset value. Peek's equation is used to find the onset level in air [18]:

$$E_0 = 3.1 \times 10^6 \delta \left(1 + \frac{0.308}{\sqrt{\delta R}} \right) \left[\frac{V}{m} \right] \quad (4-5)$$

where R is the electrode radius in cm, and δ is a coefficient depending to pressure and temperature.

It must be emphasized that Peek's equation can be used only if the electric field is the same at all the points on the discharge electrode and the values of the charge density should be selected in order to satisfy the Kaptzov condition. The initial value for the space charge density has to be guessed or taken from the previous solution. After the problem is solved, the electric field on the electrode surface is compared with Peek's value and the electric charge updated. While some well-established techniques are often advised, here the following simple formula has been used to update the space charge density on the surface of corona electrode [18]:

$$(\rho_c)_{new} = (\rho_c)_{old} + \beta(E - E_0) \quad (4-6)$$

where β is an experimentally found constant and E is the actual value of the electric field. Practically, this approach provides an indirect boundary condition for the space charge density. Its distribution on the corona electrode surface is iterated until the corona electrode electric field is sufficiently close to Peek's value.

The boundary conditions for the airflow are straightforward: two collecting plates and the wire surface act as stationary walls. The outside boundary of the domain is defined as

the velocity inlet and outflow. Since the computational domain is open in this area, the air is free to flow in both directions. All boundary conditions are summarized in Table 4.1.

TABLE 4.1
Boundary conditions for the EHD pump model

Edge	Electric potential	Airflow
Inlet	$\frac{\partial V}{\partial n} = 0$	Inlet velocity
Outlet	$\frac{\partial V}{\partial n} = 0$	Outlet pressure (outflow)
Grounded electrodes	$V = 0$	No-slip sidewalls ($u_x = 0, u_y = 0$)
Corona wire	$V = V_{ap}$	No-slip sidewalls ($u_x = 0, u_y = 0$)

4.3 Numerical Algorithm

An iterative numerical algorithm for the EHD gas pump simulation has been developed. The simulation starts from some initial guess of the space charge density and then the FEM is employed to obtain the Poissonian component of the electric potential. Using the values of calculated electric field, the new charge density distribution is obtained. For the charge transport model a partial differential equation was employed and artificial diffusion has been added to obtain a stable algorithm. After convergence is reached in the corona simulation program, the body force is calculated and substituted in Equation (4.4) for the airflow simulation. This equation is again solved iteratively and when the residuals of both of the velocity components, the turbulence kinetic energy and its rate of dissipation satisfy certain minimum conditions the airflow simulation process is terminated. As already mentioned, the contribution of the charge convection has been ignored in the electrical model because it is small compared to the charge drift. The calculations can provide detailed information on the local electrical parameters of the electric discharge, including the space charge density, the current density, the electric field, the potential distribution and the consumed power. Moreover, the mechanical parameters of the airflow, such as the stream functions, path lines, velocity, and the pressure distributions can also be predicted.

4.4 Simulation results and discussion

4.4.1 Electric current

In this study, the formula for the discharge current is derived for the general electrode geometry from the energy balance equation, in which the displacement current is explicitly taken into account. For the single species corona model, without considering electrons and after a few simplifications, the corona current can be calculated as [22]:

$$I = \frac{1}{V_{ap}} \iiint \rho_c \mu_e \vec{E} \cdot \vec{E}_s dv \quad (4-7)$$

where \vec{E}_s is the static applied field without the effect of space charge and \vec{E} is the field considering effect of the space charge. Figure 4.2 shows the numerical results for the discharge current per unit length of corona wire as a function of applied voltage for two different wall angles:

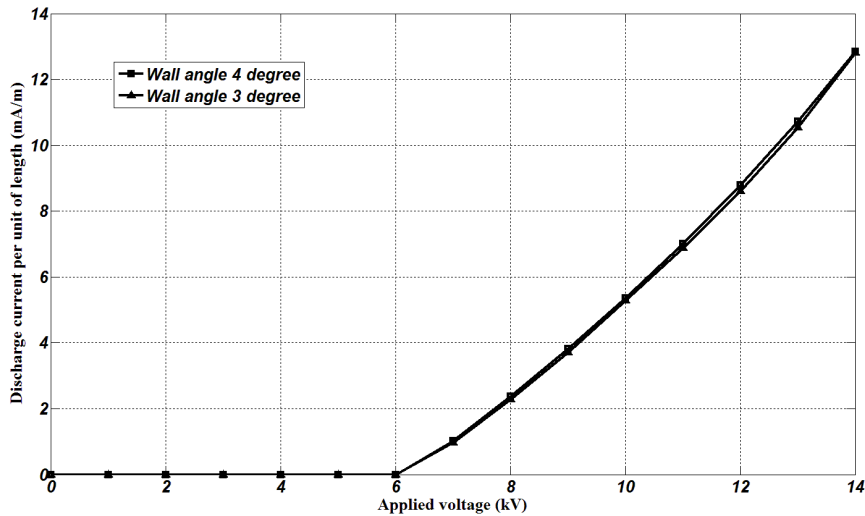


Figure 4.2: Discharge current per unit length of corona wire for EHD gas pump as a function of applied voltage

For the voltage levels below the onset value (6 kV) there is no space charge and, as a result, there is no current in the domain. As the voltage increases above the onset level the total corona current increases and agrees with the simplified analysis of Sigmond [23]. We know that the voltage onset level depends on the distribution of the electric field intensity just around the corona wire. The maximum electric field intensity occurs on the surface of the

corona wire at points facing the ground plate. The maximum charge would be injected from those points. Since the distance between the corona wire and the plate is constant and the plates are placed far enough from corona wire the current vs. voltage characteristics should be nearly the same for different plate angle.

4.4.2 Flow pattern

In order to investigate the evolution of the airflow pattern, many authors assume that the external airflow velocity is kept at some level and they observe the EHD flow pattern by gradually increasing the applied voltage [8, 14]. Since in this investigation the main goal is to study the pumping effect, the pressure difference between the inlet and outlet of the pump has been kept constant instead. The flow-pattern regime map for different voltages applied to the corona wire for the basic model described above is shown in Figure 4.3. In this figure the arrow shows the pumping direction from inlet to outlet.

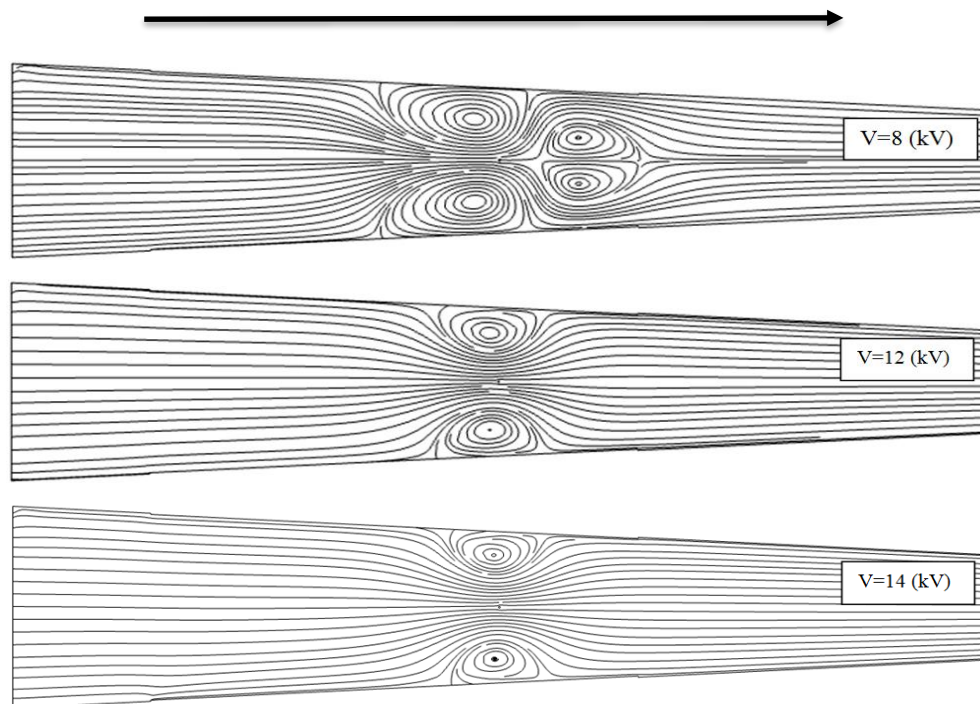


Figure 4.3: Flow patterns under different applied voltage for the same level of pressure difference ($\Delta P = 0.02 \text{ Pa}$, wall angle = 3°)

The level of pressure difference for the cases shown in Figure 4.3 has been kept equal to 0.02 Pa and the process was simulated for the increased applied voltage. For the same

level of pressure difference, at a higher level of input voltage a better pumping effect with higher level of the outlet velocity might form and consequently the vortices of the flow are smaller. Table 4.2 shows the average outlet velocity of the pump for five different values of the applied voltage.

TABLE 4.2

Average outlet velocity for the same pressure difference ($\Delta P = 0.02$ Pa) for the basic configuration

Applied voltage (kV)	Average outlet velocity (m/s)
8	0.0744
9	0.126
11	0.234
12	0.262
14	0.295

It should be noted that in this study air at room temperature and atmospheric pressure was assumed and the average mobility of the ions is considered to be $2.2 \times 10^{-4} (m^2/V.s)$, while in the real experiments this term may be dependent on the environmental conditions. In real cases the charge carriers might include heavier ions with smaller mobility, which will have greater effect on the air flow resulting in higher velocities.

4.4.3 Pressure vs. velocity characteristics

EHD pumps are characterized by two main parameters: velocity and pressure. The velocity through a channel between the inlet and outlet depends on the pressure difference across the pump, but this pressure is also controlled by the flow path outside of the pump. Therefore, a pump at a specific level of voltage is characterized by the velocity vs. pressure characteristics. It has been found that there is an analogy between the velocity vs. pressure characteristics of a pump and the current vs. voltage characteristics of a voltage source. The two main points on the current vs. voltage characteristics of a real voltage source are the short circuit current and the open circuit voltage. To derive the velocity vs. pressure curve of the pump, the same philosophy can be used. By assuming zero pressure difference between the inlet and outlet of the pump, the short circuited condition is modeled and the maximum velocity inside the pump can be determined. On the other hand, blocking the

pump, i.e. velocity equal to zero on the inlet and outlet is analogous to the open circuit condition and the pressure difference between the two sides of the pump reaches its maximum.

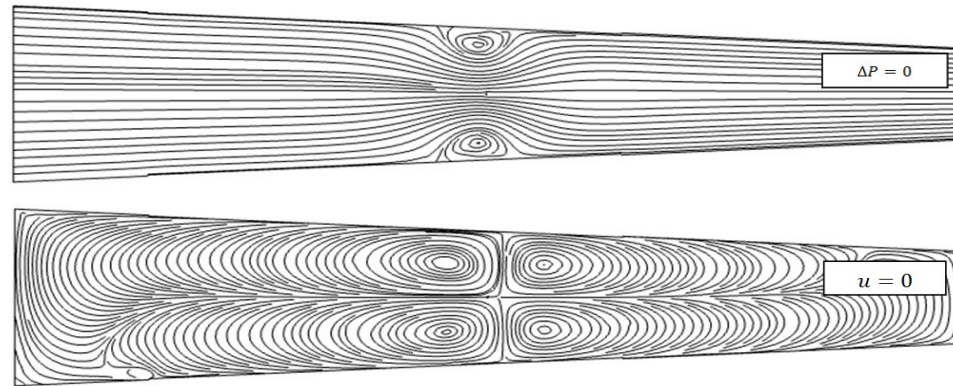
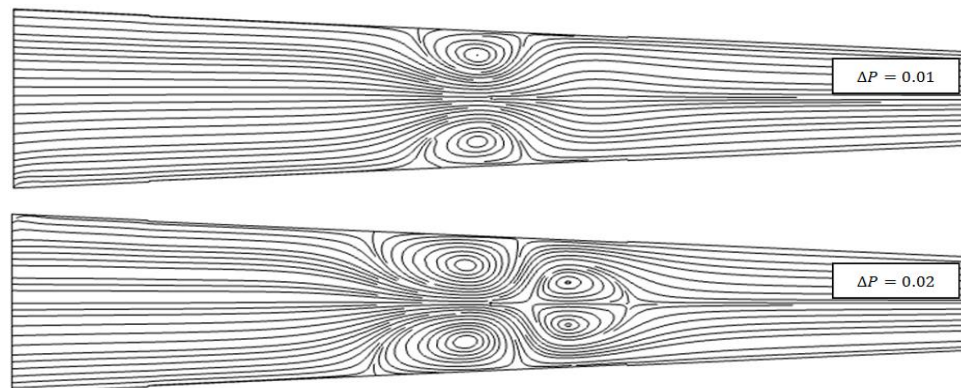


Figure 4.4: Short circuit and blocked mode of the EHD pump (wall angle = 3°)

Figure 4.4 shows these two modes of operation for the modeled pump. For $\Delta P = 0$, which in real condition corresponds to the case of a cascade of pumps forming a closed loop, the maximum capacity of the pump is observed and the velocity at the outlet reaches its maximum level. When both inlet and outlet are blocked; $u = 0$; four vortices are formed in the pump and the maximum pressure difference can be observed. By varying the pressure difference from zero up to this maximum value, the entire pump characteristics can be derived for a specific level of the applied voltage.

Figure 4.5 shows the variation of the flow pattern in the basic described model by increasing the reverse pressure for the same applied voltage equal to 8 kV. By increasing the reverse pressure, the flow velocity is reduced and eventually it is completely blocked, when the reverse pressure is equal to maximum pressure difference generated by the pump.



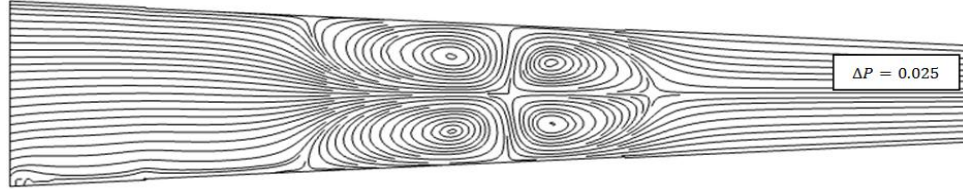


Figure 4.5: Flow patterns of the pump by changing the reverse pressure from zero up to maximum pressure for the same level of wire voltage (wall angle = 3°)

Robinson [11] has analytically proven that the relation between velocity and current is:

$$u = C_1 \sqrt{I} \quad (4-8)$$

where C_1 is the coefficient including loss, and geometry coefficients, and I is the corona current. Moreover, the relation between the current and the applied voltage has been derived in [11, 18, and 23] as:

$$I = C_2 V \times (V - V_0) \quad (4-9)$$

where C_2 is the coefficient and V is the applied voltage above the corona onset level. For voltages much higher than the corona onset voltage the Eq. (4.9) can be rewritten as:

$$I \approx C_2 V^2 \quad (4-10)$$

By merging Eq. (4.8) and (4.10):

$$u \propto V$$

Moreover, air will move through the EHD pump at the velocity at which the forward electrical pressure is matched by the aerodynamic back pressure. The latter quantity may be expressed as [11]:

$$P \approx C_3 u^2 \quad (4-11)$$

where C_3 is the coefficient and P is the pressure.

Therefore, it can be concluded that:

$$P \propto u^2 \propto V^2$$

Figure 4.6 shows the velocity vs. pressure characteristics of the studied pump for five different levels of the input voltage.

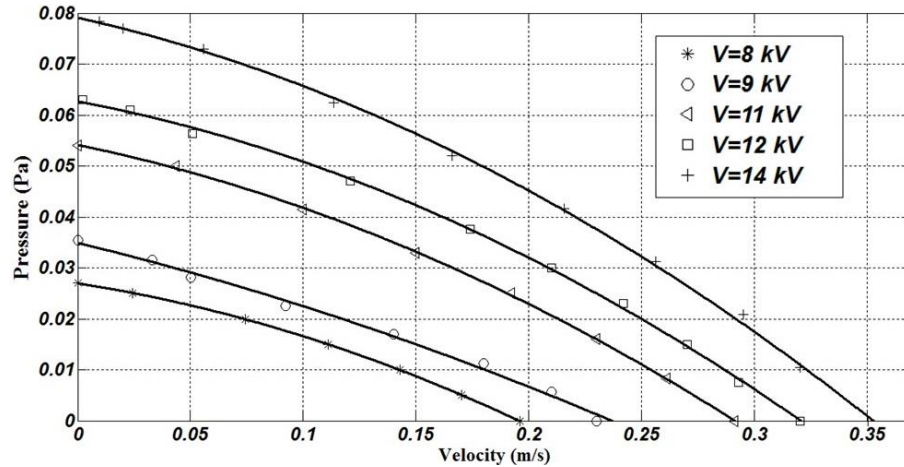


Figure 4.6: Predicted pressure vs. velocity characteristics for different levels of the applied voltage

The following can be concluded from this graph:

- 1) A higher input voltage produces a better pumping effect with a higher maximum velocity and a larger pressure difference.
- 2) The maximum velocity varies linearly with the applied voltage.
- 3) The maximum pressure varies as the square function of the applied voltage.

This relationship between the maximum pressure difference and the input voltage can be supported by the fact that the pressure difference is proportional to the momentum of air molecules in the channel and the kinetic energy's formula is a function of the velocity square:

$$P \propto \text{Kinetic energy} \propto u^2$$

Knowing that:

$$u \propto V \rightarrow \frac{u_1}{u_2} = \frac{V_1}{V_2}$$

Therefore,

$$\frac{P_1}{P_2} = \left(\frac{u_1}{u_2}\right)^2 = \left(\frac{V_1}{V_2}\right)^2$$

However, it must be noted that all the formulation in this section are based on the results for 2D model and for the full 3D model other factors might affect the velocity vs. pressure characteristics.

4.4.4 Efficiency

From the velocity profiles, the gas kinetic power and then the electromechanical efficiency of such a system may be calculated. Different techniques for computing the mechanical energy have been presented by Moreau [24]. The following formulations are used in this study in order to find the efficiency of the pump. The total current of the system can be derived from Eq. (4.7). Therefore, the consumed electric power is:

$$P_{elec} = V_{ap}I[W] \quad (4-12)$$

One problem of the previous models for the efficiency calculations [23] is that they do not consider the velocity variations inside the pump. In this work we suggest an approach, which can handle this. The mechanical power at the outlet which represents the real pumping effect is calculated. Under the assumption of a stationary flow, the mechanical power corresponds to the kinetic energy flow rate and may be expressed by:

$$P_{mech(outflow)} = \int_0^H 0.5w\rho V^3 dy [W] \quad (4-13)$$

where H and w are the height and the width of the pump, respectively.

The electro-mechanical efficiency of the pump is given by:

$$\eta = \frac{P_{mech}}{P_{elec}} \times 100 \%$$

Table 4.3 shows the variation of the system efficiency for different levels of the voltage and the 3° tilt of the wall angle.

TABLE 4.3
Total energy conversion and efficiency of the pump

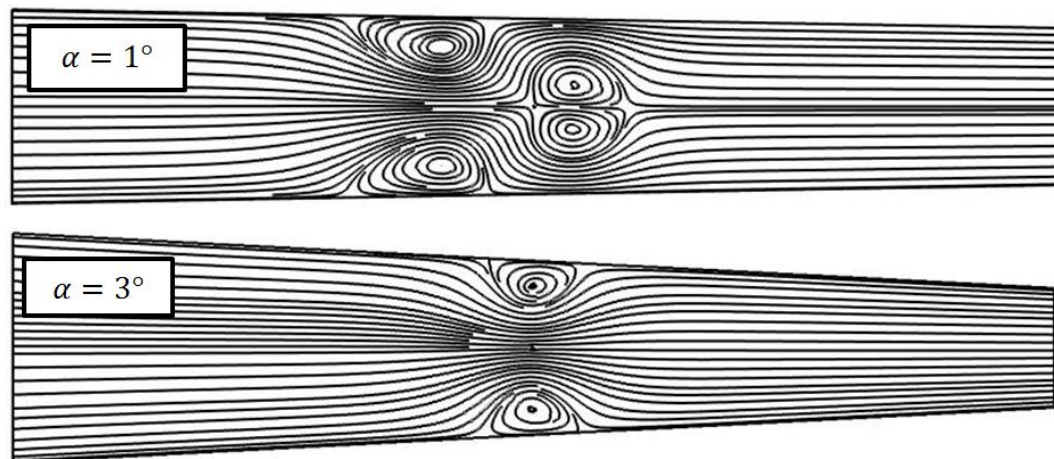
<i>Voltage (kV)</i>	<i>Current (μA)</i>	<i>P_{elec}(W)</i>	<i>P_{mech,outflow} (μW)</i>	<i>η(%)</i>
8	81.92	0.66	1	1.5e-4
9	130.5	1.17	4.3	3.7e-4
11	237.2	2.61	20	7.7e-4
12	296.8	3.56	31.6	8.9e-4
14	435.9	6.10	55.08	9e-4

Although, the electrical power consumption is fairly small, the maximum efficiency of the basic model for 3° wall angle is in order of 0.001%. Comparing the results from the

simulation with experimental data from other corona configurations shows that the derived efficiencies are much smaller than that for these experimental pumps. Although, this value is highly dependent on the configuration, dimensions of the pump and the voltage level, the differences are still higher than expected. It should be noted that in real experimental conditions, not all the ions have the mobility of negative O_2 ion, equal to $2.2 \times 10^{-4} (m^2/V.s)$. Some may, for example, consist of clusters of the water molecules, which have much smaller mobility [25]. At the same level of charge, heavier ions would cause stronger effect on the velocity profile and, as a result, the output mechanical power would be larger. This effect can be modeled by assuming a smaller effective mobility. It was found that for assumed smaller ion mobility in this case equal to $1.5 \times 10^{-4} (m^2/V.s)$ the efficiency of the pump can reach 0.01% for the same configuration as above.

4.4.5 Wall angle effect

Up to this point all the simulations have been done for the configuration with 3° tilt of the wall angle. In order to investigate the effect of this angle, the problem was also simulated for different wall angles. As before, the corona wire is always centered between the grounded electrodes and at the fixed horizontal distance from the pump outlet. All the simulations in this section have been performed for the fixed level of the supply voltage equal to 8kV. The velocity streamlines for the different wall angles and at the case of $\Delta P = 0$ are shown in Figure 4.7.



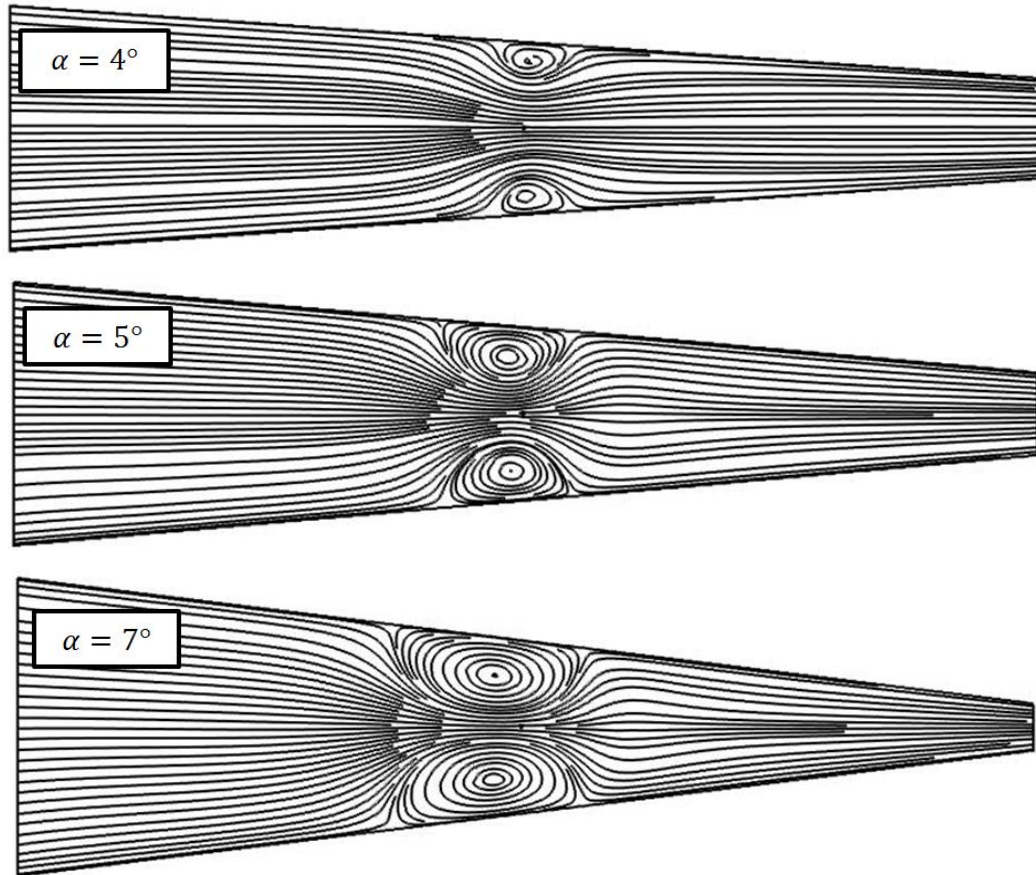


Figure 4.7: Flow streamlines for different wall angles at $V=8$ kV and $\Delta P = 0$

The flow streamlines give us a very good understanding of the pump operation. At a very small wall angle, the plates are nearly parallel and it is obvious that the pumping effect is weak with two vortices upstream and two others downstream the corona wire. As the wall angle increases up to some level, two vortices downstream the corona wire disappear and two upstream the wire get smaller, which results in an improved pumping effect. After further increasing the wall angle, the two vortices upstream the corona wire again get bigger and this somehow weakens the pumping effect. Obviously, as it was already pointed out, the size of the wakes have a direct relation with the workable kinetic energy. Bigger vortices store greater energy and this is the energy loss in the system that cannot be used for pressure generation. The effect of the wall angle on the maximum velocity, the maximum pressure difference and the maximum flow rate has been summarized in Table 4.4.

TABLE 4.4
Wall angle effect on velocity, pressure and air flow rate

Wall angle	Pressure difference $\Delta P [Pa] (u = 0)$	Outlet velocity $[m/s] (\Delta P = 0)$	Volumetric flow rate $[L/min]$
1°	0.009	0.082	3
2°	0.014	0.128	4.13
3°	0.027	0.196	5.48
4°	0.040	0.259	6.13
5°	0.050	0.272	5.32
7°	0.067	0.308	3.45

Table 4.4 shows that the maximum velocity and the maximum pressure difference at the pump outlet increases with increasing the wall angle. On the other hand, the flow rate reaches the maximum level at around 4° angle and then it starts to decrease at higher values of the wall angle. Therefore, there is an optimum value for the wall angle for which the pump produces the largest volumetric flow rate. The gas flow rate is related to the outflow velocity and the outlet cross section:

$$M \left[\frac{L}{min} \right] = V \left[\frac{m}{s} \right] \times A [m^2] \times 6 \times 10^4$$

For two different wall angles at the same level of the input voltage and for the same channel width the relation between two flow rates is:

$$\frac{M_1}{M_2} = \frac{V_1}{V_2} \times \frac{10 - 60 * \sin(\alpha_1)}{10 - 60 * \sin(\alpha_2)}$$

By increasing the wall angle the output velocity increases, but at the same time the outlet height of the pump gets smaller. As a result, there is the maximum of the flow versus wall angle curve at some point near 4° angle.

4.4.6 Conclusions

In this chapter, the results of a numerical simulation of the EHD pump have been presented for the pump model based on a single-species corona discharge model. The governing equations considering the electric field, charge transport and the gas motion were solved. For the charge transport an artificial diffusion has been added to obtain a stable algorithm.

The main objectives of this study were the investigation on both the electrical behavior of the system including the electric field intensity, the space charge distribution and the total corona current in addition to the mechanical properties of the system, including the velocity vs. pressure characteristics of the pump, the velocity streamlines. From this it was possible to derive the optimum configuration and the efficiency of the system. The results show that:

- a) At the same level of the pressure difference a higher voltage results in a higher outlet velocity and a better pumping effect.
- b) An analogy was found between the EHD pump and the real voltage source in order to capture the velocity vs. pressure characteristics of the pump, based on the short circuit and open circuit tests.
- c) The maximum velocity of the pump varies linearly with the applied voltage and the maximum pressure difference is a square function of the applied voltage.
- d) Mechanical power converted in the channel is found to be much smaller than the input power. The efficiency of the system is in the order of 0.001%. It was found that the efficiency of the system increases by considering heavier ions with smaller mobilities.
- e) For the assumed pump length and the vertical distance between corona wire and ground plates, an optimum wall angle of the pump considering the maximum volumetric gas flow rate is about the 4°.

Acknowledgments

The paper was partially supported by the Natural Science and Engineering Research Council (NSERC) of Canada. The authors would like to thank CMC MICROSYSTEM for providing access to the COMSOL commercial software.

References

- [1] T. Ullum, P.S. Larsen, O. Özcan, “Three-dimensional flow and turbulence structure in electrostatic precipitator by stereo PIV”, *Exp. Fluids*, Vol.36:1, pp.91–9, 2004
- [2] J.H. Davidson, E.J. Shaughnessy, “Turbulence generation by electric body forces,” *Exp. Fluids*, Vol.4:1, pp.17–26, 1986

- [3] P. Bequin, K. Castor, J. Scholten, "Electric wind characterization in negative point-to-plane corona discharges in air," *J. Eur. Phys., Appl. Phys.*, Vol.22:1, pp.41–9, 2003
- [4] A. Yabe, Y. Mori, K. Hijikata, "EHD study of the corona wind between wire and plate electrodes", *J. AIAA*, Vol.16:4, pp. 340–5, 1978
- [5] L. Zhao, K. Adamiak, "EHD flow in air produced by electric corona discharge in pin-plate configuration", *J. Electrostat.*, Vol.63, pp. 337-50, 2005
- [6] L. Zhao, K. Adamiak, "Numerical simulation of the electrohydrodynamic flow in a single wire-plate electrostatic precipitator", *IEEE Trans. Ind. App.*, Vol.44:3, pp. 683-91, 2008
- [7] K. Adamiak, P. Atten, "Numerical simulation of the 2-D gas flow modified by the action of charged fine particles in a single-wire ESP", *IEEE Trans. Dielectr. Elec. Ins.*, Vol.16:3, pp.608-14, 2009
- [8] W.J. Liang, T.H. Lin, "The characteristics of ionic wind and its effect on electrostatic precipitators", *Aerosol Sci. Tech.*, Vol.20:4, pp. 330–44, 1994
- [9] Y. N. Chun, A. A. Berezin, J. Mizeraczyk, J. S. Chang, "Numerical modeling of near corona wire electrohydrodynamic flow in a wire-plate electrostatic precipitator," *IEEE Trans. Dielec. Electr. Insul.*, Vol.14:1, pp.119-124, 2007
- [10] T. Yamamoto, H.R. Velkoff, "Electrohydrodynamics in an electrostatic precipitator", *J. Fluid Mech.*, Vol.108, pp. 1–18, 1981
- [11] M. Robinson, "Movement of air in the electric wind of the corona discharge", *AIEE Trans.*, pp.143–50, 1961
- [12] J. S. Chang, K. Urashima, "Electrohydrodynamic gas flow regime map in a wire-plate type electrostatic precipitator", *Int. J. Plas. Env. Sci. Tech.*, Vol.3:2, pp.2597-600, 2009
- [13] H. Tsubone, J. Ueno, B. Komeili, S. Minami, G.D. Harvel, K. Urashima, C.Y. Ching, J.S. Chang," Flow characteristics of DC wire-non-parallel plate electrohydrodynamic gas pumps", *J. Electrostat.*, Vol.66, pp.115–121, 2008
- [14] M. Kocik, J. Podliński, J. Mizeraczyk, J.S. Chang, "Particle image velocimetry measurements of wire nonparallel plates type electrohydrodynamic gas pump", *IEEE Tran. Dielec. Electr. Insul.*, Vol.16:2, pp. 312-319, 2009

- [15] M. Kocik, J. Podliński, J. Mizeraczyk, K. Urashima, J.S. Chang, “Flow distribution measurement in wire-nonparallel plate type electrohydrodynamic gas pump by a particle image velocimetry”, *IEEE Trans. Dielec. Electr. Insul.*, Vol.16:3, pp. 601-7, 2009
- [16] J.S. Chang, H. Tsubone, Y.N. Chun, A.A. Berezin, K. Urashima, “Mechanism of electrohydrodynamically induced flow in a wire-non-parallel plate electrode type gas pump”, *J. Electrostat.*, Vol.67, pp. 335–9, 2009
- [17] J. S. Chang, H. Tsubone, N. Buenconsejo Jr., J. Ueno, G. D. Harvel, J. Mizeraczyk, and K. Urashima, “Corona Discharge and Flow Characteristics of Wire-Plate Type Electrohydrodynamic Gas Pumps : Ground Plate Convergent Angle Effect”, 28th ICPIG, Prague, Czech Republic, 2007,
- [18] K. Adamiak, P. Atten, “Simulation of corona discharge in point-plane configuration”, *J. Electrostatics*, Vol.61, pp. 85-98, 2004
- [19] P. Sattari, G. S. P. Castle, K. Adamiak, “FEM FCT based dynamic simulation of corona discharge in point–plane configuration”, *IEEE Trans. Ind. App.*, Vol.46, pp. 1699-706, 2010
- [20] S.B. Pope, “Turbulent Flows”, Cambridge, 2000
- [21] H. Tennekes, J. L. Lumley, “A First Course in Turbulence”, MIT Press, 1972
- [22] N. Sato, “Discharge current induced by the motion of charged particles”, *J. Phys. D: Appl. Phys.*, Vol.13, pp. L3-6, 1980
- [23] R.S. Sigmond, “Simple approximate treatment of unipolar space-charge-dominated coronas: the Warburg law and the saturation current”, *J. Appl. Phys.*, Vol.53, pp. 891–8, 1982
- [24] E. Moreau, “Airflow control by non-thermal plasma actuators”, *J. Phys. D: Appl. Phys.*, Vol.40, pp. 605–36, 2007
- [25] P. Giubbilini, “Mobility measurement of large ions in air from a point-to-ring corona source”, *J. Appl. Phys.*, Vol.81, pp. 2101–04, 1997

Chapter 5

5 Numerical Modeling of Electrohydrodynamic Interactions in the Boundary Layer of Air Flows

In this study, the physics of a 2D corona system is numerically simulated in order to study the physical mechanisms associated with the DC corona discharge to actively modify low-velocity airflow along a flat plate. The model involves mutual interaction between the electric field, space charge density and gas flow. A single species model for positive corona discharge has been developed in this study. Velocity profiles within the boundary layer of the flat plate are presented for a free air stream velocity up to a few meters per second. The effect of voltage level and inlet air velocity on the electrical current level has been discussed. The numerical model was used to investigate the air control characteristics of the corona actuator as a function of voltage and plate orientation. Their effects on the mechanical drag and electro-kinetic efficiency were also studied. The results show that the velocity of the ionic wind at the wall increases with applied voltage and the EHD actuator causes a drag reduction.

5.1 Introduction

When a voltage above the corona onset level is applied between two electrodes, ions are created in the ionization layer and they drift from the high voltage electrode towards the grounded electrode due to the Coulomb force. The whole process involves mutual interaction between an electric field, ionic space charge and gas flow. This phenomenon of inducing the gas motion by corona discharge is known as the electric wind, corona wind or secondary electrohydrodynamic (EHD) flow [1]. The studies for utilizing high voltage discharge induced EHD applications have been conducted in a variety of fields, such as air flow control [2-4], separation control over airfoils [5], cooling of electronic circuits, dust particle collections, etc. [6, 7]. The main advantage of this process is that it directly converts electrical energy into kinetic energy of moving gas without any mechanical elements. The gas motion generated by corona discharge could be used to modify the airflow profile, or to control the laminar-turbulent transition regime around exposed obstacles. This objective can be achieved by controlling the airflow velocity magnitude in

the layer very close to the surface of the object. By using EHD, fluid motion shows a better mechanical behavior and improved flow stability by eliminating unsteadiness, unwanted vibrations, noise and losses [8-11].

For the past several decades, experimental and analytical investigations have been conducted to study the EHD phenomena for the boundary layer control. Experimental investigations of velocity distributions in the EHD flow have been carried out using various techniques, such as particle-image velocimetry (PIV) [12, 13]. Léger in [8] has conducted a series of measurements by PIV techniques in order to determine the influence of a DC corona discharge established between a wire and a grounded plane electrode on the properties of airflow around a flat plate for different angle of attack. Results showed that the kinetic energy induced by the ionic wind inside the boundary layer allows a reduction of the drag force for low external velocities. However, in their experimental set-up, the effect of the corona discharge did not take place as close to the wall as desired, probably because of the not optimized configuration.

Electrodes placed on the surface can be viewed as a form of surface roughness. Such roughness contributes to the drag formation directly through re-arrangement of the flow field, and indirectly through changes in the laminar-turbulent transition process. Effect of roughness geometry can be captured using the reduced-order geometry model [14, 15] and its proper distribution can lead to drag reduction [16- 19]. It might also be possible to combine the effect of plasma injection with the proper electrode distribution to take advantage of both drag reducing effects.

Study on different electrode configurations was investigated in detail [20] and the configuration which showed the best performance consisted of two wires with different radii of curvature as anode and cathode placed inside a groove downstream on the plate. Finally, an experimental study was performed [21] in order to investigate the influence of the external velocity on system performance for velocities up to $25m/s$. It has been noted that the corona system has lower impact on the higher external velocities. However, a significant drag reduction has been measured even at higher velocities. Another interesting result of this study was the relation between the inlet velocity and the discharge current. It

has been claimed that the discharge current could double in some cases by increasing the external velocity. In almost all the experimental investigations an ionic wind of several meters per second was reported; it contributed to enhance the velocity profile and consequently drag reduction. Study on AC corona discharge was carried out by Soetomo [22], who experimentally observed a drag reduction effect induced by AC and DC corona discharges along a flat plate in the case of flow velocities up to 2m/s.

Series of numerical studies on the boundary layer control based on previous experiments were done by Colver [23-25]. Important aspect of the study is the ability of the model to consider ion deposition and removal on the plate surface assuming a uniform small surface conductivity. Therefore, the positive ions can migrate along the plate surface. The development of a corona discharge was evaluated numerically over a finite region of a semi-infinite flat plate in the presence of flowing gas. In this study the authors used the Finite Difference Method (FDM) to solve the problem using a simple discretization of the computational domain. Because the corona discharge has a strongly non uniform behavior around the corona wire, alternative numerical techniques, like the Finite Element Method (FEM), might be more useful. Moreover, this study was limited to low-velocity airflows.

Until now, the published articles have been based either on experimental investigations or simplified numerical techniques. The aim of this paper is to numerically investigate the electrical and mechanical properties of the corona system around a flat plate using FEM. In order to simulate the model, a single species model for a DC positive input voltage is presented in this paper. In the case of a DC positive-corona discharge, positive ions produced at the anode collide with neutral gas molecules and exchange their momentum. The governing equations: the Poisson equation for electric field, continuity equation for charge transport and the momentum equation for flow pattern using a turbulent model were solved using the FEM with a highly non-uniform mesh distribution. The equation for the total force on the air in the boundary layer including the effect of the electrostatic body force is developed in this study. The efficiency of the system has been calculated by defining a control volume contour around the corona wire. The effect of voltage level on the velocity profile and the effect of external velocity on the discharge current as well as a study on the tilted configuration have been done. Results show the drag reduction occurs

even at higher velocities, but the corona system has a smaller effect at the higher external velocities and the efficiency of the system decreases at higher voltage levels.

5.2 Model description

5.2.1 Geometry

Figure 5.1 shows the two-dimensional model of a flat plate with corona and grounded wires mounted on the insulating surface. It must be noted that the electrodes should be placed in a way to perturb the flow as minimum as possible when the discharge is not acting on the airflow, and the corona system should have the ability to create a tangential EHD force in close vicinity to the wall. In order to fulfill those requirements the corona system was assumed to consist of two electrodes placed on the insulating surface of the plate. The values for the corona and grounded wire thickness, and the distance between these two wires are the same as it was reported by Moreau [21]. The corona wire consists of a 0.7mm diameter copper wire electrode mounted on the surface of the plate and located 10cm downstream of the leading edge. The cathode is a 2mm diameter wire, located 4cm downstream of the corona wire.

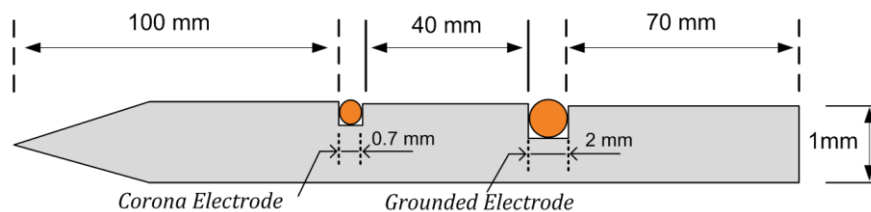


Figure 5.1: Configuration for the corona wire and grounded wire

5.2.2 Boundary layer

When a viscous fluid flows along a rigid surface, an essential condition is that the velocity at any point on the wall is zero. If the viscosity is small without being negligible, the modifying effect appears to be confined within narrow regions adjacent to the solid surfaces called the boundary layer. The flow adjacent to the plate is retarded and the velocity gradually grows from zero to the free-stream value at some distance from the wall [26]. Let's consider a homogeneous free-stream flow with speed U_∞ parallel to an infinitely thin, flat plate located along the positive x-axis (Figure 5.2).

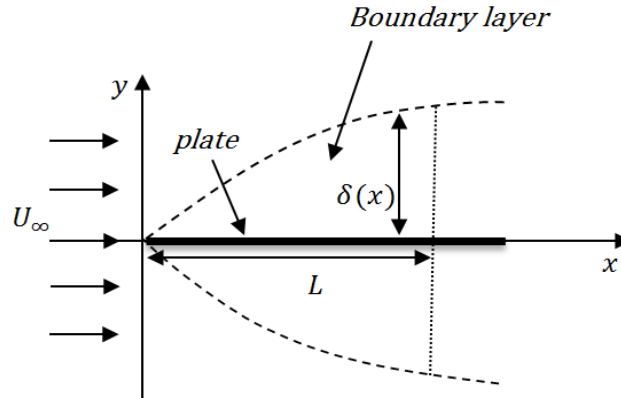


Figure 5.2: Flow over a flat plate

It has been shown that the boundary layer thickness, which is the distance between the surface and the point where the velocity is equal free-stream value, is proportional to the square root of the kinematic viscosity [26]. Since the effect of the viscosity in the boundary layer decreases as we move outward from the wall, the boundary layer thickness at any point on the plate would depend on the distance of the point from the leading edge of the plate. Details of the formulations and the numerical techniques for solving this equation have been published in numerous articles [26, 27]. Generally, if the boundary layer thickness being defined as the point that the velocity of the position is equal to 99 percent of the free air velocity, it has been shown that the boundary layer thickness on the flat plate would be equal to [26]:

$$\delta_{99}(x) \cong 5.0 \sqrt{\frac{x\mu}{\rho U_\infty}} \quad (5-1)$$

Where ρ is the fluid density, μ is the dynamic viscosity of the fluid, and x is the distance from leading edge. This x -dependent value will be used later on for the drag force formulation.

5.2.3 Fluid flow model

Detailed descriptions of the governing equations are given in [26]. The summary of the equations of motion for the two-dimensional flow are:

$$\frac{\partial u}{\partial x} + \frac{\partial v}{\partial y} = 0$$

$$\frac{\partial u}{\partial t} + u \frac{\partial u}{\partial x} + v \frac{\partial u}{\partial y} = -\frac{1}{\rho} \frac{\partial P}{\partial x} + \frac{\mu}{\rho} \frac{\partial^2 u}{\partial y^2} + \frac{1}{\rho} F$$

$$-\frac{1}{\rho} \frac{\partial P}{\partial y} = 0$$
(5-2)

In this case Equation (5.2) could be simplified since the simulation is in steady state condition. Moreover, for the flow along a plate parallel to the stream velocity, it was assumed there is no pressure gradient, so the momentum equation in the x direction for steady motion in the boundary layer is:

$$u \frac{\partial u}{\partial x} + v \frac{\partial u}{\partial y} = \lambda \frac{\partial^2 u}{\partial y^2} + \frac{\rho_c}{\rho} E_x$$
(5-3)

where u and v are the velocity components in the x and y directions, respectively, λ is the fluid kinematic viscosity, E_x is the electric field strength in the x direction, and ρ_c is the positive ion charge density. To solve the system of equations above we need to specify initial and boundary conditions. At the plate surface there is no flow across it, which implies that:

$$v = 0 \text{ at } y = 0$$

Due to the viscosity we have the no slip condition at the plate. In other words,

$$u = 0 \text{ at } y = 0$$

At infinity, outside the boundary layer and away from the plate, we have

$$u \rightarrow U_\infty \text{ as } y \rightarrow \infty$$

5.2.4 Electrical model

A full dynamic model of the corona discharge is quite complicated, because it involves many ionic species and reactions [28]. In order to investigate EHD effects of the corona discharge a much simpler single species model is usually sufficient. The physics and governing equations for modeling this model have been well established in the literature

[29]. In the model used in this paper, the ionization layer around the corona wire has been neglected, and the ions, with the same polarity as the polarity of the wire voltage, are assumed to be injected from the corona electrode surface, accelerated by the Coulomb force and transported toward the ground electrode. This means that the electric field, space charge and gas flow are involved in the governing equations. Poisson's equation governs the electric potential, and consequently the electric field intensity distribution for a given charge distribution [30]:

$$\nabla^2 V = -\frac{\rho_c}{\varepsilon} \quad (5-4)$$

The charge drift creates the electric current with a density defined as:

$$\vec{J} = \rho_c(\mu_e \vec{E} + \vec{u}) - D \nabla \rho_c \quad (5-5)$$

where \vec{J} is the electric current density, \vec{E} is the electric field intensity, \vec{u} is the gas velocity, ε is the gas permittivity, μ_e is the mobility of ions and D is the ions diffusion coefficient. Three terms on the right hand side of Equation (5.5) are drift, convection and diffusion currents, respectively. Under steady-state conditions, the current density must satisfy the charge conservation equation:

$$\nabla \cdot (\rho_c(\mu_e \vec{E} + \vec{u}) - D \nabla \rho_c) = 0 \quad (5-6)$$

Generally, since the drift velocity of ions is usually about two orders of magnitude larger than the typical velocity of the gas flow [31], the convective component in the ionic current density can be neglected. As a result the electric field and space charge density will be independent of the fluid motion. However, in this study in the glow discharge regime we are interested to see the effect of the flow velocity rate on the current level; so, a fully coupled model has been developed.

The problem of the corona discharge is governed by two partial differential equations with unknown electric potential and space charge density. The boundary conditions for the potential are straightforward: a given DC electric potential (V_{ap}) on the corona electrode and zero potential on the grounded planes [29]. However, formulation of proper boundary conditions for the space charge density is not so easy because the ionization layer has been

neglected. One possible approach is to use Kaptzov's hypothesis which assumes that when the corona discharge occurs at some point on the electrode, the electric field at this point remains at the corona onset value. Peek's equation is used to find the onset level in air [29]:

$$E_0 = 3.1 \times 10^6 \left(1 + \frac{0.308}{\sqrt{R}}\right) \left[\frac{V}{m}\right] \quad (5-7)$$

where R is the electrode radius in cm.

It must be emphasized that Peek's equation can be used only if the electric field is the same at all the points on the discharge electrode and the values of the charge density should be selected in order to satisfy the Kaptzov condition. The initial value for the space charge density has to be guessed or taken from the previous solution. After the problem is solved, the electric field on the electrode surface is compared with Peek's value and the electric charge updated. While some more elegant techniques are often advised, here the following simple formula has been used to update the space charge density on the surface of corona electrode [29]:

$$\rho_c^{new} = \rho_c^{old} + \beta(E - E_0) \quad (5-8)$$

where β is an experimentally found constant and E is the actual value of the electric field. Practically, this approach provides an indirect boundary condition for the space charge density. Its distribution on the corona electrode surface is iterated until the corona electrode electric field is sufficiently close to Peek's value.

5.3 Numerical method

It must be noted that the ionic wind in this case is mainly caused by the ion drift and electrons have negligible effect due to their small mass compared to the ion mass. Therefore, an iterative numerical algorithm based on a single species model for the boundary layer control simulation has been developed. The simulation starts from some initial guess of the space charge density, velocity component and then the conventional FEM procedure is employed to obtain the Poisson component of the electric potential. For the charge transport model a partial differential equation is solved, but an artificial diffusion has been added to obtain a stable algorithm. After calculating the potential

distribution, the electric field is calculated by differentiating the potential distribution. Using the values of calculated electric field, the new charge density distribution is obtained. This process continues and the iterative algorithm also updates the injected charge density on the corona electrode surface until the electric field values are sufficiently close to Peek's value. After convergence is reached in the corona simulation program, the body force is calculated and substituted in Eq. (5.3) for the airflow simulation. This equation is again solved iteratively and when the residuals of both of the velocity components, the turbulence kinetic energy and its rate of dissipation satisfy certain minimum conditions the airflow simulation process is terminated. At this point, the new values for velocity components need to be entered into the charge continuity equation and the whole process will continue to the point that all variables satisfy a certain error criterion. The calculations can provide detailed information on the local electrical parameters of the electric discharge, including the space charge density, the current density, the electric field, the potential distribution and the consumed power. Moreover, the mechanical parameters of the airflow, such as velocity, the pressure distributions and drag force can also be calculated.

5.4 Results and discussion

5.4.1 Current

In this study, the formula for the discharge current is derived for the general electrode geometry from the energy balance equation, in which the displacement current is explicitly taken into account. For the single species corona model, without considering electrons and after a few simplifications, the corona current can be calculated as [32]:

$$I = \frac{1}{V_{ap}} \iiint \rho_c \mu_e \vec{E} \cdot \vec{E}_s dv \quad (5-9)$$

where \vec{E}_s is the static applied field without the effect of space charge and \vec{E} is the field considering effect of the space charge.

Figure 5.3 shows the numerical results for the discharge current per unit length of corona wire as a function of applied voltage for zero input velocity. In order to check the

accuracy of the model, the numerical results have been compared with the experimental results [21].

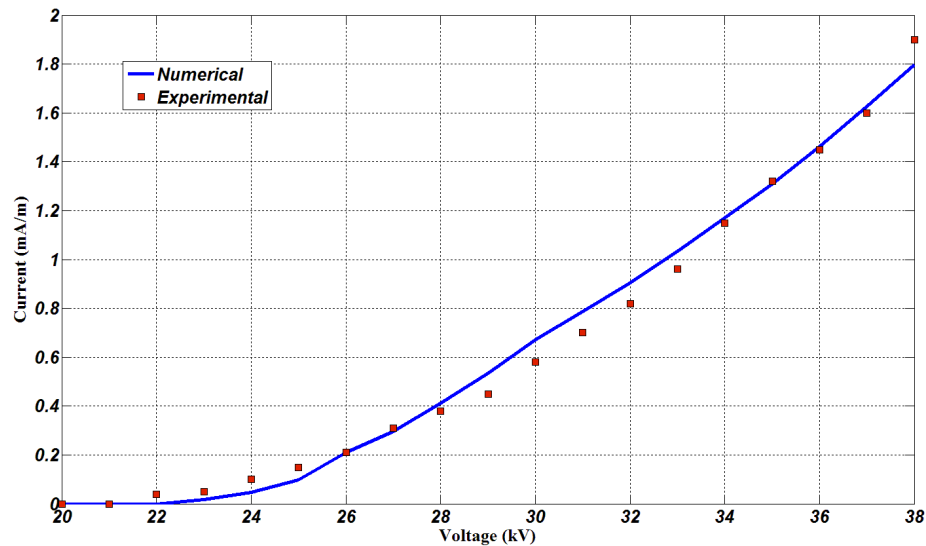


Figure 5.3: Corona discharge current versus voltage

For the voltage levels below the onset value (22 kV) there is no space charge and, as a result, there is no current in the domain. As the voltage increases above the onset level the total corona current increases and agrees with the simplified analysis of Sigmond [33]. One of the issues that need to be addressed is the effect of the gas velocity on the discharge current level, and whether it has a major effect in the glow regime velocity range or not. Moreau [21] has studied the effect of free air velocity on the current level for both glow discharge and streamer regimes. It has been mentioned that in the configurations used in their study, the glow regime is preferable, and the streamer regime appears when the ambient air humidity and the free air stream velocity are higher than some threshold values. Based on their results below 12m/s the discharge is of the glow type, while above 12m/s it becomes the streamer discharge. They have shown that by increasing the free air velocity (U_{∞}) the discharge current increases almost linearly due to the convection of positive ions by the airflow from the anode to the cathode. In our computational model, there is some effect of the ion convection on the current density level; however, for the velocity spectrum that we have studied, the current density at 12m/s is not more than 6% higher than that at the zero velocity. Moreover, El-Khabiry and Colver [25] have presented a graph which shows the effect of the air velocity on the current magnitude for 0 and 15m/s. In their work,

even for such big input velocities, the corona current for 15m/s, which supposedly is in the streamer regime, is only about 20% higher than for zero stream velocity. By looking at the results presented by Moreau et al. [21] up to 12m/s the rate of the current increase is very smooth and the slope of the current versus velocity curve is small. However, when the velocity is larger than 12m/s, the velocity effect on the current level is much stronger. Apparently, effect of the free air velocity on the current level would be strong when the regime of operation will change from the glow discharge to the streamer discharge.

5.4.2 Velocity profile

In order to study the corona effect the velocity profile for inlet velocity equal to 2m/s has been shown in Figure 5.4 for a system with/without corona discharge. The effect of the corona generated EHD flow on the air flow in the boundary layer is clearly visible: the velocity streamlines would be attracted to the area close to the surface and re-emerging as a wall jet. By using this feature, momentum would be injected in regions of boundary layer. Depending on the geometry and the configuration of the corona electrodes, the corona discharge contributes up to a few meters per second to the velocity profile enhancement.

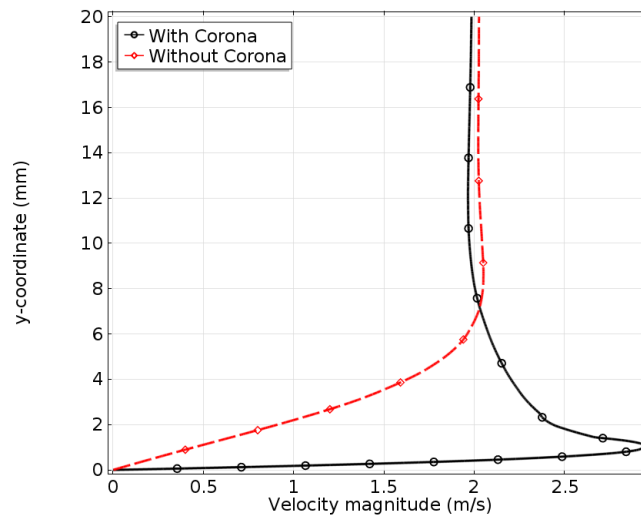


Figure 5.4: Velocity profile for the system with/without corona at $x=1\text{cm}$ ahead of corona wire for $U_\infty=2\text{ m/s}$.

After increasing the velocity level, this type of pattern, where the maximum velocity is greater than the input velocity, is not dominant anymore. Figure 5.5 compares the velocity profiles for different input velocities up to 12m/s. As it can be seen, up to 5m/s there is still

an overshoot pattern for the velocity profile with corona discharge effect. However, for higher velocity levels, for example 10 or 12 m/s, the velocity profile for the system with corona is nearly the same as for the system without discharge, and the only effect of corona discharge is to increase the velocity level close to the surface of the solid wall, which, as it will be discussed later, results in a smaller drag force level. From Figure 5.5 it can also be noted that the corona system has a smaller effect at higher input velocities. It can be described by the fact that the discharge energy is almost constant for different air velocities while the energy of the airflow in these regions increases with its velocity.

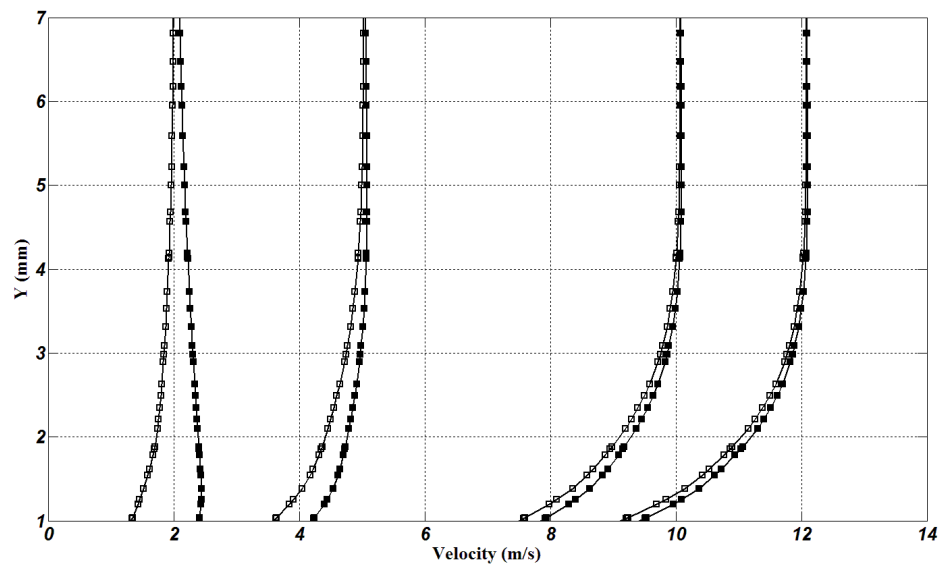


Figure 5.5: Velocity profiles without discharge (□) and with corona discharge (■) at $x=1\text{ cm}$ for $U_\infty=2, 5, 10$ and 12 m/s .

Obviously, the velocity profiles are different for different x positions. Figure 5.6 shows the velocity profiles for input voltage equal to 38kV and different x positions ahead of the corona wire, assuming the input velocity value $U_\infty=1\text{ m/s}$.

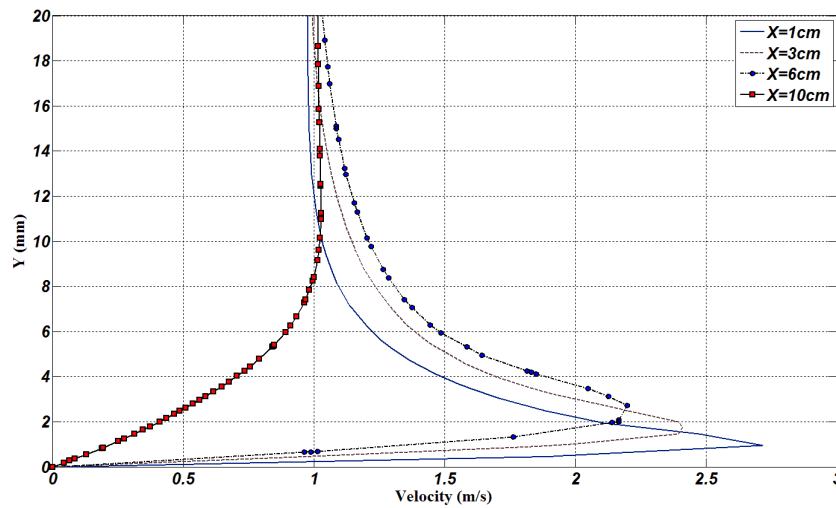


Figure 5.6: Velocity profiles induced by corona discharge for the input voltage 38kV for different x values

At points closer to the corona wire the body force is greater and the effect of corona discharge on the velocity profile is more pronounced, while at distances further from corona wire the maximum velocity level and the effect on the velocity profile decreases. However, the electric corona discharge always improves the velocity profile for all points along the x axis as compared with the system without corona discharge.

5.4.3 Effect of the Voltage Level

The onset voltage for this configuration is about 22kV. When the applied voltage increases above that level, the capability of the system to increase the airflow velocity closer to the wall is enhanced. The maximum velocities obtained are 0.89, 1.78, 2.37 and 2.87m/s for voltages equal to 26, 30, 34 and 38kV, respectively. This is due to the fact that electric field intensity and ionic current is larger at higher voltages and, as a result, the body force is higher. Figure 5.7 shows the evolution of the velocity pattern for different applied voltages. By looking at this Figure it can be seen that the velocity level close to the wall has the maximum value and further from the flat plate it reaches the free stream velocity. In this figure the input velocity is equal to zero and the ionic wind is the only effect.

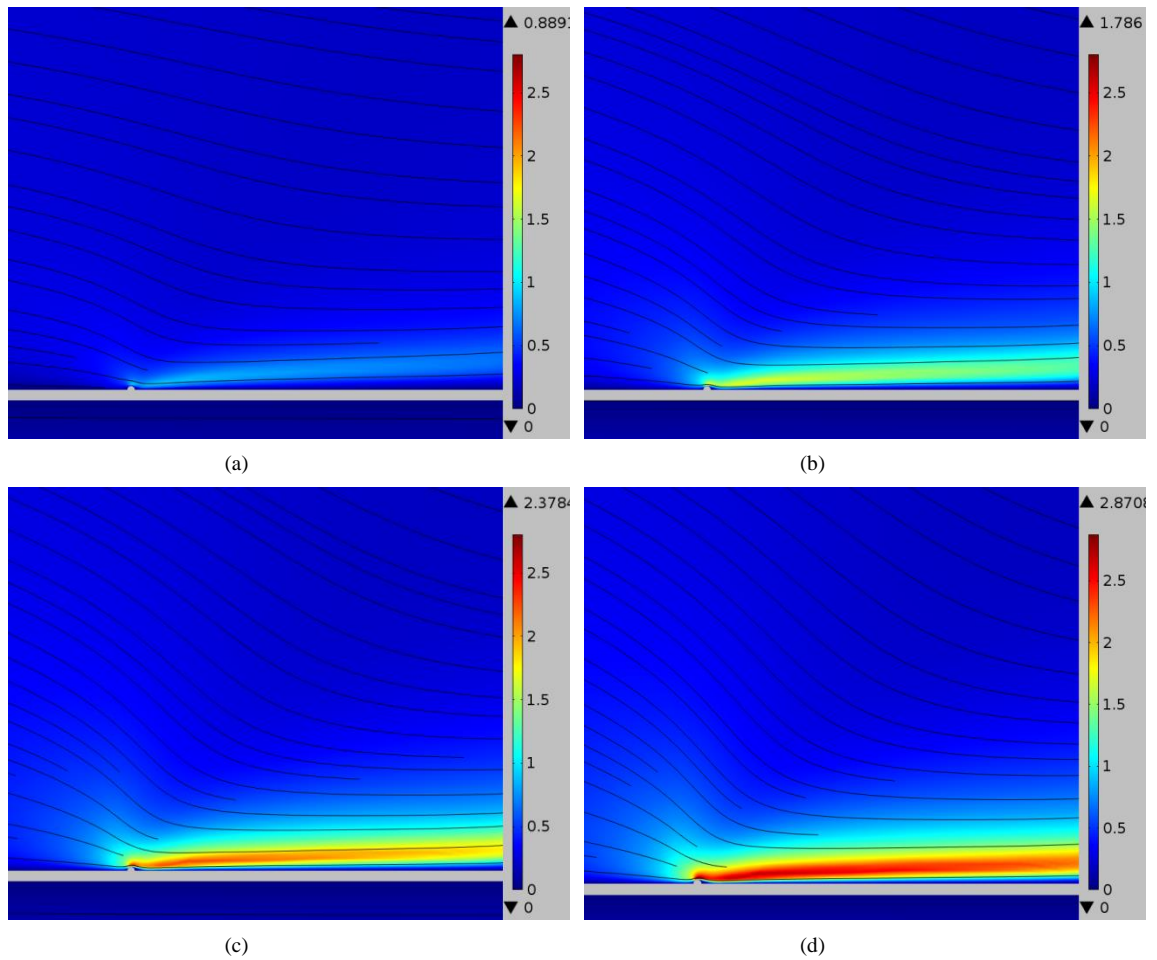


Figure 5.7: Velocity profiles for $U_\infty \approx 0$ and different applied voltages (a) 26kV, (b) 30kV, (c) 34 kV, (d) 38kV

Figure 5.8 shows the velocity distribution along a line normal to the wall at $x=1\text{cm}$ ahead of the corona wire for different applied voltages. Higher voltages at the same level of air stream velocity have a greater effect on the velocity profile close to the flat plate surface.

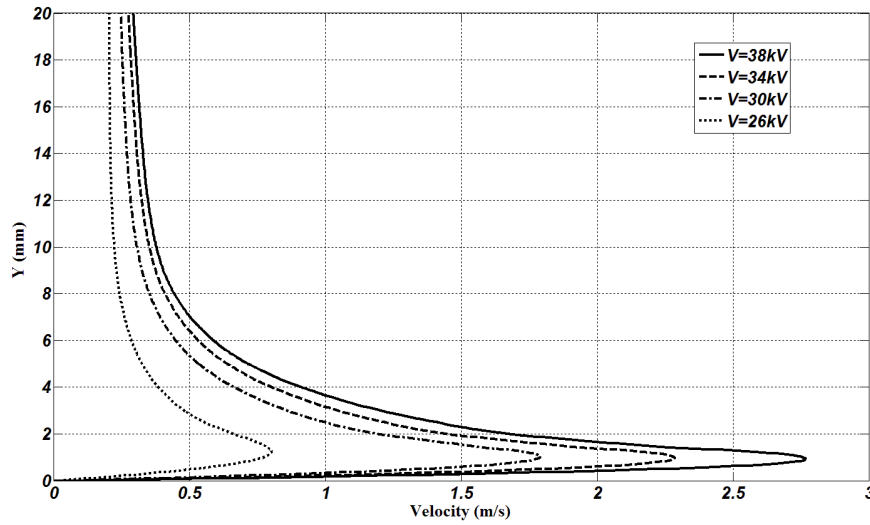


Figure 5.8: Velocity profiles induced by the ionic wind along a line normal to the wall for different applied voltages at $x=1\text{cm}$ ahead of the corona wire

5.4.4 Total force

Our goal is to determine the total force acting on air flow in the boundary layer resulted by corona discharge. This force is the accumulation of the frictional drag force and the body force produced by the corona system. Let us consider the boundary layer developing over a flat plate, as shown in Figure 5.9.

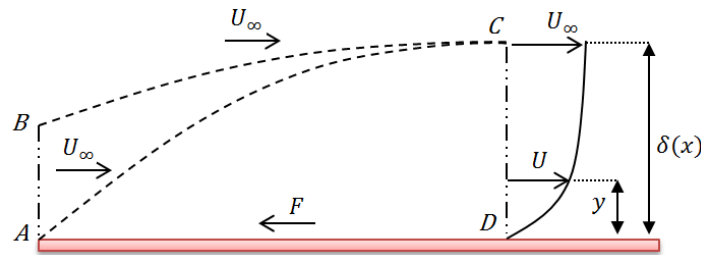


Figure 5.9: Boundary layer formation around the flat plate

The total force can be found by applying the momentum theorem:

$$\sum \vec{F} = (w \int \rho \vec{U} |U| dy)_{Outlet} - (w \int \rho \vec{U} |U| dy)_{Inlet} \quad (5-10)$$

where w is the plate width. By defining the control volume:

$$-\sum F = w \int_D^C \rho U^2 \cos(\theta) dy - w \int_A^B \rho U_\infty^2 dy$$

Since U_∞ is constant all over $|AP|$:

$$\int_A^B U_\infty^2 dy = U_\infty^2 |AB|$$

Continuity equation gives:

$$\int_A^B U_\infty^2 dy = U_\infty^2 |AB| = \int_D^C U dy = \int_0^\delta U dy$$

Therefore,

$$\sum F = w U_\infty \int_0^\delta \rho U dy - w \int_0^\delta \rho U_\infty^2 \cos(\theta) dy$$

For low-viscosity fluids, total force:

$$\sum F = w \rho \int_0^\delta U_\infty (U_\infty - U) dy \quad (5-11)$$

Figure 5.10 shows the total force over the flat plate for different input velocity levels at 38 kV applied voltage. Simulation results confirm the reduction of the total force in the velocity levels up to 12m/s. Moreover, it was found that for the velocities up to 3.5 m/s, the electrostatic force not only compensates the effect of the drag force but also changes the direction of the total force.

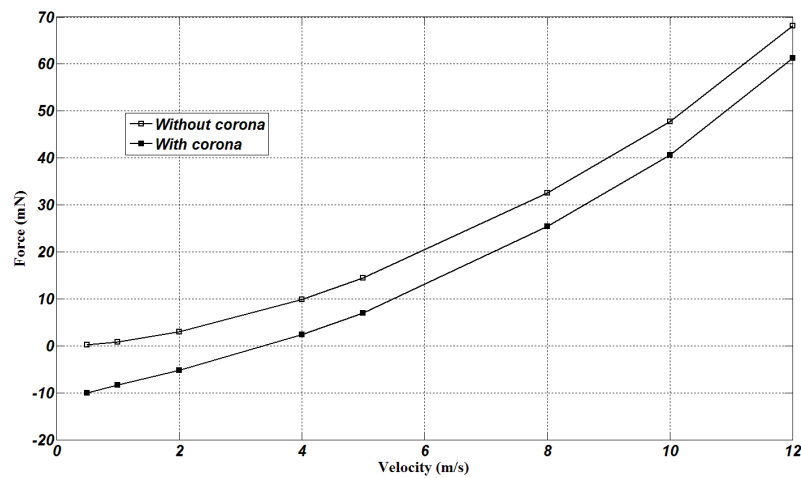


Figure 5.10: Total force calculation at $x=1$ cm ahead of corona wire versus airflow velocity U_∞ in absence and in presence of the corona discharge

In order to find the total force at $x=1\text{cm}$ ahead of corona wire, Eq.(5.11) is applied for the section of the velocity distribution up to the point when the velocity reaches its steady state value. For the system with corona effect up to 3.5m/s , velocity reaches a maximum value larger than U_∞ , and then it starts to decrease to the point that it is nearly equal to input velocity. So, the value of $(U_\infty-U)$ in Eq. (5.11) would be negative in almost all the points on the graph with corona, while it is positive for almost all the points on the graph for the system without corona. As a result the force value for the system with corona is negative at those velocity levels.

5.4.5 Efficiency

The purpose of using electric discharge is to convert electrical energy into kinetic energy inside the boundary layer in order to accelerate the flow close to the wall. From the velocity profiles, the gas kinetic power and then the electromechanical efficiency of the investigated system may be calculated. The total current of the system can be derived from Eq. (5.9). Therefore, the consumed electric power is:

$$P_{elec} = V_{ap} \cdot I [W] \quad (5-12)$$

In order to find the efficiency of the model, the same algorithm as presented by Moreau [21], has been used in this study. The concept is that a control volume has been defined at a certain distance upstream and downstream of the corona wire. It was proven that the total power loss could be calculated from:

$$P_{loss} = \left(w \int \frac{1}{2} \rho U^2 \vec{U} \cdot \vec{n} dy \right)_{inlet} - \left(w \int \frac{1}{2} \rho U^2 \vec{U} \cdot \vec{n} dy \right)_{outlet} \quad (5-13)$$

The total electrical power converted to the mechanical power could be calculated from:

$$P_{mech} = (P_{loss})_{off} - (P_{loss})_{on} \quad (5-14)$$

The mechanical power added to the airflow by the electrical discharge thus corresponds to the power loss without discharge $(P_{loss})_{off}$ minus the power loss with discharge $(P_{loss})_{on}$. Then, the efficiency is defined as:

$$\eta = \frac{P_{mech}}{P_{elec}}$$

Figure 5.11 shows the efficiency of the electrokinetic energy conversion for the free air velocity equal to 5m/s. It is obvious that the higher applied voltages result in smaller efficiency levels. It was already discussed that the relative effect of the corona discharge at higher velocities is smaller than at lower velocities. It also looks that the efficiency has a reverse linear relation with the applied voltage.

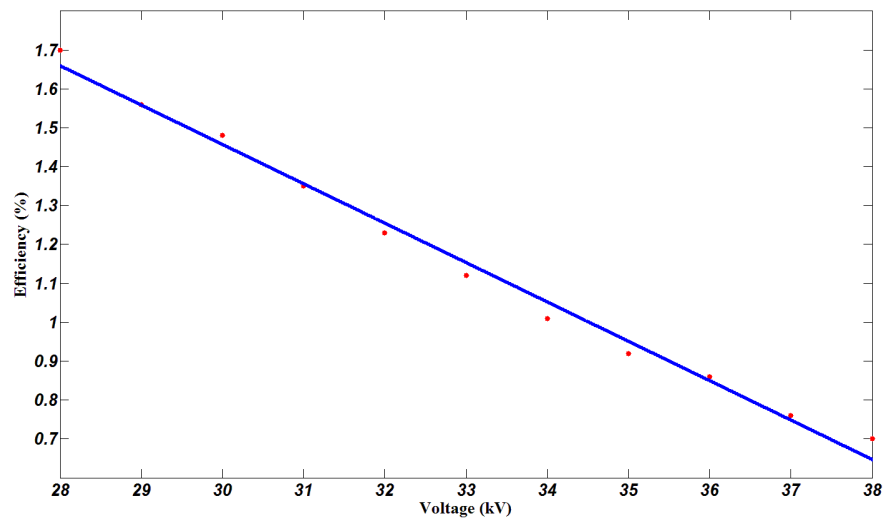


Figure 5.11: Efficiency versus applied voltage for $U_{\infty}=5$ m/s.

5.4.6 Angle of attack

In Figure 5.12, we can see the airflow around the flat plate with zero, 10° and 20° degree of orientation with a free airstream velocity 0.5m/s in the absence and presence of the DC discharge. Without the corona effect the air flow separates from the wall at the leading edge, forming a significant wake just above the flat plate. In the case of corona discharge, the airflow is reattached to the wall. This process modifies the laminar–turbulent transition inside the boundary layer and reduces the drag. Moreover, this results shows that the DC discharge creates the airflow parallel to the wall.

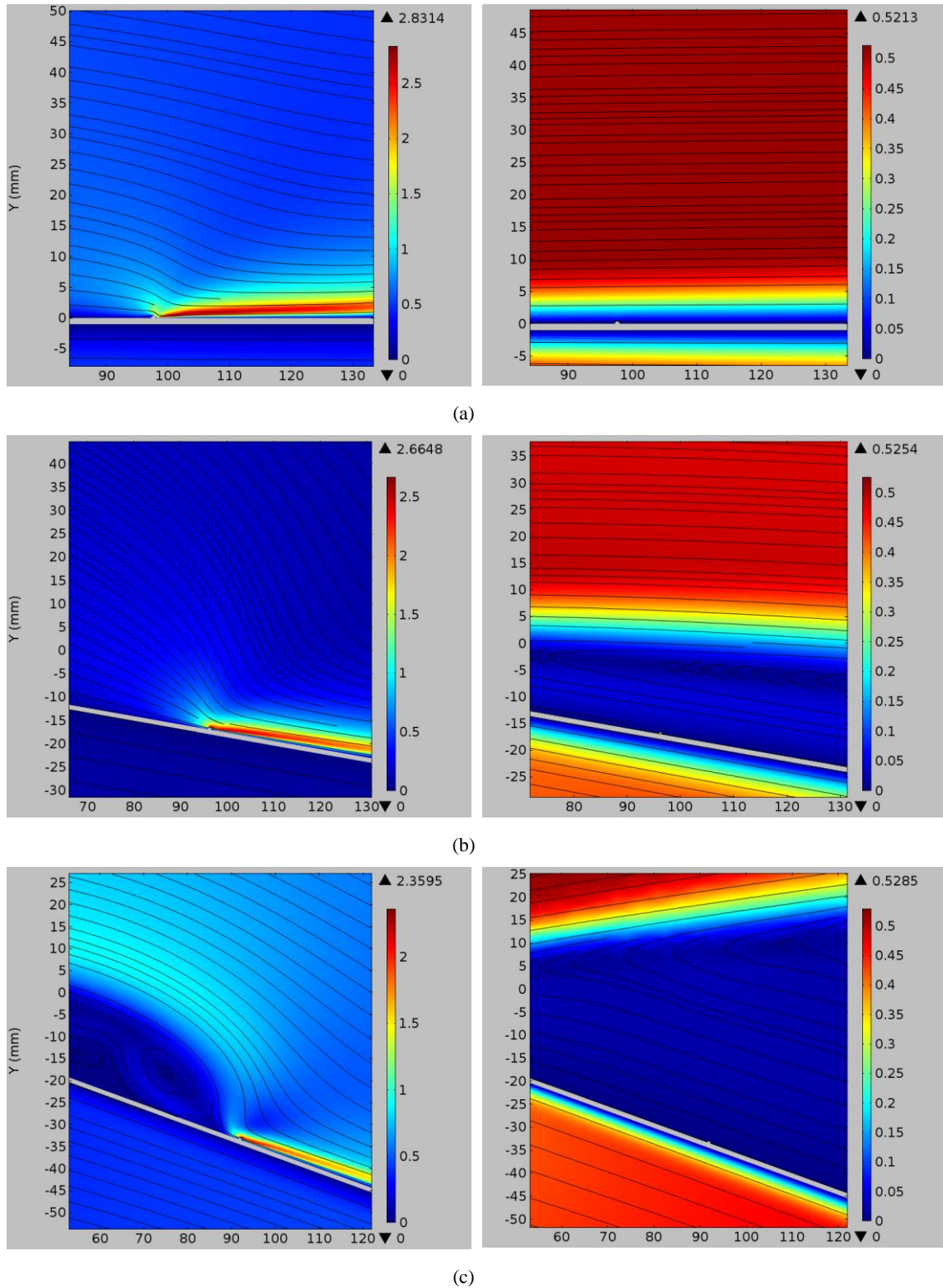


Figure 5.12: Velocity distribution with (left) and without (right) the corona effect for input velocity $U_\infty=0.5$ m/s and a flat plate at (a) 0° , (b) 10° , (c) 20° .

5.5 Summary

In this paper, we have studied the use of positive DC corona discharge to control low velocity airflow along a flat plate. Velocity profiles within the boundary layer of the flat plate have been investigated for air velocities up to 12m/s. For the velocities below this value the corona discharge is in the glow regime and the total behavior of the system is stable. The corona system consisting two cylindrical wires with different radii mounted on the plate surface, which was found to be the most efficient geometry, has been used in this study. In the case of free air velocity equal to zero, the ionic wind produced by the corona reaches the value of about 2.5m/s. The current is formed mostly by the drift of ionic species, with the diffusion and convection components much smaller. Even though after increasing the free air velocity the current density increases, but since for all the simulations the discharge is in the glow regime, the current increase is not more than 6%. While in the streamer regime the current level would be doubled for an increased free stream velocity.

Regardless of the current level, a consistent drag reduction has been shown for velocities up to 12m/s. Also, up to some velocity level the forces produced by corona system not only compensate the effect of the drag but also changes the force vector direction. It is shown that the effect of the corona discharge at higher free air velocity gets smaller. This phenomenon has been illustrated clearly by showing the velocity profiles. Although the kinetic energy induced by corona discharge is greater for higher voltage levels, the efficiency of the system has a reverse relation with the voltage level. In general, the maximum efficiency of such model is about 2%.

References

- [1] L. Zhao, K. Adamiak, "EHD flow in air produced by electric corona discharge in pin-plate configuration", *J. of Electrost.*, Vol.63, pp.337-50, 2005
- [2] T. Corke, C. Enloe, S. Wilkinson, "Dielectric barrier discharge plasma actuators for flow control", *Ann. Rev. Fluid Mech.*, Vol. 42, pp.505–29, 2010
- [3] E. Moreau, "Airflow control by non-thermal plasma actuators", *J. Phys. D: Appl. Phys.*, Vol.40, pp. 605–36, 2007

- [4] J. D'Adamo, G. Artana, E. Moreau, G. Touchard, "Control of the airflow close to a flat plate with electrohydrodynamic actuators", Proc. ASME Flow Ins. & Con., pp. 1339- 44, Montreal, Canada, 2002
- [5] T. Corke, E. Jumper, M. Post, D. Orlov, T. McLaughlin, "Applications of weakly-ionized plasmas as wing flow-control devices", 40th AIAA Aero. Sci. Meeting & Exhibit, Pap. No. 2002-0350, Reston, USA, 2002
- [6] H. Tsubone, J. Ueno, B. Komeili, S. Minami, G.D. Harvel, K. Urashima, C.Y. Ching, J.S. Chang, "Flow characteristics of DC wire-non-parallel plate electrohydrodynamic gas pumps", J. Electrostat., Vol.66, pp.115–21, 2008
- [7] K. Adamiak, "Numerical models in simulating wire-plate electrostatic precipitators: A review", J. Electrostat., Vol.71, pp. 673-80, 2013
- [8] L. Leger, E. Moreau, G. Artana, G. Touchard, "Influence of a DC corona discharge on the airflow along an inclined flat plate", J. Electrostat., Vol.51-52, pp.300-6, 2001
- [9] L. Leger, E. Moreau, G. Touchard, "Electrohydrodynamic airflow control along a flat plate by a DC surface corona discharge - Velocity profile and wall pressure measurements", 1st AIAA Flow Control Conf., Pap. No. 2002-2833, St. Louis, USA, 2002
- [10] G. Artana, G. Diprimio, G. Desimone, E. Moreau, G. Touchard, "Electrohydrodynamic actuators on a subsonic airflow around a circular cylinder", 32nd AIAA Plasma Dynamics & Laser Conf., Pap. No. 2001-3056, Anaheim, California, 2001
- [11] G. Artana, J. D'Adamo, L. Leger, E. Moreau, G. Touchard, "Flow Control with Electrohydrodynamic Actuators", J. AIAA, Vol.40:9, pp.1773–9, 2002
- [12] T. Ullum, P.S. Larsen, O. Özcan, "Three-dimensional flow and turbulence structure in electrostatic precipitator by stereo PIV", Exp. Fluids, Vol.36:1, pp.91–9, 2004
- [13] M. Kocik, J. Podliński, J. Mizeraczyk, J.S. Chang, "Particle image velocimetry measurements of wire nonparallel plates type electrohydrodynamic gas pump", IEEE Trans. Dielectr. Elec. Ins., Vol.16:2, pp. 312-9, 2009
- [14] J.M. Floryan, "Stability of wall-bounded shear layers in the presence of simulated distributed surface roughness", J. Fluid Mech., Vol.335, pp.29–55, 1997

- [15] J.M. Floryan, “Three-dimensional instabilities of laminar flow in a rough channel and the concept of hydraulically smooth wall”, *Euro. J. Mech. B: Fluids*, Vol.26, pp. 305–329, 2007
- [16] A. Mohammadi, J.M. Floryan, “Mechanism of drag generation by surface corrugation”, *Phys. Fluids*, Vol.24, pp.013602, 2012
- [17] A. Mohammadi, J.M. Floryan, “Pressure losses in grooved channels”, *J. Fluid Mech.*, Vol.725, pp. 23–54, 2013
- [18] H.V. Moradi, J.M. Floryan, “Flows in annuli with longitudinal grooves”, *J. Fluid Mech.*, Vol.716, pp.280–315, 2013
- [19] H.V. Moradi, J.M. Floryan, “Stability of flow in a channel with longitudinal grooves”, *J. Fluid Mech.*, Vol.757 pp. 613–648, 2014
- [20] L. Leger, E. Moreau, G. Touchard, “Effect of a DC corona electrical discharge on the airflow along a flat plate”, *IEEE Trans. Ind. Appl.*, Vol.38: 6, pp.1478-85, 2002
- [21] E. Moreau, L. Leger, G. Touchard, “Effect of a DC surface-corona discharge on a flat plate boundary layer for air flow velocity up to 25 m/s”, *J. Electrostat.*, Vol.64, pp. 215–25, 2006
- [22] F.S. Soetomo, “The influence of high-voltage discharge on flat plate drag at low Reynolds number air flow”, M. S. Thesis, Iowa State University, 1992
- [23] G.M. Colver, S. El-Khabiry, “Modeling of DC corona discharge along an electrically conductive flat plate with gas flow”, *IEEE Trans. Ind. Appl.*, Vol.35:2, pp. 387-94, 1999
- [24] S. El-Khabiry, G.M. Colver, “A semi-theoretical development of drag reduction on a thin plate in low Reynolds number flow with corona discharge”, *Proc. ESA Annual Meeting*, pp.135–138, Rochester, USA, 1995
- [25] S. El-Khabiry, G.M. Colver, “Drag reduction by DC corona discharge along an electrically conductive flat plate for small Reynolds number flow”, *Phys. Fluids*, Vol. 9, pp.587-99, 1997
- [26] H. H. Schlichting, “Boundary layer theory”, New York: McGraw-Hill, 2000
- [27] J. Hoffman, C. Johnson, “Turbulent incompressible flow, applied mathematics: body and soul, Vol. 4”, New York: Springer, 2006
- [28] P. Sattari, C.F. Gallo, G.S.P. Castle, K. Adamiak, “Trichel pulse characteristics – negative corona discharge in air”, *J. Phys. D: Appl. Phys.*, Vol.44, pp.155502, 2011

- [29] K. Adamiak, P. Atten, "Simulation of corona discharge in point-plane configuration", *J. Electrostat.*, Vol.61, pp.85-98, 2004
- [30] P. Sattari, G.S.P. Castle, K. Adamiak, "FEM FCT based dynamic simulation of corona discharge in point-plane configuration", *IEEE Trans. Ind. Appl.*, Vol.46, pp. 1699-706, 2010
- [31] M. Robinson, "Movement of air in the electric wind of the corona discharge", *AIEE Trans.*, pp.143-50, 1961
- [32] N. Sato, "Discharge current induced by the motion of charged particles", *J. Phys. D: Appl. Phys.*, Vol.13, pp.L3-6, 1980
- [33] R.S. Sigmond, "Simple approximate treatment of unipolar space-charge-dominated coronas: the Warburg law and the saturation current", *J. Appl. Phys.*, Vol.53, pp. 891-898, 1982

Chapter 6

6 Modeling of dielectric barrier discharge actuator for airflow control

In this study, a two-dimensional model of dielectric barrier discharge (DBD) is numerically simulated in order to study the ability of such a system to actively modify low-velocity airflow along a flat plate. The investigated model involves mutual interaction between the electric field, space charge density and gas flow. A single species model valid for either positive or negative ions has been adopted for this study. In order to improve our understanding of the physical mechanisms associated with the system, velocity profiles within the boundary layer of the flat plate are presented for a free air stream velocity up to a few meters per second. The effect of voltage and frequency as well as the system configuration on the actuator performance has been discussed. The results show the EHD actuator can cause a reduction in drag.

6.1 Introduction

When a high voltage is applied between two electrodes, ions are produced in air and they drift from the discharge electrode to the collector under the Coulomb forces. These ions exchange momentum with air molecules and induce a fluid motion, called electrohydrodynamic flow (EHD) [1]. It has been proven that the glow discharge at atmospheric pressure using a dielectric barrier discharge (DBD) can induce gas flow and operate as an actuator for flow control. The plasma jet generated by a DBD actuator is able to alter the velocity inside the boundary layer and can modify the interaction between the fluid and body surface without any mechanical moving parts [2]. Such EHD phenomenon directly converts electric energy into kinetic energy with very small response time compared to the characteristic times of the fluid dynamics.

There are many articles that review the use of AC surface DBD actuators applied to airflow control [2, 3]. The idea of using weakly ionized gas formed at the surface of a dielectric material for producing an air jet close to the surface of an insulator was first demonstrated by Roth [4]. Later both the electrical and mechanical characteristics of a surface DBD were presented and discussed by a few research groups. However, because

of its complicated physics, most of the investigations on DBD actuators for flow control are experimental in application such as boundary layer flow control [5-8], or flow separation control drag reduction [9-11]. Focusing on the instantaneous evolution of the velocity at a given point, Forte [12] observed the non-stationary evolution of instantaneous velocity for different points. It has been shown that the actuator generates a pulsed induced flow at the same frequency as the frequency of the high voltage. In their experiments the authors have shown that at points close to the exposed electrode negative corona discharge induces higher velocities as compared with the positive corona. It was already revealed that the structure of the plasma is not exactly the same during both half cycles [13]. However, just a few millimeters downstream of the exposed electrode the experiment shows almost the same behavior during both positive and negative half cycles with a very small fluctuation of velocity around a mean value. A reason for this decreased difference between the two half cycles is that far enough from the exposed electrode, there is no effect of electrons and the net body force results from positive and negative ions that have very small differences in their mobility.

Plasma actuator models can be generally classified into two categories, defined by the method in which the charge density is calculated. Several authors tried to model the whole process taking into account the chemistry of the discharges in various gases. The chemistry based models typically track the chemical species, electrons and ions, solving a set of transport equations. Essential features, such as ionization, recombination, and streamer propagation, are all included in the model. Based on such a model, Boeuf *et al.* [14, 15] showed that for a sinusoidal voltage, the discharge current consists of short pulses with large amplitude along with a low frequency current discharge of the corona type. However, the contribution of the low frequency current to the total force may be predominant in comparison with the pulse contribution, because the force induced during the corona phases acts over a much larger volume and for a longer time. Likhanskii *et al.* [16] conducted a simulation taking into account the chemistry of the discharge including both positive and negative ions. This model is capable of accurately resolving and predicting the plasma phenomena that occur with plasma actuator operation. Although the chemistry model proposed by the authors has the potential to resolve the plasma phenomena directly, the computational cost presents a significant limitation in its implementation since the

parameters in the model are non-constant and depend on the electric field intensity. Additionally, no investigation has been performed into the solution of this model over commonly used kilo hertz frequencies. In order to control the number of pulses happening during a half period of voltage, they had to increase the level of frequency up to 100 kHz. In most of the existing experiments the working frequency for DBD actuators is between a few hundred hertz to a few kilo hertz. Therefore, such an approach can be useful for detailed study of some physical processes, but not as a design or optimization tool in engineering applications.

The researchers interested in engineering applications of DBD often ignore the processes in the ionization layer by using algebraic models approximated by the solution of the Poisson and charge transport equations. The significant difference between the two approaches is that the latter generally requires assumptions on the behavior of either the charge density or electric field intensity produced by the actuator. One of the first suggested plasma actuator models was proposed by Shyy et al. [17]. In this study, an assumption was imposed suggesting that the electric field decays linearly in the horizontal and vertical directions from its prescribed maximum value located at the trailing edge of the exposed electrode. So, there is no accurate calculation of the spatial charge density, which is maintained at a constant value. As we know the plasma charge density is an important indicator of force intensity and is highly dependent on the applied electric field; neglecting its spatial variance can have a significant effect on the overall force distribution and accuracy of the model.

A slightly more sophisticated approach was proposed by Suzen et al. [18]. They assumed that the charge density on the dielectric surface follows a half Gaussian distribution. The maximum value of the half Gaussian distribution is assumed to match the experimental flow results. Since this value was defined for the specific actuator geometry and is thus constant, this parameter is not able to account for geometrical changes or voltage and frequency variation.

Based on the description above, in this study the DBD model is numerically simulated in order to study the ability of the discharge to actively modify low-velocity airflow along

a flat plate. It involves mutual interaction between the electric field, space charge density and gas flow. A single species model valid both for positive and negative ions, has been developed in this study assuming AC input voltage. Since the ionic wind in this case is mainly caused by ions, the effect of the electrons in the model has been ignored. The main contribution in this study is that that real time space charge density is calculated to satisfy the semi-empirical Peek's criterion and no other assumptions are made in order to include the effect of body force in Navier- Stokes equation. Also, in order to improve our understanding of the physical mechanisms associated with the system, velocity profiles within the boundary layer of the flat plate are presented for a free air stream velocity up to a few meters per second. The effect of the voltage and the frequency level as well as the geometrical characteristics of the model on the system performance has been discussed. The results show that the EHD actuator causes air drag reduction. This study could help researchers in optimization of the actuator.

6.2 Model description

The general idea of the DBD actuator is shown in Figure 6.1. The electrodes should be placed in a way to minimize the perturbation of the air flow when the discharge is not present and the DBD system should have the ability to create a tangential EHD force in close vicinity to the wall. In order to fulfill those requirements the DBD system consists of two electrodes, one placed on the insulating surface of the plate and exposed to high voltage and the other one buried inside the dielectric material and grounded. The exposed electrode is a copper strip with rounded edges having 0.02mm curvature radius, 5mm wide mounted on the surface of the insulator and located 2mm downstream of the leading edge of the plate. The buried electrode has 15mm width and 0.1mm thickness, shifted 4mm away downstream of the corona wire. Vertical distance from the grounded electrode to the surface of the insulator is 2mm.

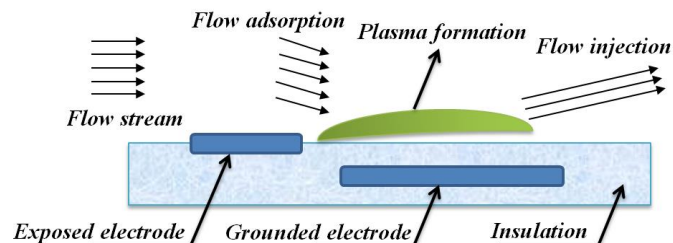


Figure 6.1: Idea of DBD actuator (not to scale)

Although, optical measurements of the plasma indicate that it is composed of a series of micro discharges, generally in a specific range of the voltage the plasma appears as a relatively uniform diffuse discharge. So, instead of the full three dimensional model of the system, a 2D model seems accurate enough to govern all essential interactions inside the boundary layer. The governing equations for the two-dimensional, single species model are as follows:

6.2.1 Fluid flow model

Detailed descriptions of the boundary layer governing equations are given in [19]. The summary of the equations of motion for high enough Reynolds number and for the two-dimensional flow are:

$$\begin{aligned} \frac{\partial u}{\partial x} + \frac{\partial v}{\partial y} &= 0 \\ \frac{\partial u}{\partial t} + u \frac{\partial u}{\partial x} + v \frac{\partial u}{\partial y} &= -\frac{1}{\rho} \frac{\partial P}{\partial x} + \lambda \frac{\partial^2 u}{\partial y^2} + \frac{\rho_c}{\rho} E_x \\ -\frac{1}{\rho} \frac{\partial P}{\partial y} &= 0 \end{aligned} \quad (6-1)$$

where u and v are the velocity components in the x and y directions, respectively, ρ is the fluid density, μ is the dynamic viscosity, $\lambda = \mu/\rho$ is the fluid kinematic viscosity, E_x is the electric field strength in the x direction and ρ_c is the net ion charge density.

To solve the above system of equations it is necessary to specify initial and boundary conditions. The fluid flow is run once without effect of the electric field and charge density distribution, body force effect and the distribution of the free air velocity in domain is put as the initial condition in the fluid flow model. At the plate surface there are no slip conditions.

$$u = 0 \text{ and } v = 0 \text{ at } y = 0$$

At infinity, outside the boundary layer and away from the plate, the flow is undistorted

$$u \rightarrow U_\infty \text{ as } y \rightarrow \infty$$

6.2.2 Electrical model

In the model used in this paper, Poisson's equation governs the electric potential, and consequently the electric field intensity distribution, for a given charge distribution [20]:

$$\nabla^2 V = -\frac{\rho_c}{\varepsilon} \quad (6-2)$$

The charge drift creates the electric current with a density defined as:

$$\vec{J} = \rho_c(\mu_e \vec{E} + \vec{u}) - D \nabla \rho_c \quad (6-3)$$

where \vec{J} is the electric current density, \vec{E} is the electric field intensity, \vec{u} is the gas velocity, ε is the gas permittivity, μ_e is the mobility of ions and D is the ions diffusion coefficient. The current density must satisfy the charge conservation equation:

$$\frac{\partial \rho_c}{\partial t} + \nabla \cdot \left(\rho_c (\mu_e \vec{E} + \vec{u}) - D \nabla \rho_c \right) = 0 \quad (6-4)$$

So, the problem of the corona discharge is governed by two partial differential equations with unknown electric potential and space charge density. The boundary conditions for the potential are straightforward: a given AC electric potential (V_{ap}) on the corona electrode and zero potential on the grounded plane [9]. However, formulation of proper boundary conditions for the space charge density is not so easy because the ionization layer has been neglected. One possible approach is to use Kaptzov's hypothesis which assumes that when the corona discharge occurs at some point on the electrode, the electric field at this point remains at the corona onset value. Peek's equation is used to find the onset level in air [21]:

$$E_0 = 3.1 \times 10^6 \left(1 + \frac{0.308}{\sqrt{R}} \right) \left[\frac{V}{m} \right] \quad (6-5)$$

where R is the electrode radius in *cm*.

The initial value for the space charge density has to be guessed or taken from the previous solution. After the problem is solved, the electric field on the electrode surface is compared with Peek's value and the electric charge updated. The following formula has been used to update the space charge density on the surface of corona electrode [21]:

$$\rho_c^{new} = \rho_c^{old} + \beta(E - E_0) \quad (6-6)$$

where β is an experimentally found constant and E is the actual value of the electric field.

An important point in simulating DBD is to include surface charge accumulation on the dielectric surface. This surface charge produces a field directed against the electric field produced by the voltage source to an extent that the ionization eventually stops. Actually, the surface charge accumulation plays a controlling role for the self-limiting feature of DBD preventing transition from a corona to a spark discharge. According to Maxwell equations, the tangential and normal components of the electrical intensity and electrical displacement at the interface between air and dielectric material must satisfy the following conditions [22]:

$$\vec{n} \times (E_d - E_a) = 0 \quad (6-7)$$

$$\vec{n} \cdot (D_d - D_a) = \rho_s \quad (6-8)$$

In the above equations, ρ_s is the accumulated surface charge density, and the subscripts d and a , correspond to dielectric or air. The time derivative of surface charge density is related to the normal current density [23]:

$$\frac{\partial \rho_s}{\partial t} = \vec{n} \cdot \vec{J} \quad (6-9)$$

The current density \vec{J} is defined in Eq. (6.3), so, the surface charge accumulation can be calculated as:

$$\rho_s = \int J_n dt + C_0 \quad (6-10)$$

The integral form of the surface charge density on the dielectric is a superposition of the charge added at a given time steps and C_0 , which defines the total charge accumulated in previous time steps.

6.3 Numerical algorithm

The processes occurring in the dielectric barrier discharge during a cycle of AC voltage are more complicated than that for a corona discharge. By applying an electric field larger than the breakdown field local ionization occurs, which initiates the electric current in the domain. During the positive half cycle the positive ions will accumulate on the dielectric surface. So, the total electric field intensity is a combination of the electric field produced by the voltage source and the field produced by the space charge collected on the dielectric surface. As the discharge progresses, the charge accumulated on the dielectric surface reduces the local electric field to such an extent that ionization stops and the current is quenched. When the sign of the applied voltage reverses, the electric field due to external voltage is reinforced due to the surface charge accumulation. This enhanced field at the beginning of the new half cycle initiates a current in the opposite direction, which transfers negative charge to the dielectric surface. The process continues until the opposing field due to the built up surface charge once again extinguishes the ionic current across the gap [23].

Following this description, an iterative numerical algorithm based on a single species model for the boundary layer control simulation has been developed. The simulation starts from some initial guess of the space charge density, air velocity components and then the conventional FEM procedure is employed to obtain the Poisson component of the electric potential. For the charge transport model a partial differential equation is solved, but an artificial diffusion has been added to obtain a stable algorithm. After calculating the potential distribution, the electric field is calculated by differentiating the potential distribution. Using the values of calculated electric field, the new charge density distribution is obtained. This process continues and the iterative algorithm also updates the injected charge density on the corona electrode surface until the electric field values are sufficiently close to Peek's value. After convergence is reached in the corona simulation program, the body force is calculated and substituted in Eq. (6.1) for the airflow simulation. This equation is again solved iteratively and when the residuals of both of the velocity components, the turbulence kinetic energy and its rate of dissipation satisfy certain minimum conditions the airflow simulation process is terminated. At this point, the new values for velocity components need to be entered into the charge continuity equation and

the whole process will continue to the point that all variables satisfy a certain error criterion. The calculations can provide detailed information on the local electrical parameters of the electric discharge, including the space charge density, the current density, the electric field, the potential distribution and the consumed power. Moreover, the mechanical parameters of the airflow, such as velocity, the pressure distributions and drag force can also be calculated.

It should be noted that the electric field varies strongly in both space and time. Near the discharge electrode the electric field variation is particularly steep, which demands a very fine spatial mesh, while in the remaining region the electric field is more uniform. A non-uniform spatial mesh is therefore essential for an accurate numerical treatment.

6.4 Results and discussion

All simulations have been performed for a single surface DBD actuator immersed in air at atmospheric pressure. The most important issue in the simulation that needed to be tackled is the different timescale involved in the electrical and fluid flow models. The time scale suitable for the simulation of the plasma actuator is defined by the period of the AC cycle that drives the alternating current discharge. This time scale is on the order of 1ms, which is approximately 10 times smaller than the time scale of the movements of the neutral fluid responding to the plasma actuator, which is on the order of 10ms. It means that the electrical part of the model reaches its quasi-steady-state much faster than the mechanical part, but the model should run up to the point that the mechanical error in two consecutive time step reaches a reasonably small value. Following this description the results of the numerical model are shown below.

6.4.1 Electric field intensity

Figure 6.2 shows the distribution of the electric field intensity at the tip of the exposed electrode with and without the effect of accumulated charges in space and on the surface of the dielectric.

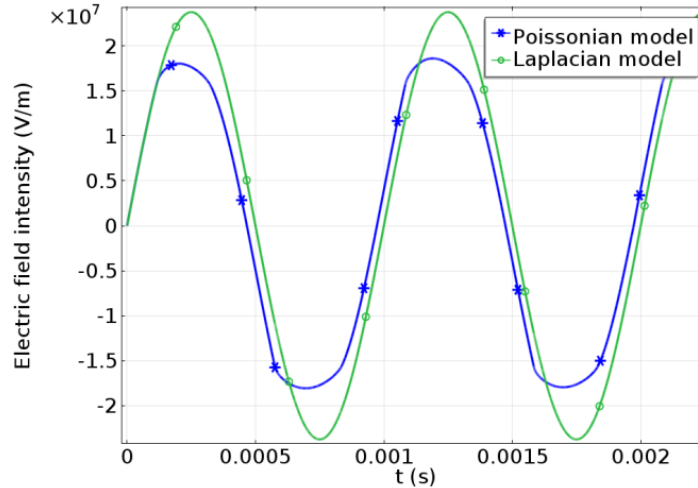


Figure 6.2: Electric field intensity on the tip of exposed electrode with (Poissonian model) and without (Laplacian model) the effect of the charge accumulated in air and dielectric surface

Two observations are dominant in Figure 6.2. First, the electric field is distorted due to effect of injected space charge from the tip of the exposed electrode and the accumulated surface charge on the dielectric. Thus, the electric field intensity reaches the value above Peek's value just after the voltage zero crossing. The second observation relates to the value of the maximum electric field intensity on the exposed electrode's tip. The iterative algorithm used modifies the injected charge and the iterations are terminated when the difference between both fields reaches an assumed value. So, the electric field magnitude is pretty close to Peek's value equal to $1.73 \times 10^7 (V/m)$, over a longer time interval.

6.4.2 Electric current

Typical voltage and current waveforms are presented in Figure 6.3 assuming a frequency of 1kHz and amplitude of 15kV. In this study, a formula for the discharge current for a general electrode geometry is derived from the energy balance equation. With a few simplifications the current equation can be calculated as [24]:

$$I = \frac{1}{V_{ap}} \iint (\mu_{e,p} \rho_{c,p} - \mu_{e,n} \rho_{c,n}) \vec{E} \cdot \vec{E}_s ds + \frac{\varepsilon}{V_{ap}} \iint \frac{\partial \vec{E}_s}{\partial t} \cdot \vec{E}_s ds \quad [A/m] \quad (6-11)$$

As already mentioned, in this model the effect of the electrons has been neglected, but in order to make the model as accurate as possible two factors were adjusted in the positive and negative half cycles: the mobility of the ions and Peek's value. The mobility of the negative ions in this study is assumed $2.5 \times 10^{-4}(\text{m}^2/\text{V}\cdot\text{s})$, which is slightly higher than the positive ions with $2.2 \times 10^{-4}(\text{m}^2/\text{V}\cdot\text{s})$ mobility. The Peek's value for the negative ions is taken equal to $1.6 \times 10^7(\text{V}/\text{m})$ and so is slightly lower for negative ions compare to positive ions. Even though these changes in the physics are very small, they result in a visible difference in positive and negative current.

The conduction current is shown in Figure 6.3 below with the electrostatic displacement current neglected.

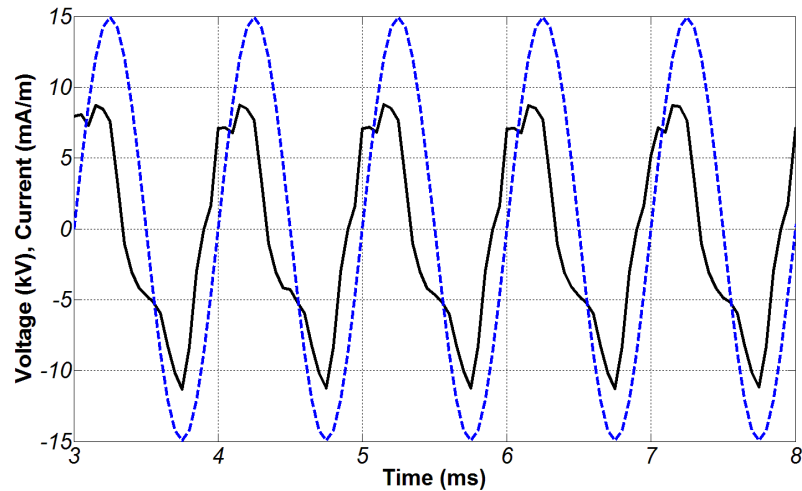


Figure 6.3: Voltage (kV) and current (mA/m) waveforms in DBD

As shown in Figure 6.3, the electric charge accumulated on the dielectric surface has a choking effect on the current waveform and the current is not in phase with the applied voltage.

6.4.3 Flow velocity

In order to study the DBD effect, the velocity profile for an inlet velocity equal to 1m/s is shown in Figure 6.4 for systems with and without discharge. The effect of the DBD generated EHD flow on the air flow in the boundary layer is clearly visible: the velocity profile in the boundary layer of the airflow is enhanced. Due to this effect, momentum is

injected in the boundary layer. However, for higher input velocities the profile it was found that the DBD discharge had less influence and showed a smaller effect. This can be explained by the fact that the discharge energy is almost constant for different air velocities, while the energy of the airflow in these regions increases with its velocity.

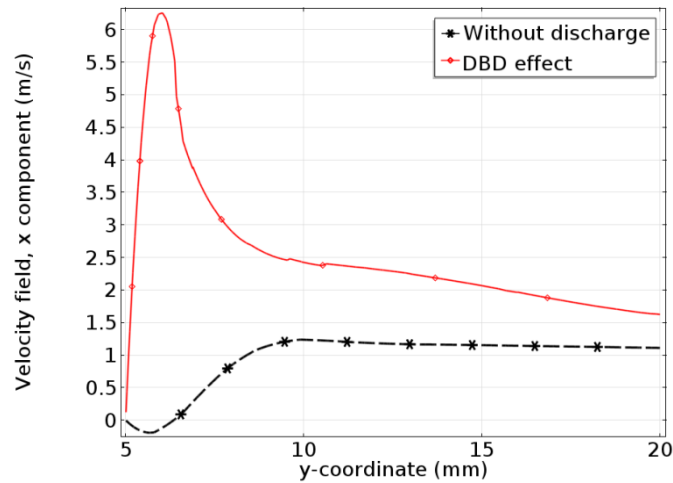


Figure 6.4: Velocity profile along a direction normal to the surface at $x=10\text{mm}$ ahead of the exposed electrode

Figure 6.5 shows the effect of the DBD generated EHD flow on the air flow in the boundary layer. The velocity streamlines are attracted towards the surface and form a wall jet. Depending on the geometry and the configuration of the electrodes, the DBD can contribute up to few meters per second to the velocity profile enhancement.

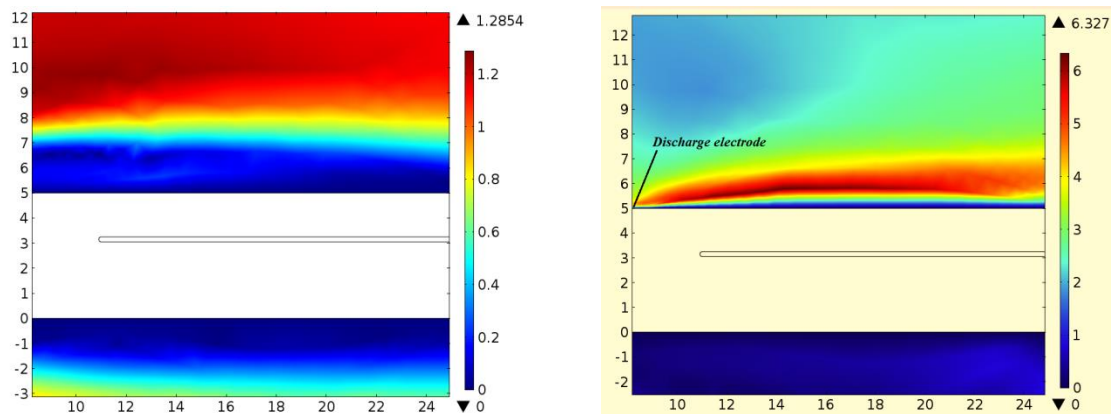


Figure 6.5: Velocity distribution around the object without (left) and with EHD flow (right)

Velocity profiles above a DBD actuator for different x values are shown in Figure 6.6. The higher velocity is reached at x closer to the exposed electrode. Away from the

discharge electrode the value of the maximum velocity decreases, but the point of maximum moves farther from the wall.

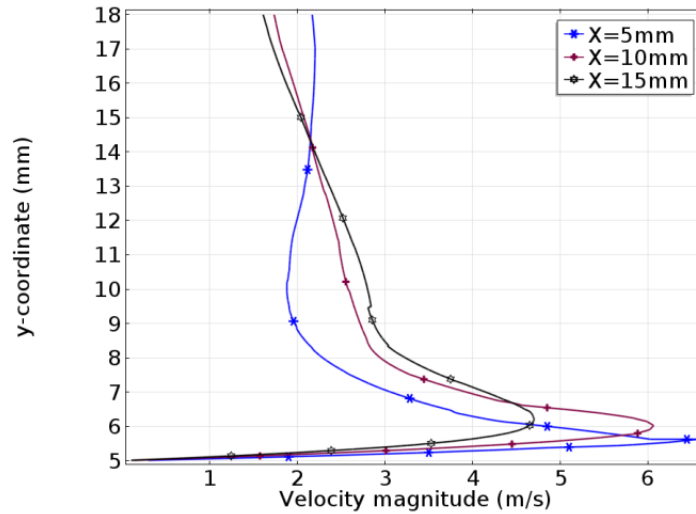


Figure 6.6: Velocity profiles above the DBD actuator for different distances from the discharge electrode

Time evolution of the horizontal component of the air velocity (u) is presented in Figure 6.7 for two different positions.

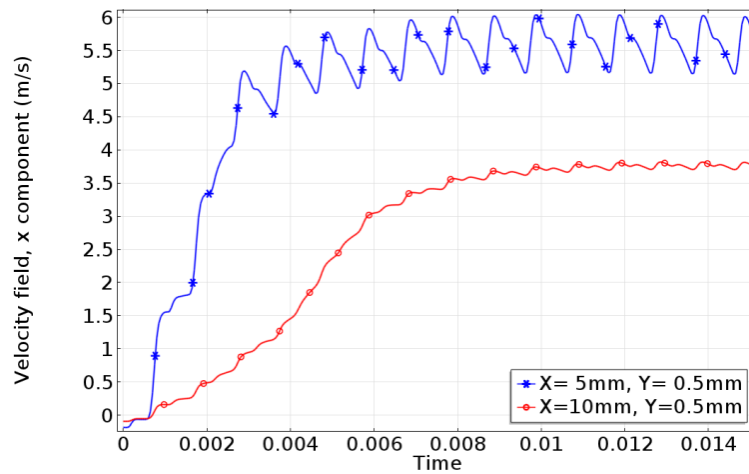


Figure 6.7: Time evolution of the x velocity component

The following can be observed from the calculated distributions:

- A pulsed induced air flow is generated at the same frequency as the frequency of high voltage.

- Velocity fluctuations disappear at larger distances from the discharge electrode and the horizontal velocity stabilizes around a mean value.
- The velocity profile stabilizes after around ten cycles of the voltage period.

6.4.4 Force calculation

The total force acting on the air flow in the boundary layer resulted from the corona discharge is an important parameter of the actuator. This force is the sum of the frictional drag force and the body force produced by the DBD system. For low-viscosity fluids the total force per unit length is equal to [25]:

$$\sum F = \rho \int_0^{\infty} (U_{\infty} - U) U_{\infty} dy [N/m] \quad (6-12)$$

Figure 6.8 shows the total force over the flat plate for different input velocity levels. Simulation results confirm the reduction of the total force for the velocity levels up to a few meters per second. Moreover, it was found that for the velocities up to some critical value, equal to 2.15m/s, the electrostatic force not only compensates for the effect of the drag force, but also changes the direction of the total force.

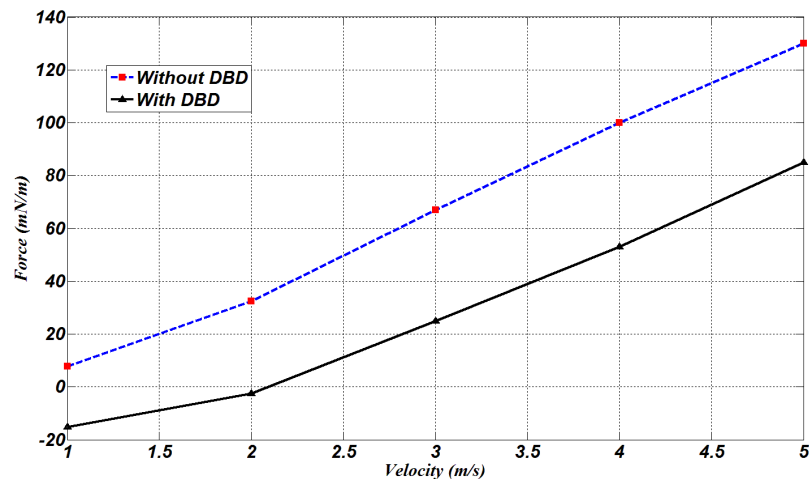


Figure 6.8: Total force calculation at $x=5$ mm ahead of exposed electrode versus free airflow velocity U_{∞} in absence and in presence of the DBD

6.4.5 Parametric study

There are several geometrical and physical parameters that have strong effects on actuator performance. A parametric study of those features would be useful for optimized design of the system. In this study the system was analyzed for different voltage levels and frequencies, exposed electrode dimensions, grounded electrode width, and for different gaps between the electrodes.

6.4.5.1 Voltage level

The evolution of the velocity with the applied voltage for different frequencies is shown in Figure 6.9. At the same frequency by increasing the maximum input voltage, the current level is increases. Thus, the momentum electrically transferred to the fluid is larger, and, as a result, the maximum velocity in domain just ahead of the corona electrode reaches greater values.

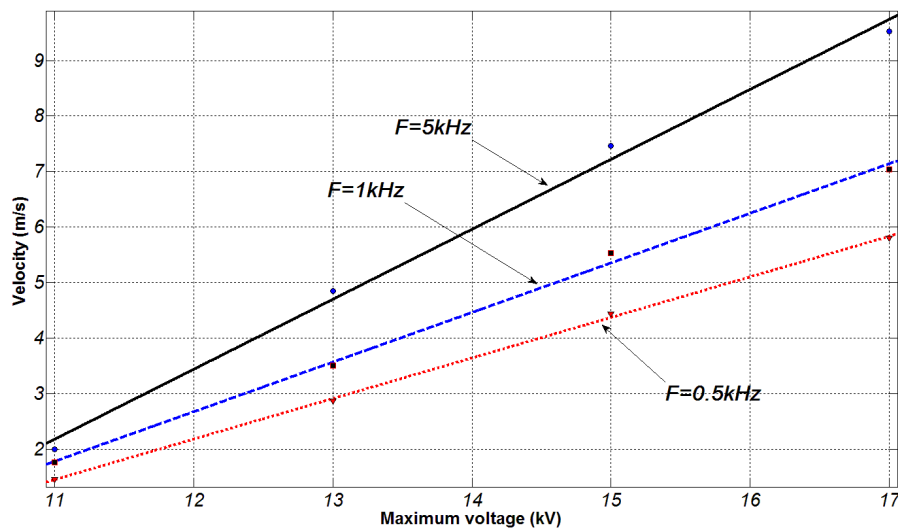


Figure 6.9: Evolution of the maximum induced air velocity with voltage magnitude and frequency

Likewise, at the same input voltage, higher frequency results in higher induced velocity in the domain. Figure 6.10 presents the maximum current versus the voltage amplitude for the three different frequencies modeled. It has been already proven [23] that by increasing the frequency the total charge in the domain is larger and so the maximum current level, consumed power and the maximum induced electrokinetic energy all increase.

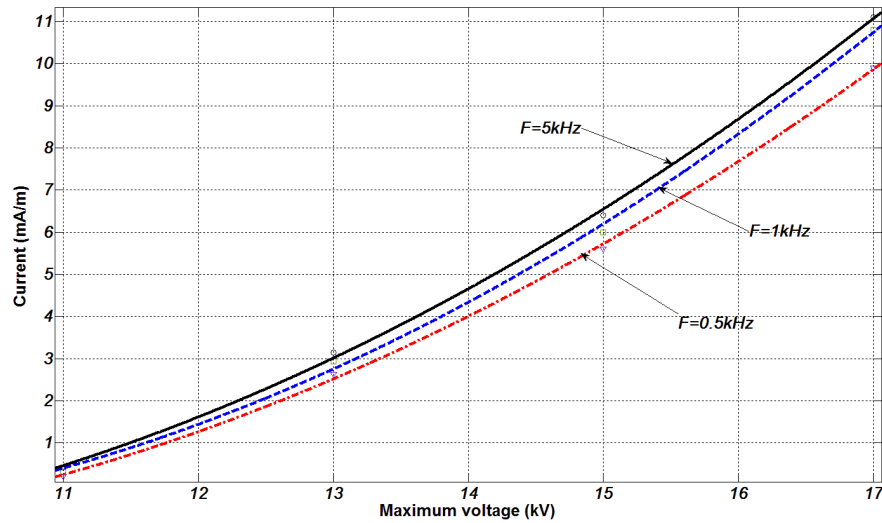
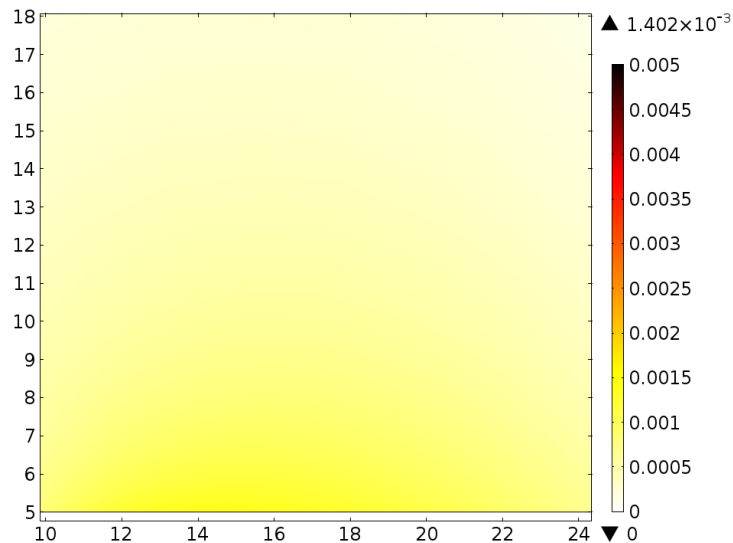


Figure 6.10: Maximum current for different voltage magnitudes and frequencies

Another interesting result regarding the maximum applied voltage is related to the plasma region extension over the insulating surface. It has been already shown [13] that the maximum extent increases linearly with the voltage amplitude. This can be seen in Figure 6.11 which shows space charge density distribution of the plasma for three voltages at the same time. Here the plasma is more extended in both the horizontal and vertical directions at the higher input voltages.



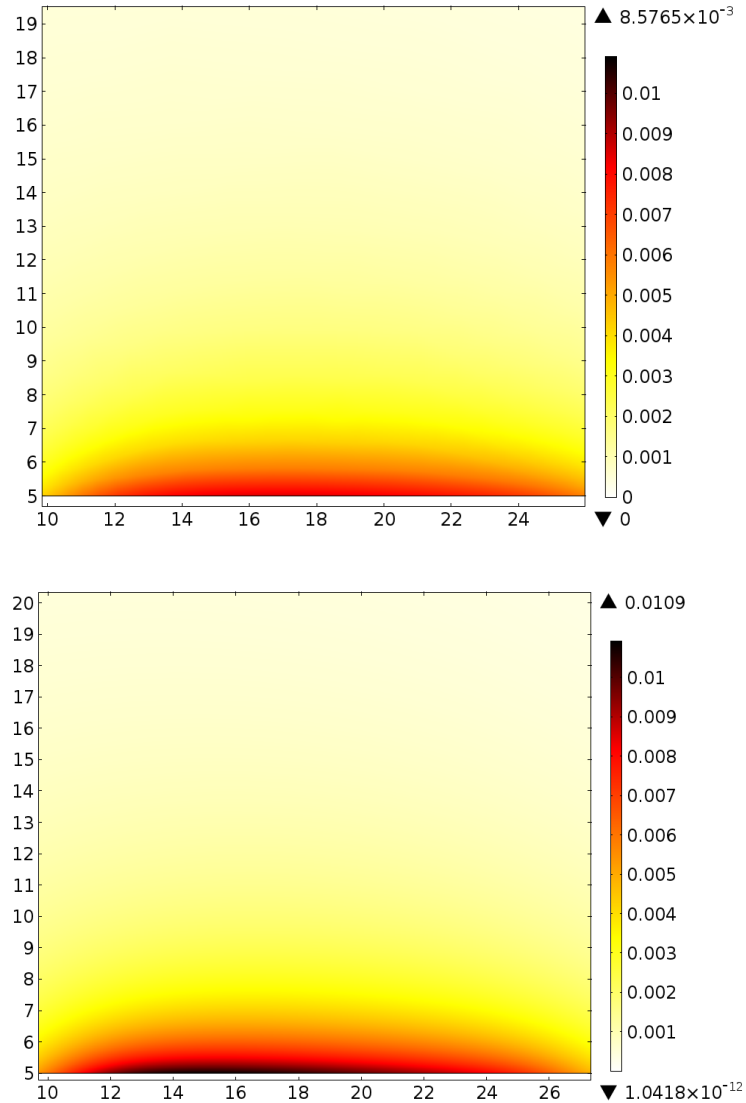


Figure 6.11: Space charge density distribution (plasma extension) for different applied voltages

6.4.5.2 Frequency

Figure 6.12 shows the variation of the velocity at the same point for two different frequencies. It should be noted that at the lower frequency the velocity reaches its quasi-stationary form after a smaller number of cycles, but the velocity fluctuations are much larger compared to that at the higher frequency. In addition as already discussed, the higher frequency results in a greater magnitude of the mean velocity.

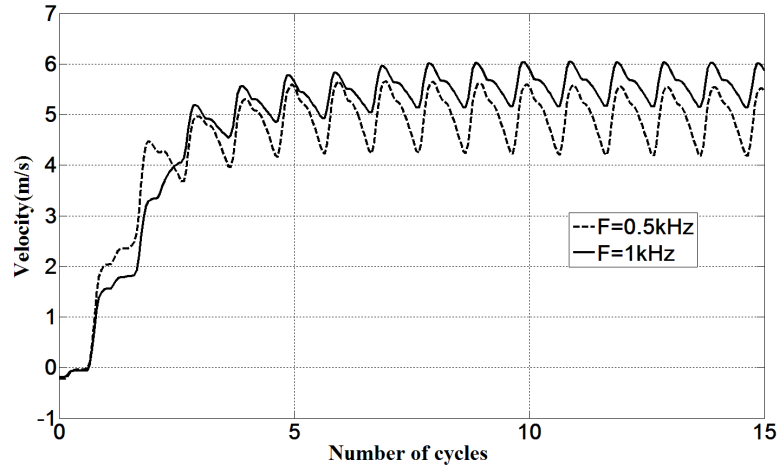


Figure 6.12: Velocity evolution at the same point for two different frequencies of the applied voltage

Figure 6.13 shows how the fluctuation in the velocity changes with the frequency for several values of voltage. For all cases after increasing the voltage frequency the fluctuation level decreases. The reason for this behavior results from the fact that at higher frequencies, the intervals during which the ions are injected to the domain are shorter, and ions do not have enough time to accumulate on the insulator surface. Thus, the body force, which is the product of the charge density and field intensity, at higher frequencies is more stable compared to that at the lower frequencies.

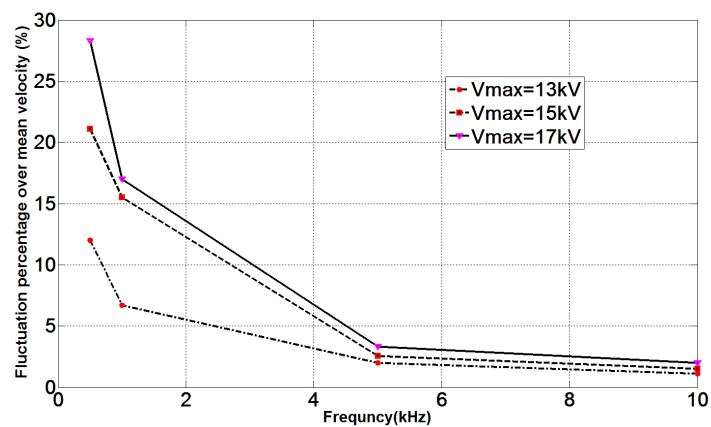


Figure 6.13: Normalized fluctuation level for different frequency levels

6.4.5.3 Exposed electrode thickness

One of the major geometrical parameters, which affect the actuator performance, is the exposed electrode thickness. By increasing the radius of curvature of the corona electrode

edge, based on Eq.(6.5) the value for Peek's value gets smaller. Meantime, the local electric field around the corona electrode would be smaller. So, for the same level of input voltage, space charge density would be smaller for larger radii of the exposed electrode since less charge is needed to satisfy Kaptzov hypothesis on the corona wire. In order to illustrate this, Figure 6.14 shows the space charge density distribution for the basic case, and the new model with an exposed electrode with 0.08mm radii.

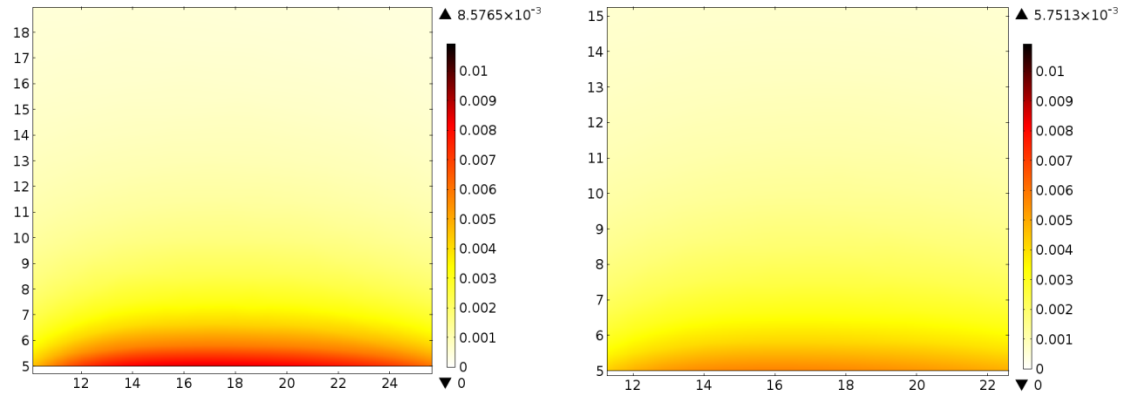


Figure 6.14: Plasma extension (space charge density) for two different radii of the exposed electrode (left) 0.04mm, (right) 0.08mm

As shown in Figure 6.14, the plasma extension in both the horizontal and vertical direction is larger for the smaller radii of curvature. Figure 6.15 shows the velocity fluctuation for these two cases at a point 5mm ahead of the exposed electrode.

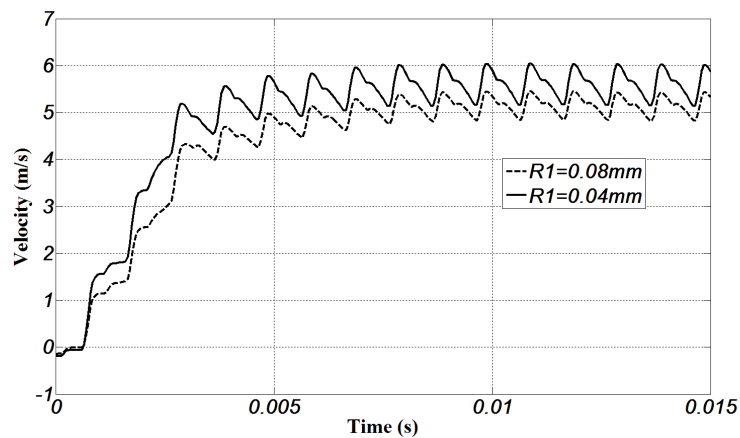


Figure 6.15: Velocity evolution at the same point for two different radii of the exposed electrode

Also, a thinner exposed electrode results in a larger velocity, since both the electric field intensity and space charge density have greater values. As a result, the body force would

be greater in the thinner electrode case. However, for a thicker electrode the velocity pattern is smoother. Generally, it can be said that a thinner exposed electrode produces stronger impact in the air moving above the wall at the same level of input voltage. Meantime, by choosing a thinner electrode we can minimize the disturbance of the corona electrode on moving air, when the system is not working.

6.4.5.4 Grounded electrode width

Figure 6.16 shows the velocity profile extension for two different widths of the grounded electrode. It has been found that the velocity profile extends up to the rightmost point of the grounded electrode on the surface. Beyond that, the effect of the *DBD* disappears.

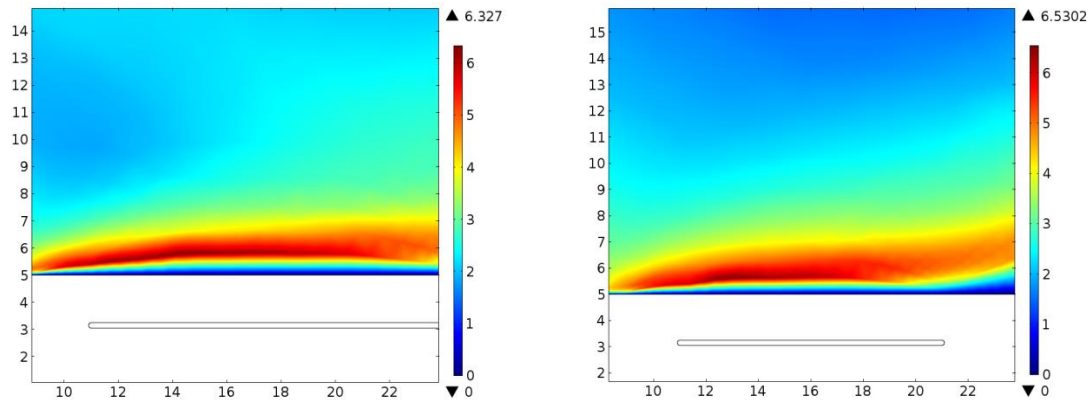


Figure 6.16: The effect of DBD on boundary layer for 15mm (left), and 10mm (right) electrode width

However, since the distance between the tip of the exposed electrode and the grounded electrode is constant, the onset voltage level, and consequently the maximum current, is the same for both cases. Therefore, almost the same level of the electric energy is transferred to the air, which will reduce the maximum velocity. This is confirmed by the results in Figure 6.17, where, the maximum velocity in the domain for different cases is shown: the narrower the grounded electrode, the greater the velocity magnitude.

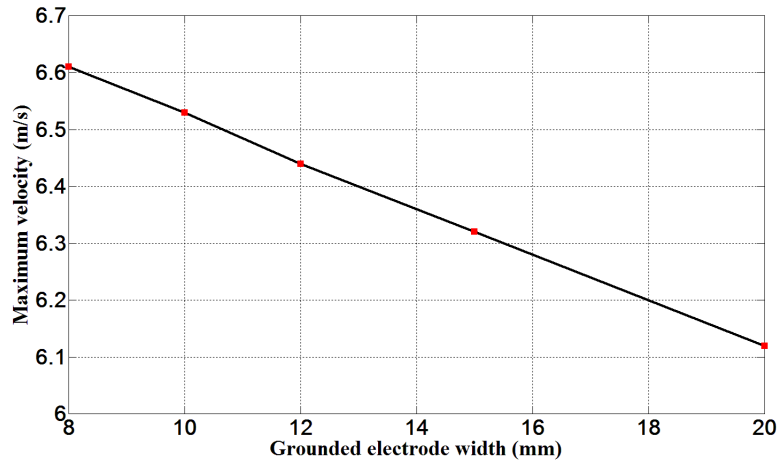


Figure 6.17: Maximum velocity for different widths of the ground electrode

6.5 Conclusions

The DBD has been shown to have a significant effect on the velocity profile in the boundary layer, even for small values of electrical power consumption. The following conclusions follow from the performed simulations:

- Single species model provides the results, which agree with experimental data published in literature.
- The DBD system results in drag reduction for air velocities, which correspond to the glow discharge regime.
- The extent and magnitude of the velocity profile depends on the configuration of the system. Both the exposed and grounded electrode have an impact on the velocity extension: a thinner exposed electrode results in greater velocity magnitude with larger fluctuations. The wider the grounded electrode, the longer the velocity profile, but with a smaller magnitude.
- Higher frequencies show better actuator performance with less velocity fluctuations.
- Frequency seems to have the strong effect on controlling the fluctuation level. By increasing the frequency, at every level of the input voltage, the fluctuation can be eliminated, or at least reduced.
- Both higher voltage and higher frequency result in higher current level and consequently higher velocity magnitude.

- The maximum velocity is almost a linear function of the voltage, while the maximum current is a square function of the voltage.

Acknowledgments

We would like to acknowledge NSERC for their financial support and CMC Microsystems for the providing an access to COMSOL commercial software.

References

- [1] L. Zhao, K. Adamiak, “EHD flow in air produced by electric corona discharge in pin-plate configuration”, *J. Electrostat.*, Vol.63, pp.337-50, 2005
- [2] N. Benard, E. Moreau, “Electrical and mechanical characteristics of surface AC dielectric barrier discharge plasma actuators applied to airflow control”, *Exp. Fluids*, Vol.55, pp.1-43, 2014
- [3] T. Corke, C. Enloe, S. Wilkinson, “Dielectric barrier discharge plasma actuators for flow control”, *Annul. Rev. Fluid Mech.*, Vol.42, pp.505–29, 2010
- [4] J. Roth, M. Sherman, S. Wilkinson, “Boundary layer flow control with a one atmosphere uniform glow discharge surface plasma”, 36th AIAA Aerospace Sci. Meeting & Exhibit, Pap. No. 1998-0328, Reno, USA, 1998
- [5] G. Neretti, A. Cristofolini, C. Borghi, A. Gurioli, R. Pertile, “Experimental results in DBD plasma actuators for air flow control, dielectric barrier discharge control of a turbulent boundary layer in a supersonic flow”, *IEEE Trans. Plasma Sci.*, Vol. 40:6, pp.1678-87, 2012
- [6] S. Im, H. Do, M. Cappelli, “Dielectric barrier discharge control of a turbulent boundary layer in a supersonic flow”, *Appl. Phys. Let.*, Vol. 97, pp.041503, 2010
- [7] A. Cristofolini, G. Neretti, F. Roveda, C. Borghi, “Schlieren imaging in a dielectric barrier discharge actuator for airflow control”, *J. Appl. Phys.*, Vol.111, pp.033302, 2012
- [8] A. Cristofolini, G. Neretti, C. Borghi, “Effect of the charge surface distribution on the flow field induced by a dielectric barrier discharge actuator”, *J. Appl. Phys.*, Vol. 114, pp.073303, 2013
- [9] T. Jukes, K. Choi, “Dielectric-barrier-discharge vortex generators: characterization and optimization for flow separation control”, *Exp. Fluids*, Vol.52, pp.329-45, 2011

- [10] C. Marks, R. Sondergaard, M. Wolff, R. Anthony, “Experimental comparison of DBD plasma actuators for low Reynolds number separation control”, *J. Turbomachinery*, Vol.135, pp.011024, 2013
- [11] S. Walker, T. Segawa, “Mitigation of flow separation using DBD plasma actuators on airfoils: A tool for more efficient wind turbine operation *Renewable Energy*”, Vol. 42, pp.105-10, 2012
- [12] M. Forte, J. Jolibois, J. Pons, E. Moreau, G. Touchard, M. Cazalens, “Optimization of a dielectric barrier discharge actuator by stationary and non-stationary measurements of the induced flow velocity: application to airflow control”, *Exp. Fluids*, Vol.43, pp.917–28, 2007
- [13] C. Enloe, T. McLaughlin, R. VanDyken, K. Kachner, E. Jumper, T. Corke, “Mechanisms and responses of a single dielectric barrier plasma actuator: plasma morphology”, *J. AIAA*, Vol.42:3, pp.589–94, 2004
- [14] J. Boeuf, L. Pitchford, “Electrohydrodynamic force and aerodynamic flow acceleration in surface dielectric barrier discharge”, *J. Appl. Phys.*, Vol.97, pp.103307, 2005
- [15] J. Boeuf, Y. Lagmich, T. Unfer, T. Callegari, L. Pitchford, “Electrohydrodynamic force in dielectric barrier discharge plasma actuators”, *J. Phys. D: Appl. Phys.* Vol.40, pp.652–62, 2007
- [16] A. Likhanskii, M. Shneider, S. Macheret, R. Miles, “Modeling of dielectric barrier discharge plasma actuator in air”, *J. Appl. Phys.*, Vol.103, pp.053305, 2008
- [17] W. Shyy, B. Jayaraman, A. Andersson, “Modeling of glow discharge-induced fluid dynamics”, *J. Appl. Phys.*, Vol.92:11, pp.6434-43, 2002
- [18] Y. Suzen, P. Huang, J. Jacob, “Numerical simulations of plasma based flow control applications”, 35th AIAA Fluid Dynamics Conf. & Exhibit, Pap. No. 2005-4633, Toronto, Canada, 2005
- [19] H. Schlichting, “Boundary layer theory”, New York: McGraw-Hill, 2000
- [20] P. Sattari, G.S.P. Castle, K. Adamiak, “FEM-FCT based dynamic simulation of corona discharge in point–plane configuration”, *IEEE Trans. Ind. Appl.*, Vol.46, pp.1699-706, 2010

- [21] K. Adamiak, P. Atten, "Simulation of corona discharge in point-plane configuration", *J. Electrostat.*, Vol.61, pp.85-98, 2004
- [22] J. Shang, P. Huang, "Modeling of ac dielectric barrier discharge", *J. Appl. Phys.*, Vol.107, pp. 113302, 2010
- [23] M.R. Ghazanchaei, K. Adamiak, G.S.P Castle, "Quasi-stationary numerical model of the dielectric barrier discharge", *J. Electrostat.*, Vol.72, pp.261-69, 2014
- [24] N. Sato, "Discharge current induced by the motion of charged particles", *J. Phys. D: Appl. Phys.*, Vol.13, pp.L3-6, 1980
- [25] E. Moreau, L. Leger, G. Touchard, "Effect of a DC surface-corona discharge on a flat plate boundary layer for air flow velocity up to 25 m/s", *J. Electrostat.*, Vol.64, pp.215–25, 2006

Chapter 7

7 Conclusions and Future Study

7.1 Conclusions

This chapter presents the summary and conclusions from the studies reported in this thesis related to the secondary EHD flow generated by the corona and dielectric barrier discharges. It also makes recommendations for possible future work.

In this thesis, a series of problems dealing with DC positive corona discharge and dielectric barrier discharge in air were simulated under quasi stationary conditions. The effect of electrostatic forces on various fluid dynamics problems in gaseous media was investigated. In order to make the models computationally time effective, a comprehensive FEM based technique including all the essential phenomena involved in the problems was developed. This single species discharge model is capable to solve the Poisson equation in order to calculate the electric field and potential distribution, charge transport equation to calculate the charge distribution in domain, and momentum equation to calculate the air velocity distribution in a fully coupled algorithm. Different steps in the FEM algorithm were mathematically explained and formulated. One of the main contributions of this study is to provide a numerical algorithm to predict the level of injected charge density to the domain based on the voltage level. Series of coefficient have been specified and the best fit would be selected, based on the voltage level and the maximum applied voltage. This algorithm gives us a real time monitoring of the injected charge to the system. A non-uniform discretization of the domain was considered, where the elements in the vicinity of the discharge electrode were much finer than in the other areas. It is important that for such a complicated geometry a distributed mesh was used.

7.1.1 Single-Species Model of Dielectric Barrier Discharge

A key feature in the modeling of DBD is to include the accumulation of charges on the dielectric surface. The electric circuit models with the combination of capacitive and resistive elements are commonly used for modeling the DBD. Those elements are time-dependent, and the difficulty of defining them prevents extensive application of such

models. Beside, in many cases empirical calibration is needed, and a significant concern arises in the implementation of each of these models when extrapolating to new geometries that are different from the ones in which the calibration was performed.

In order to solve those issues, a 2D FEM single species model was proposed for modelling the dielectric barrier discharge without any geometrical or physical calibration. This model confirmed that a single species model was capable of successfully modeling the DBD. In this model, the ionization layer was completely disregarded. The behaviour of the total corona current and space charge density under the AC voltage was studied. Kaptzov's hypothesis was used as a supplementary boundary condition for calculating the charge density in the whole air gap and on the surface of the corona electrode.

It was shown that the numerical model for the dielectric barrier discharge is similar to that for the corona discharge with just one additional boundary condition on the dielectric material in order to include the effect of surface charge accumulation.

Two observations are dominant in the electric field distribution: horizontal zero crossing distortion due to effect of injected space charge from the tip of the needle and the accumulated surface charge on the dielectric, and the other one about the maximum electric field intensity on the needle's tip which is going to be around Peek's value for all the points participating in charge injection.

The time evolution of the space charge density and surface charge accumulation were shown. The shapes of charge clouds at different time instants and for different applied voltages were presented.

The effect of different parameters such as frequency and the magnitude of applied voltage on the DBD characteristics, like the average current, were investigated.

It was found that the current changes parabolic and the space charge almost linearly as the voltage increased above the onset level.

At the fixed voltage, by increasing the frequency, the current level increases due to the fact that transition time from positive cycle to negative cycle gets smaller and clouds of

both positive and negative ions are formed. However, the net charge in whole domain is smaller at higher frequencies, because at lower frequencies ions with the same polarity are dominant in a half cycle, and starting from following cycle almost all the ions are settled on the dielectric layer.

At higher frequencies, the ion transition time from the discharge electrode to the dielectric surface can be longer than the voltage period, therefore, at some points of the air gap there are still charges of one polarity, when the charges of opposite polarity start to be injected from the needle which is the main reason for clouds of ions formation.

7.1.2 Wire-nonparallel plate electrohydrodynamic gas pump

The 2D characteristics of the EHD flow patterns were studied in a wire-to-nonparallel plate EHD blower. The EHD flow body force was calculated from the corona discharge model and used in the flow velocity calculations.

The detailed distributions of all essential parameters for the electric and flow field were predicted. The effect of corona discharge electrode geometry and applied voltage on the corona discharge characteristics and EHD flow pattern was discussed.

An analogy was found between the EHD pump and an equivalent voltage source in order to capture the velocity vs. pressure characteristics of the pump, based on the short circuit and open circuit tests.

Mechanical power converted in the channel was found to be much smaller than the input electrical power, but the efficiency of the system increases by considering heavier ions with smaller mobilities.

For the assumed pump length and the vertical distance between corona wire and ground plates, an optimum wall angle of the pump for the maximum volumetric gas flow rate was found.

Due to the facts that the distance between the corona wire and the plate is constant and the plates are placed far enough from corona wire the current vs. voltage characteristics was found to have nearly the same for different plate angle.

7.1.3 Electrohydrodynamic Interactions in the Boundary Layer of Air Flows

A 2D model to study the electromechanical interaction between the corona discharge and air flow over a flat plate for different angle of attack was developed. The major challenge in this model is to effectively capture the behavior of the space charge density without extensive modeling of the fundamental chemical reactions that occur. Thus, a single species model for a DC positive input voltage was presented.

The tangential body force acting on the gas is directed downstream and is created by the downstream motion of the positive ions.

The effect of voltage level on the velocity profile and the effect of external velocity on the discharge current were investigated. Velocity profiles within the boundary layer of the flat plate were predicted for air velocities up to 12m/s. For the velocities below this value the corona discharge is in the glow regime. In the case of free air velocity equal to zero, the ionic wind produced by the corona reaches the value of about 2.5m/s.

The equation for the total force on the air in the boundary layer including the effect of the electrostatic body force was developed. Regardless of the current level, a consistent drag reduction has been shown for velocities up to 12m/s.

The efficiency of the system has been calculated by defining a control volume contour around the corona wire. Higher voltages at the same level of air stream velocity have a greater effect on the velocity profile close to the flat plate surface. However, higher applied voltages result in smaller efficiency levels. The efficiency has an inverse linear relation with the applied voltage since the relative effect of the corona discharge at higher velocities is smaller than at lower velocities.

For different angles of attack and in the absence of the DC discharge the air flow separates from the wall at the leading edge, forming a significant wake just above the flat plate. In the case of corona discharge, the airflow is reattached to the wall. This process modifies the laminar–turbulent transition inside the boundary layer and reduces the drag.

7.1.4 DBD plasma actuator for airflow control

The major difference between the DBD and the surface corona discharge actuators is the presence of a dielectric barrier separating the anode and cathode in the former configuration. The dielectric barrier introduces a region of large electric breakdown strength, allowing for the application of larger potential differences and thus larger electric field intensities in the plasma region. In addition, the presence of the dielectric barrier increases the stability of the plasma, preventing a glow-to-arc transition at typical potentials for which this would occur on the surface corona discharge.

In this study, a new DBD plasma actuator model has been proposed which relies upon several significant modifications to the existing models. These modifications include a new criterion to evaluate the electric field strength required for plasma ignition, an accurate model for including the electrostatic body force based on real time variation of charge distribution, a new integrative approach to calculating the surface charge density on the dielectric barrier, complete reformulation of the discharge current with different onset levels and mobilities for positive and negative ions. Meantime, the displacement current has been included in current calculation.

The mutual interaction between three fields: electrostatic, airflow and ion flow was taken into account. The developed DBD can be used for many different configurations.

This accurate model is capable of predicting the output of the actuator under variations in geometry, voltage, and frequency, and can alleviate the current trial-and-error design approach that is typically implemented. Furthermore, optimizing the performance of the plasma actuator is most easily achieved since the physics of the plasma is understood through an accurate model.

The effect of the applied voltage amplitude on the discharge characteristics was investigated. For this, the AC frequency was kept constant, and the amplitude of the applied voltage was varied. The total current from the plasma actuator was found to be a parabolic function of applied voltage, while the maximum velocity above the plate changes linearly with the applied voltage. It should be noted that the voltage versus maximum velocity variation might show different pattern based on the actuator geometry, especially the dielectric thickness, and the voltage range used in the study.

A pulsed induced air flow is generated with double the frequency of the input voltage. Velocity fluctuations disappear at larger distances from the discharge electrodes and the horizontal velocity stabilizes around a mean value.

The effect of the frequency of the applied AC voltage was also studied. It was found that the extent of the plasma over the dielectric surface depends on the AC frequency. Frequency seems to have a strong effect on the velocity fluctuation level. Also the driving frequency controls how many times the plasma is ignited within a specific time period.

By increasing the frequency, at every level of the input voltage, the fluctuation can be eliminated, or at least reduced. Higher frequencies show better actuator performance with less velocity fluctuations.

It was found that the extent and magnitude of the velocity profile depends on the configuration of the system. Geometry of both the exposed and grounded electrode has an impact on the velocity extension.

7.2 Recommendations for Future Study

It is believed that the research reported in this thesis answers some fundamental questions about EHD flow and effect of different parameters on this phenomenon, assuming complicated discharge electrode geometries. However, there are number of issues which deserve further investigation.

7.2.1 Modeling

The models presented in this work provide a step forward in predicting the characteristics of EHD systems, but further development efforts would be desired. Numerical models could be improved to include; a wide range of non-symmetric geometries, details of plasma formation, geometry optimization for maximum performance.

7.2.2 Experimental studies

A database of experimental setups and measurements could also be used to identify strengths of the discussed models which may be further implemented in different applications.

7.2.3 EHD pump design for cooling an electronic circuit

One of the main applications of EHD pumps is in cooling of electronic circuits. As we know, to initiate and sustain a corona discharge process required in an EHD pump, the electric field in the area of ion creation must exceed the dielectric strength of air, which under standard conditions is approximately equal to three kilovolts per millimeter. For most practical devices, this requires an operating voltage greater than a kilovolt and often multiple kilovolts. As most electronic applications do not have an existing power source suitable to directly power an EHD air mover, a compact high voltage power supply must be included as part of the EHD system design. For compact applications, such as many consumer electronics, the development of small, efficient and low cost high voltage power supplies is essential. Such power supply devices are critical for commercial EHD applications.

7.2.4 Sliding Discharge

A relatively new design for plasma actuators is based on a sliding discharge. The concept is based on utilizing the AC DBD to weakly ionize the air, and then to superpose a DC electric field to establish a corona discharge between spatially separated electrodes. The DC component induces the sliding discharge. This design is based on the three-electrode geometry: two air-exposed electrodes flush mounted on the wall surface of a dielectric material (Electrodes 1 and 2) and another planar electrode on the other side of the dielectric wall (Electrode 3). The electrode placed below the dielectric may also be encapsulated in the dielectric wall. Electrodes 2 and 3 are connected together, and usually grounded, whereas Electrode 1 is excited. If Electrode 1 is excited by an AC HV, without a DC component, then there is a typical DBD between Electrodes 1 and 3. On the other hand, if one applies simultaneously a sufficient AC component to establish a DBD, plus a DC component sufficient to establish a typical corona between Electrodes 1 and 2, then a sliding discharge is produced. In fact, it seems that the DBD plays the role of ionizer around Electrode 1, and the DC component induces a sliding corona discharge between Electrodes 1 and 3. The advantages of this concept are that large plasma sheets can be produced and the plasma is stable with no glow-to-arc transition, except when the DC component is above the DC breakdown limit for the air.

7.2.5 Different applications of plasma actuators

There are an ever growing number of applications of DBD plasma actuators. New applications continue to appear as more investigators gain experience in using the concept of EHD actuator design. A partial list of these includes low-pressure turbine blade separation control, turbine tip-clearance flow control, unsteady vortex generation and control, and airfoil leading-edge separation control as well as boundary layer control. Study on real industrial applications and optimization of the EHD actuator for practical cases mentioned above looks a promising area for future work.

Curriculum Vitae

Name: Mohammadreza Ghazanchaei

Post-secondary Education and Degrees: Iran University of Science & Technology
Tehran, Iran
2004-2008 B.Sc.

Iran University of Science & Technology
Tehran, Iran
2008-2010 M.Sc.

Western University
London, Ontario, Canada
2011-2015 Ph.D.

Honors and Awards: First rank among the M.Sc. Power electronics students of the Electrical Engineering Department, Iran University of Science & Technology, Sep. 2010

Graduate research scholarship at Western Univ., London, Ontario, Sep. 2011

Second place best presentation award at ESA conference, University of Waterloo, ON, Canada, June 2012

Third place best presentation award at ESA conference, University of North Dame, IN, USA, June 2014

Related Work Experience Teaching Assistant
Western University
2011-2015

Research Assistant
Western University
2011-2015

Research Engineer & Research Assistant, Advanced Electrical Machine Design & Drive Lab, IUST, Power Engineering Department, 2008-2010

Publications:

M.R. Ghazanchaei, K. Adamiak, G.S.P. Castle, "Predicted flow characteristics of a wire-nonparallel plate type electrohydrodynamic gas pump using the Finite Element Method," *J. Electrostat.*, Vol. 73, pp. 103-111, Feb. 2015

M.R. Ghazanchaei, K. Adamiak, G.S.P. Castle, "Modeling of dielectric barrier discharge actuator for airflow control," under review: *J. phys. D: Appl. Phys.*, Mar. 2015

Mohammadreza Ghazanchaei, Kazimierz Adamiak, G.S. Peter Castle, "Numerical Modeling of EHD Interaction in the Boundary Layer of Air Flows," under review: *Int. J. Flow Control*, Feb. 2015

Mohammadreza Ghazanchaei, Kazimierz Adamiak, G.S. Peter Castle, "Numerical study on the DC corona discharge for the active airflow control along the flat plate," *Ins. Phys., IOP: Electrostatics*, Vol.1, pp.85, Southampton, UK, April, 2015

Mohammadreza Ghazanchaei, Kazimierz Adamiak, G.S. Peter Castle, "Quasi-stationary numerical model of the dielectric barrier discharge," *J. Electrostat.*, Vol.72:4, pp. 261-269, Aug.2014

Mohammadreza Ghazanchaei, Kazimierz Adamiak, G.S. Peter Castle, "Investigation on dielectric barrier discharge actuator to control airflow boundary layer," *Electrostatic Society of America (ESA) Annual Meeting on Electrostatics*, Pomona, USA, June 2015

Mohammadreza Ghazanchaei, Kazimierz Adamiak, G.S. Peter Castle, "Modeling of dielectric barrier discharge actuator for airflow control," *CANCAM 2015*, London, Canada, June 2015

Mohammadreza Ghazanchaei, Kazimierz Adamiak, G.S. Peter Castle, "Predicted flow characteristics of a wire-nonparallel plate type electrohydrodynamic gas pump using the Finite Element Method," *Electrostatics Society of America (ESA)*, Notre Dame, USA, June 2014

M.R. Ghazanchaei, K. Adamiak, G.S.P. Castle, "Numerical Modeling of EHD Interaction in the Boundary Layer of Air Flows," *Cage Club Student Conference on High Voltage Engineering and Applied Electrostatics*, Hamilton, ON, Aug. 2014

M.R. Ghazanchaei, K. Adamiak, G.S.P. Castle, "Quasi-stationary numerical model of the dielectric barrier discharge," *Electrostatics Society of America (ESA)*, Cocoa Beach, USA, June 2013

M.R. Ghazanchaei, K. Adamiak, G.S.P. Castle, "Adaptation of Comsol software to the simulation of corona discharge phenomenon," *IEEE/ESA Joint Conference*, Cambridge, Canada, June 2012